CFD SIMULATION OF HYDROCYCLONE FOR DESALINATION PROCESS

MISS JITSOPIN SRUDHIPROM

A THESIS SUBMITTED IN PARTIAL FULFILLMENT

OF THE REQUIREMENTS FOR

THE DEGREE OF MASTER OF ENGINEERING (CHEMICAL ENGINEERING)

FACULTY OF ENGINEERING

KING MONGKUT'S UNIVERSITY OF TECHNOLOGY THONBURI

2011

CFD Simulation of Hydrocyclone for Desalination Process

Miss Jitsopin Srudhiprom B.Eng. (Chemical Engineering)

A Thesis Submited in Partial Fulfillment of the Requirement for
the Degree of Master of Engineering (Chemical Engineering)
Faculty of Engineering
King Mongkut's University of Technology Thonburi
2011

Thesis Committee

…… Chairman of Thesis Committee
(Lect. Warinthorn Songkasiri, Ph.D.)

……. Member and Thesis Advisor
(Assoc.Prof. Dr.*Thongchai* Srinophakhun, Ph.D.)

……. Member
(Asst. Prof. *Jindarat Pimsamarn*, Ph.D.)

……. Member
(Asst. Prof. Dr.*Wanwilai Kraipech* Evans, Ph.D.)

Special Research project Title	CFD Simulation of Hydrocyclone for Desalination Process
Special Research Project Credits	6
Candidate	Miss Jitsopin Srudhiprom
Special Research Project Advisor	Assoc. Prof. Dr. Thongchai Srinophakun
Program	Master of Engineering
Field of study	Chemical Engineering
Department	Chemical Engineering
Faculty	Engineering
B.E.	2554

Abstract

The separation of ice from brine slurry with a hydrocyclone was simulated using computational fluid dynamics method. Reynolds Stress Model (RSM) and Eulerian-Granular approach were used to model the flow behavior of ice-sea water slurry inside the hydrocyclone. The overall size of the hydrocyclone was 5 cm in diameter and 116 cm in height. The simulation was separated into two parts: in the first part, the effects of the operating parameters were studied. The inlet velocity of ice-sea water slurry feed was varied from 11 to 25 m/s, while the ice solid volume fraction was kept at 0.2. The separation efficiency reached 80%, when the inlet velocity was higher than 20 m/s. The increase in the inlet velocity generated higher centrifugal force which improved the separation efficiency. The solid volume fraction was varied from 0.1 to 0.4 based on the inlet velocity at 20 m/s. While the ice solid fraction was varied from 0.1 to 0.4, the separation efficiency significantly decreased from 94 to 48%, because the increase in the solid concentration raised the drag force. The separation efficiency finally reduced. In the second part, the effects of the overflow diameter and the overflow diameter on the separation efficiency and the flow pattern of ice slurry were investigated. The enlargement of the overflow diameter from 0.41 to 0.7 cm increased the mass recovery fraction of ice in the overflow stream from 59 to 96%, but the volume percent of ice exiting at the overflow side decreased from 57 to 44%. The decrease of the underflow diameter provided the results corresponding to the enlargement of overflow diameter. When the underflow diameter decreased from 0.915 to 0.5 cm, the split fraction of ice-slurry increased from 65 to 99%. A lower ice purity in the overflow stream was found at a larger overflow diameter. Either increasing overflow diameter or decreasing underflow diameter caused both ice and sea water to migrate to the overflow, but the percentage of increase in sea water exiting the overflow was higher than that of ice. Therefore, diluter flow was found at overflow when the overflow area increased. The simulation of ice and seawater separation with hydrocyclone could be used to predict the separation efficiency and also described the ice and sea water distribution inside a hydrocyclone.

Keywords: CFD/ Desalination Process/ Eulerian-Granular Model/ Hydrocyclone

หัวข้อโครงการศึกษาวิจัย	การคำนวณทางพลศาสตร์ของไหลของไฮโดรไซโคลนที่ใช้ในกระบวนการผลิตน้ำจืดจากน้ำทะเล
หน่วยกิต	6
ผู้เขียน	นางสาวจิตโสภิณ ศรุติพรหม
อาจารย์ที่ปรึกษา	รศ. ดร.ธงไชย ศรีนพคุณ
หลักสูตร	วิศวกรรมศาสตรมหาบัณฑิต
สาขาวิชา	วิศวกรรมเคมี
ภาควิชา	วิศวกรรมเคมี
คณะ	วิศวกรรมศาสตร์
พ.ศ.	2554

บทคัดย่อ

งานวิจัยนี้เป็นการศึกษาการแยกน้ำแข็งออกจากน้ำเกลือ โดยใช้ไฮโดรไซโคลนด้วยเทคนิคการคำนวณพลศาสตร์ของไหล สมการที่ใช้ในการคำนวณคือ Reynolds Stress Model (RSM) และ Eulerian-Granular model สัดส่วนขนาดของไฮโดรไซโคลนที่ใช้ในการศึกษามีเส้นผ่านศูนย์กลาง 5 เซนติเมตร สูง 116 เซนติเมตร โดยงานวิจัยนี้แบ่งการศึกษาเป็น 2 ส่วน ส่วนแรกศึกษาผลของความเร็วขาเข้าของไฮโดรไซโคลนและความเข้มข้นของน้ำแข็ง โดยแปรผันความเร็วขาเข้าของไฮโดรไซโคลนตั้งแต่ 11-25 เมตรต่อวินาที ณ ความเข้มข้นของน้ำแข็งคงที่ที่ร้อยละ 20 โดยปริมาตร เมื่อเพิ่มความเร็วขาเข้าของไฮโดรไซโคลนถึง 20 เมตรต่อวินาที ได้ประสิทธิภาพการแยกร้อยละ 80 การเพิ่มความเร็วขาเข้าของไฮโดรไซโคลนเป็นการเพิ่มแรงเหวี่ยงทำให้ประสิทธิภาพการแยกดีขึ้น ความเข้มข้นของน้ำแข็งถูกแปรผันตั้งแต่ร้อยละ 10 ถึง 40 เมื่อเพิ่มความเข้มข้นของน้ำแข็งจากร้อยละ 10 ถึง 40 ประสิทธิภาพในการแยกจะลดลงจากร้อยละ 94 ถึง 48 เนื่องจากว่า การเพิ่มความเข้มข้นของน้ำแข็งจะเป็นการเพิ่มแรงต้านการไหล ในส่วนที่สองของงานวิจัยเป็นการศึกษาผลของเส้นผ่านศูนย์กลางด้านบนและด้านล่าง โดยแสดงผลเป็น อัตราส่วนของเส้นผ่านศูนย์กลางด้านบนต่อเส้นผ่านศูนย์กลางด้านล่าง (D_o/D_u) โดยเพิ่มเส้นผ่านศูนย์กลางด้านบนจาก 0.41 ถึง 0.7 เซนติเมตร สัดส่วนมวลของน้ำแข็งที่นำกลับมาได้ อยู่ในทางออกด้านบนของไฮโดรไซโคลน โดยเพิ่มขึ้นเป็นร้อยละ 59 ถึง 96 แต่ร้อยละของปริมาตรน้ำแข็งลดลงจาก 57 ถึง 47 หลังจากที่ศึกษาเส้นผ่านศูนย์กลางด้านบนแล้วจึงศึกษาเส้นผ่านศูนย์กลางด้านล่าง พบว่าการเพิ่มเส้นผ่านศูนย์กลางด้านบนของไฮโดรไซโคลนและลดเส้นผ่านศูนย์กลางด้านล่างให้ผลคล้ายคลึงกัน เมื่อลดเส้นผ่านศูนย์กลางด้านล่างจาก 0.915 ถึง 0.5 เซนติเมตร ปริมาณน้ำแข็งที่นำกลับมาได้ ได้ในช่องด้านบนเพิ่มขึ้นจากร้อยละ 65 ถึง 99 ดังนั้น

เมื่อเพิ่มพื้นที่รูเปิดด้านบนหรือลดพื้นที่รูเปิดด้านล่างพบว่าปริมาณการไหลของช่องรูเปิดด้านบนเพิ่มขึ้น แต่ความเข้มข้นของน้ำแข็งที่ได้จากช่องรูเปิดด้านบนกลับลดลง

คำสำคัญ: การผลิตน้ำจืดจากน้ำทะเล/ไฮโดรไซโคลน/CFD/Eulerian-Granular

ACKNOWLEDGEMENTS

It is my pleasure to acknowledge those who have helped make this thesis possible. Firstly, I would like to express my gratitude to my advisors, Associate Professor Thongchai Srinophakun for advice, valuable suggestions, encouragement, enthusiasm, and great support throughout this work. He has been my most important mentor and has greatly influenced my perspective in mathematic modeling.

Appreciation is also extended to Chemical Engineering Practice School, KMUTT which gives me a lot of support, good experiences and valuable opportunity. Also, I would like to thank my committee members, Asst. Prof.Wanwilai Kraipech Evans, Dr.Warinthorn Songkasiri, and Asst. Prof.Jindarat Pimsamarn for their kind and useful recommendations.

I would like to express my great gratitude to give me the support to complete this thesis. I want to thank Wata Cluster, Faculty of Engineering, Kasetsart University for supplying a facility for running Ansys Fluent V.14

Most of all, I would like to express my deepest gratitude to my parents and my friend for their love and continuing encouragement, their sacrifices and their support, without which I could not have produced this thesis.

CONTENTS

	PAGE
ENGLISH ABSTRACT	i
THAI ABSTRACT	ii
ACKNOWLEDGEMENTS	iv
CONTENTS	v
LIST OF TABLES	vii
LIST OF FIGURES	viii
LIST OF SYMBOL	x
CHAPTER	
1 INTRODUCTION	**1**
1.1 Introduction	1
1.2 Objectives	2
1.3 Scopes of Work	2
2 LITERATURE REVIEW AND THEORY	**3**
2.1 Literature review of freeze desalination	3
2.2 Thermodynamics of freezing desalination	4
2.3 Ice slurry production	6
2.4 Physical properties of ice	8
2.5 Hydrocyclone	8
2.5.1 Basics principle of hydrocyclone	8
2.5.2 Force effect in hydrocyclone	9
2.5.3 Design factor of hydrocyclone	12
2.6 Basics of computational fluid dynamics	15
2.7 Multiphase flow modeling	16
2.8 Multiphase flow modeling	17
2.9 Fluid-solid Momentum equation	18
2.10 CFD review of hydrocyclone	22
2.11 Reynold Stress Model	23
3 METHODOLOGY	**24**
3.1 Studying freezing desalination process	24
3.2 Creating geometry by ICEM CFD	26
3.3 Mesh Independence test	30
3.4 Problem formulation	30
3.4.1 Governing equation	31
3.4.2 Multiphase model set up	31
3.4.3 Boundary and the numerical scheme	32
3.5 Analyzing the result	33
4 RESULT AND DISCUSSION	**34**
4.1 Mesh Independence test	34
4.2 Effect of inlet velocity	35
4.3 Effect of solid concentration	41
4.4 Effect of overflow diameter and underflow diameter	45

5 CONCLUSION AND RECOMMENDATION **49**
5.1 Conclusion 49
5.2 Recommendations 50

REFERENCES **51**
APPENDIX 54
A. ASPEN PLUS SIMULATION DATA 54
B. EXPERIMENTAL RESULTS 58
C. FLUENT SETTING 63

CURRICULUM VITAE **76**

LIST OF TABLES

TABLE		PAGE
2.1	Eutectic temperature of salt solution	4
3.1	Parameters for CFD Simulation	26
3.2	Hydrocyclone geometry proportions	27
3.3	Variation of overflow diameter (D_u= 1.51 cm)	28
3.4	Variation of underflow diameter (D_o= 1.16 cm)	28
3.5	Node number for mesh independence test	31
4.1	Relative difference per node	35
A.1	Aspen Plus simulation data	55

LIST OF FIGURES

FIGURE		PAGE
2.1	Eutectic freezing loop (1) Stirred tank freezer (2) High speed propeller (3) Slurry pump (4) Hydrocyclone (5) Ice filter (6) Salt filter (7) overflow brine flow meter (8) underflow brine flow meter (9) precooled heat exchanger	3
2.2	Solubility curve of NaCl in water	5
2.3	Freezing curve of salt solution	5
2.4	Phase diagram of water and brine	6
2.5	Eutectic crystallizer	7
2.6	Particle size distribution: average residence time = 13 min;wt% ice ≈ 4% =375 rpm (a) refrigeration evaporation temperature = -5.43^{O}C (b) refrigeration evaporation temperature = -4.69^{O}C	7
2.7	Shear-Strain diagram for ice at T_c=-15^{O}C	8
2.8	Fluid flow pattern in hydrocyclone	9
2.9	Tangential velocity profile	10
2.10	Vertical velocity profile	11
2.11	Radial velocity profile	12
2.12	Multicyclone arrangement	13
2.13	Effect of split ratio on the separation efficiency	15
2.14	Finite control volume approach	16
2.15	Bingham fluid	19
2.16	Granular flow regimes	19
3.1	Methodology scheme	25
3.2	Overall crystallization process	26
3.3	Hydrocyclone geometry	27
3.4	Hydrocyclone geometry of overflow diameter variation (a) D_o/D_u = 0.55 (b) D_o/D_u = 0.66 (c) D_o/D_u = 0.86 (d) D_o/D_u= 0.94	29
3.5	Hydrocyclone geometries of underflow diameter variation (a) D_o/D_u= 1.16 (b) D_o/D_u= 0.89 (c) D_o/D_u= 0.69 (d) D_o/D_u= 0.63	30
4.1	Mass flow rate at overflow and underflow (kg/s)	35
4.2	Effect of inlet velocities on the separation efficiency Condition: ice fraction = 0.2 Temperature = -30°C, pressure = 5 bar	36
4.3	Effect of inlet velocity on pressure profile below 4.5 cm of vortex finder	37
4.4	Effect of inlet velocity profile of ice (a) axial velocity (b) tangential velocity (c) radial velocity	38
4.5	pressure profile at the middle plane (a) inlet velocity =11 m/s (b) Inlet velocity = 15 m/s (c) Inlet velocity = 20 m/s (d) Inlet velocity = 25 m/s	39
4.6	contour of ice volume fraction at the symmetry plane (a) inlet velocity = 11 m/s (b) inlet velocity = 15 m/s (c) inlet velocity = 20 m/s (d) inlet velocity = 25 m/s	40
4.7	Effect of ice solid fraction on the separation efficiency	42
4.8	Bulk viscosity of ice calculated by Symlal-Orbien	40
4.9	Ice volume fraction at the middle plane of hydrocyclone (a) Inlet ice volume fraction = 0.1 (b) Inlet ice volume fraction = 0.2 (c) Inlet ice volume fraction = 0.3 (d) Inlet ice volume fraction = 0.4	43
4.10	Velocity vector plot of slurry at the middle plane of hydrocyclone (a) ice inlet fraction = 0.1 (b) ice inlet fraction = 0.4	44

4.11	percent split fraction of the overflow stream operating at the inlet velocity of 20 m/s and ice concentration of 20 % v/v	46
4.12	Purity of ice at the overflow opening operating at the inlet velocity of 20m/s and ice concentration of 20 % v/v	46
4.13	Sea water recovery in the overflow stream at the overflow opening operating at the inlet velocity of 20 m/s and ice concentration of 20 % v/v	47
4.14	Ice recovery in the overflow stream at the overflow opening operating at the inlet velocity of 20 m/s and ice concentration of 20 % v/v	47
4.15	Effect of ratio D_o/D_u on the separation efficiency	48
A.1	Aspen Plus Simulation Process	55
A.2	Filtration fraction of ice filter	57
B.1	Effect of pressure drop on the separation efficiency: HY1 nylon powder in water C_i = 0.50 % v/v ,T_c = 17°C	59
B.2	Feed Concentration Effect on the clarification efficiency: Geometry hydrocyclone HY2 brewing yeast in sucrose water 2.3 % (w/w),operating conditions: ΔP= 4.8 bar	59
B.3	Rietema design of hydrocyclone	60
B.4	Effect of ratio on the split fraction of overflow stream	61
B.5	Effect of D_o/D_u ratio on the separation efficiency of hydrocyclone	62
C.1	Thesis Problem Statement	64
C.2	Solidwork of hydrocyclone	65
C.3	ICEM CFD of Hydrocyclone	65
C.4	Reading mesh	66
C.5	Solver type setting	66
C.6	Turbulence model set up	67
C.7	Multiphase model set up	68
C.8	Creating material of sea water	68
C.9	Using Fluent Database	69
C.10	Creating ice material	69
C.11	Defining primary phase	70
C.12	Defining secondary phase	70
C.13	Defining boundary conditions	71
C.14	Defining inlet velocity	72
C.15	Pressure outlet condition	72
C.16	Solution method of CFD	73
C.17	Energy case	73
C.18	Setting adiabatic case	74
C.19	Setting heat transfer coefficient	74
C.20	Temperature contour at the middle plane of hydrocyclone	75

LIST OF SYMBOL

SYMBOL			UNIT
ρ_I	=	Density of ice	kg/m^3
T_k	=	Temperature	K
T_C		Temperature	^{o}C
μ_I	=	The viscosity of ice	kg/(m-s)
D_p	=	Particle diameter	m
ρ_p	=	Density of particle	kg/m^3
ρ_l	=	Density of liquid	kg/m^3
r	=	The radius inside hydrocyclone	m
F_C	=	Centrifugal force	kg m/s^2
v_t	=	Tangential velocity	m/s
R_f	=	Flow split ratio	-
ε	=	Efficiency of hydrocyclone	-
ρ	=	The density	kg/m^3
π	=	The molecular flux of momentum	
g	=	The gravitational acceleration	m/s^2
$\bar{u}$	=	Time smoothed velocity	m/s
u'	=	Instantaneous deviation of velocity	m/s
$\vec{v}$	=	The overall velocity vector	m/s
$\bar{F}$	=	External body force	N
μ_T	=	Turbulent viscosity	kg/(m-s)
k	=	Turbulent kinetic energy	m^2/s^2
α_s	=	Solid volume fraction	-
ρ_s	=	Density of solid phase	kg/m^3
$\vec{u}_s$	=	Velocity of solid phase	m/s
$\dot{m}_{ls}$	=	Unidirectional mass transfer between fluid and solid phase	
N	=	Total number of phases	-
$\vec{F}_{lift,s}$	=	Lift force	N
$\vec{F}_{vm,s}$	=	Virtual mass force	N
K_{sl}	=	the fluid-solid exchange coefficient	
μ_l	=	The viscosity of liquid	kg/(m-s)
τ_s	=	Particulate relaxation time	-
e_{ls}	=	the coefficient of restitution	-
$C_{fr,ls}$	=	The coefficient of friction between the lth and sth solid-phase particles	-
d_l	=	the diameter of the particles of solid l	m
d_{50}	=	Cut size diameter of hydrocyclone	m
P_s	=	Solid pressure	kg/ms^2
λ_s	=	Solid bulk viscosity	kg/(m-s)
μ_s	=	Solid shear viscosity	kg/(m-s)
$g_{0,ss}$	=	the radial distribution	-
S	=	the distance between grains	m
$\emptyset_{ls}$	=	The energy exchange between the lth fluid or solid phase and the sth solid phase	kg/(ms^3)
γ_{θ_s}	=	The collisional dissipation of energy	kg/(ms^3)

k_{θ_s}	=	The diffusion coefficient	m^2/s
$\mu_{s,col}$	=	Collisional viscosity	kg/(m-s)
$\mu_{s,kin}$	=	Kinetic viscosity	kg/(m-s)
$\mu_{s,fr}$	=	Frictional viscosity	kg/(m-s)
$\emptyset$	=	the angle of internal friction	
D_o	=	Overflow diameter	m
D_u	=	Underflow diameter	m
Δ	=	Relative difference between node	-

CHAPTER 1 INTRODUCTION

1.1 Introduction

Nowadays, the increased concern over the problem of fresh water supplies is resulted from the continuously growing of world population together with the industrial and agricultural production. About 99 % of the total surface and ground water above the ground is salty or in the form of ice in the polar region [1], hence the desalination technology is considered as the alternative way for producing the fresh water.

Several processes of the desalination have been proposed and grouped according to their process principles: Distillation, Freezing, and Membrane Technology. The earliest desalination method is the desalination distillation based on the thermal evaporation. The water vapor will be condensed to be the pure water. The membrane desalination applies the synthetic membrane to filter the dissolved salts. Reverse Osmosis (RO) use lower energy than the distillation, but its plant capacity is small compared to the distillation method [2]. The major problem of the desalination distillation occurs during the sea water is heated, the scaling of calcium, magnesium sulfate, and carbonates are formed on the heat transfer surface. The high operating temperature also results in the corrosion of the construction material, such as steel and iron. RO applies high pressure to overcome osmotic pressure, RO is economics only for the brackish water (NaCl =100-10,000 (ppm)). Due to the drawbacks of the reverse osmosis and the distillation, the freezing desalination is considered due to the low operating temperature which helps to minimize the cost and the scaling. The energy of the freeze desalination is low when compared to the distillation, because the heat of freezing is much lower than the heat of evaporation.

The freeze desalination is based on the principle that ice can be nucleated and grown separately and excludes impurities. After the freeze crystallization, the solid-liquid separation systems are applied to separate the ice crystal phase from brine liquid phase. There are many technologies of solid-liquid separation such as the gravity sedimentation equipment, hydrocyclone, and washing stage. The washing stage is used to replace the mother liquid in the solid streams with washing liquids.

The wash column is widely used to separate the ice crystal from the concentrated brine, but the limitation of wash column is that the wash column requires an average particle size of over 300 μm to function and the ice fraction in the wash column must be very high to form sufficiently porous bed. Consequently, centrifugal separation is considered. Hydrocyclone is the centrifugal separation equipment which is compact, simple devices and has a low pressure drop. It is interesting to use hydrocyclone to separate the ice slurry from the concentrated brine.

The goal of this work is to develop the CFD model of hydrocyclone for desalination process based on the eutectic freezing crystallization. The investigation of this research was, therefore, two folds: firstly, to obtain the optimum operating condition of hydrocyclone: inlet velocity and the inlet ice fraction, and secondly, to investigate the effect of overflow and underflow diameter on the flow discharge pattern of ice-sea water slurry inside hydrocyclone.

1.2 Objective

1. To develop the computational fluid dynamics model of suitable hydrocyclone for freezing desalination process
2. To study the effect of inlet velocity and pressure drop on the separation efficiency of hydrocyclone

1.3 Scope of work

1. The design and simulation of hydrocyclone will be performed by ANSYS Fluent program version 14
2. The design specification of the hydrocyclone for concentrating ice slurry from brine must provide the separation efficiency at least 80%

CHAPTER 2 LITERATURE REVIEW AND THEORY

2.1 Literature review of freeze desalination

Sea water is a salt solution which consists of inorganic salt and organic salt. The freezing desalination process is used to purify the sea water based on the principle that the ice crystal can form and exclude the impurities. The remaining liquid is the concentrated brine. After the crystallization process, the ice and brine slurry will be sent to the separation equipment in order to separate the ice from the brine. The ice will be melted to be the pure water. The freezing desalination is not commercially available now, but there are still a few researches of the freezing desalination. The previous work investigated for the freezing desalination is described below.

Nelson [3] investigated the order of formation of salts during freeze concentration of sea water. Approximately 88% of the water present in the initial sample of brine was transformed into ice before the first crystallizer. The first salt formed. Sodium sulfate decahydrate, began to separate at -8.2°C. When the temperature of the system reached -22.9°C, sodium chloride dihydrate precipitated in large quantity. Below -36°C, potassium chloride and magnesium chloride decahydrate precipitated. The calcium chloride hexahydrate began to form at -54°C.

Stepakoff [4] studied the continuous eutectic freezing process based on the technlogy developed for direct contact freeze crystalliztaion. The feed was frozen continuously by direct contact until the eutectic temperature reached. The salt solution used in the eutectic freezing experiment was potassium chloride, because it did not form a hydrate when it crystallized at low temperature. It was easier to separate and collect the ice crystal at low temperature. The hydrocyclone was applied to separate the lighter solid or ice crystal from the salt crystal. Ice and salt occured in two distinct layers. The eutectic crystallization process is shown in Figure 2.1

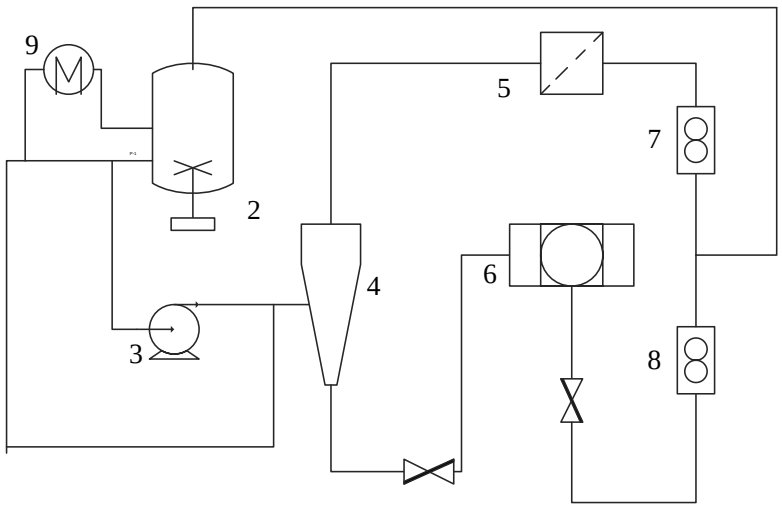

Figure 2.1 Eutectic freezing loop (1) Stirred tank freezer (2) High speed propeller (3) Slurry pump (4) Hydrocyclone (5) Ice filter (6) Salt filter (7) overflow brine flow meter (8) underflow brine flow meter (9) precooled heat exchanger [4]

The product of eutectic crystallizer consisted of two types of solids: the lighter ice crystal and the salt crystal entrained in Freon liquid. After exiting the eutectic crystallizer, they were pumped to hydrocyclone. The overflow stream and underflow stream were filtered through a fine mesh polypropylene screen in two plexiglass columns. The ice bed was collected in the overflow filter. It was melted by adding Freon 113. The Freon was able to wash residual salt crystal. The residual salt was recovered by additional filtration. The relative weights of salt and ice collected in the filters defined the separation efficiency of the hydrocyclone, about 85%. The separation efficiency could be improved by staging a second hydrocyclone after the overflow filter. The overall system gave the separation efficiency of 95%.

The economics of the freezing desalination depends on the freezing temperature. Therefore, the eutectic temperature of natural sea water must be investigated, as the sea water did not contain only the sodium chloride (NaCl), but also other salts such as, Na^{+}, K^{+}, Mg^{++},Cl^{-}, SO_4^{-}, and HCO_3^{-} . Barduhn [5] carried out the experiment for determining the temperature required for eutectic freezing of natural sea water. Their experimental result is shown in Table 2.1.

Table 2.1 Eutectic temperature of salt solution [5]

Eutectic solution composition,wt%	Eutectic temperature °C
23.3%NaCl	-21.2
20.2%NaCl+5.8%KCl	-22.9
22.8%NaCl+0.3%Na_2SO_4	-21.7
30.22%$CaCl_2$	-49.8
21.0%MgCl2	-33.6
26% $CaCl_2$ + 5% $MgCl_2$	-55
30% $CaCl_2$+ 1.6% NaCl	-52
22.7%$MgCl_2$+ 1.56%NaCl	-35

Table 2.1 shows the temperature of eutectic salt solution in which NaCl is the major liquid composition. The second salt e.g. the sulfates and bicarbonates of Mg and Ca lower the eutectic temperature by less than 2°C. Two salts: $CaCl_2$ and $MgCl_2$ combined with NaCl lower the eutectic temperature to approximately -35 and -55°C.

2.2 Thermodynamics of freezing desalination

The thermodynamic system of freeze desalination is described by the eutectic phase diagram. The eutectic phase diagram consists of three lines: eutectic curve, solubility curve, and the freezing curve. Figures 2.2 and 2.3 show the freezing curve and solubility curve respectively.

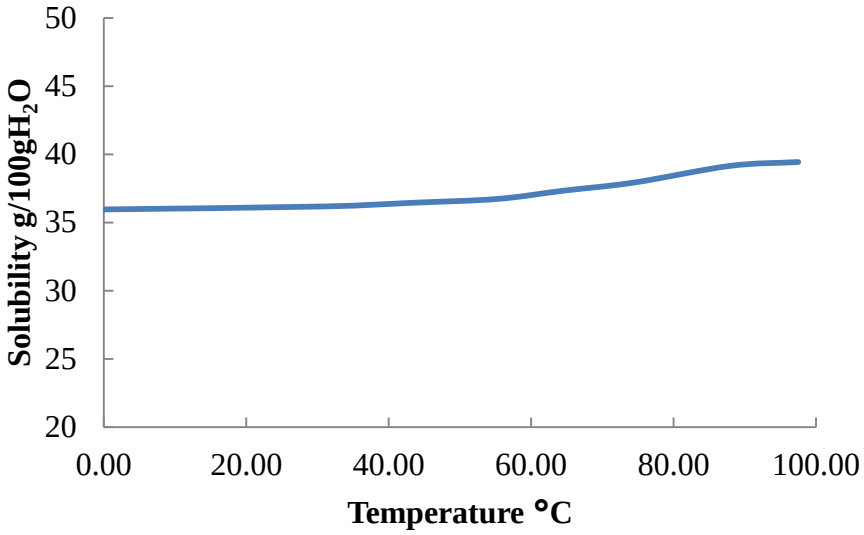

Figure 2.2 Solubility curve of NaCl in water [6]

According to Figure 2.2, the solubility of NaCl increases with the rising temperature. It can be interpreted from this figure while the salt precipitation occurs. For example, if 39 g of NaCl initially dissolves in 100 g of water at 100°C, it can be dissolved in the water very well due to the maximum solubility of 40 g at 100 °C. Then the solution is cooled to 20 °C at which solubility is approximately 35 g/100 gH_2O, and some of NaCl will no longer dissolve in water. Then salt crystal of NaCl will precipitate [7]. In contrast to solubility, the freezing temperature decreases with the increase of salt concentration. As shown in Figure 2.3, the higher concentration of NaCl is, the lower freezing point will be.

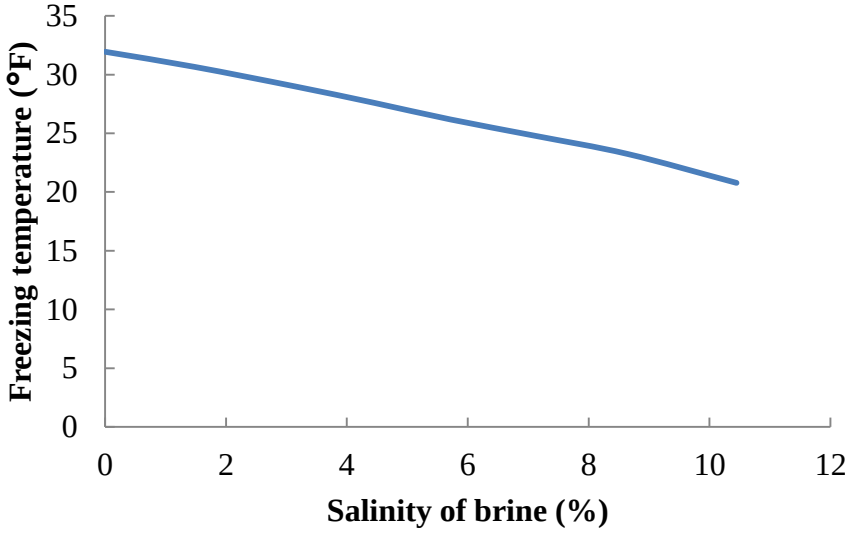

Figure 2.3 Freezing curve of salt solution [8]

Both the freezing curve and the solubility curve can be combined in eutectic phase diagram as shown in Figure 2.4

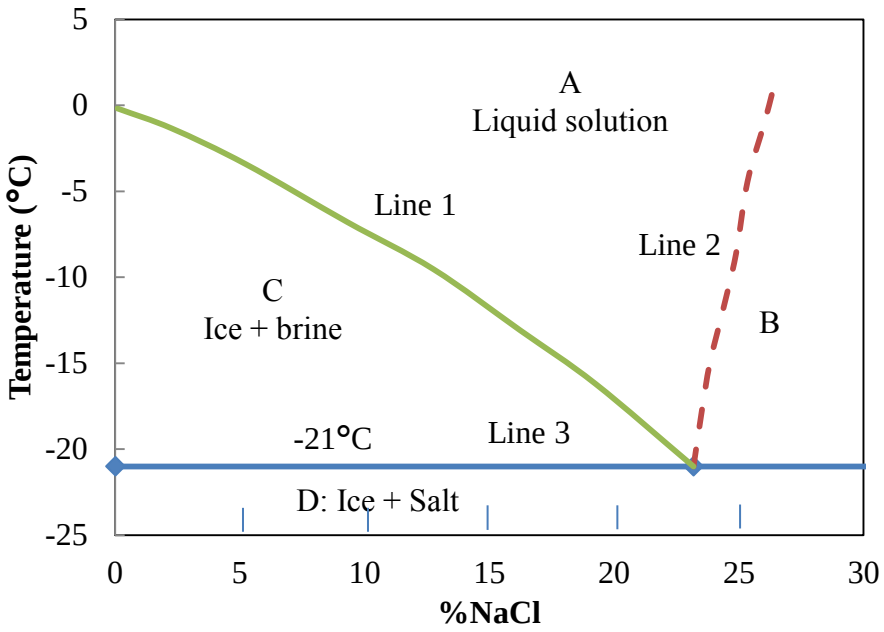

Figure 2.4 Phase diagram of water and brine [9]

Figure 2.4 consists of three lines: solubility line (line 1), freezing line (line 2), and eutectic line (line 3). These three lines separate the eutectic phase diagram into five regions as following:

Region A: The solution temperature is above the freezing curve and the solubility curve. The mixture is only simple salt solution. The natural sea water exists in this phase.
Region B: The salt concentration of sea water is higher than the maximum solubility limit, and the salt crystal will form.
Region C: The salt solution is cooled below the freezing curve, and then the ice forms exclude the impurity.
Region D: The solution temperature is lower than the eutectic temperature. All ice and salt become crystal.

2.3 Ice slurry production

Ice slurry is the water solution in which small ice crystals are present. The ice crystal form due to the nucleation process which can be divided into two stages: the primary nucleation and secondary nucleation. The primary nucleation is the direct formation of ice crystal from the solution. The secondary nucleation is the formation of new ice crystal from ice crystals already present in the solution. The growth rate of ice crystallization is dependent on the conditions in the crystallizer such as the driving force and the residence times. The ice created by slurry can be various shape e.g. large ice particles or even plate ice. Ice crystal is not ideal solid. It can break and agglomerate. Therefore, the properties of ice slurry does not depend only the crystallization process, but also transport and storage. Margolis [10] studied the performance of continuous well stirred ice crystallizer producing ice with direct contact refrigeration. The effect of residence time, agitation rate, and undercooling temperature on the particle size were investigated by manipulating the experiment of crystallization of ice from sodium

chloride solution with the direct contact of isobutylene sparged at the bottom of the crystallizer.

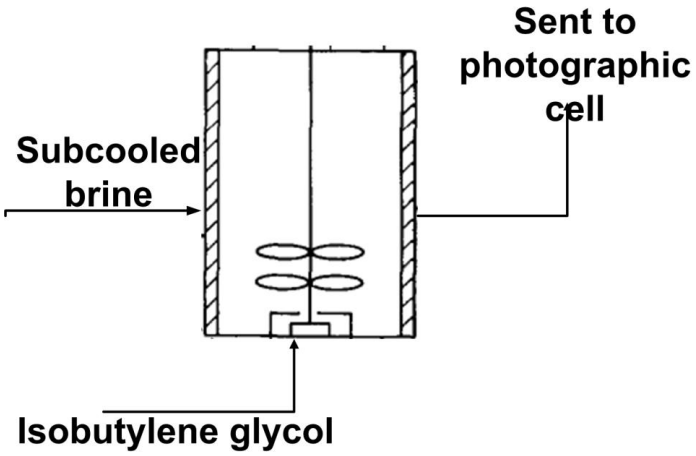

Figure 2.5 Eutectic crystallizer [11]

The effluent of crystallizer was examined photographically to determine the concentration and the characteristics of the ice particles formed.

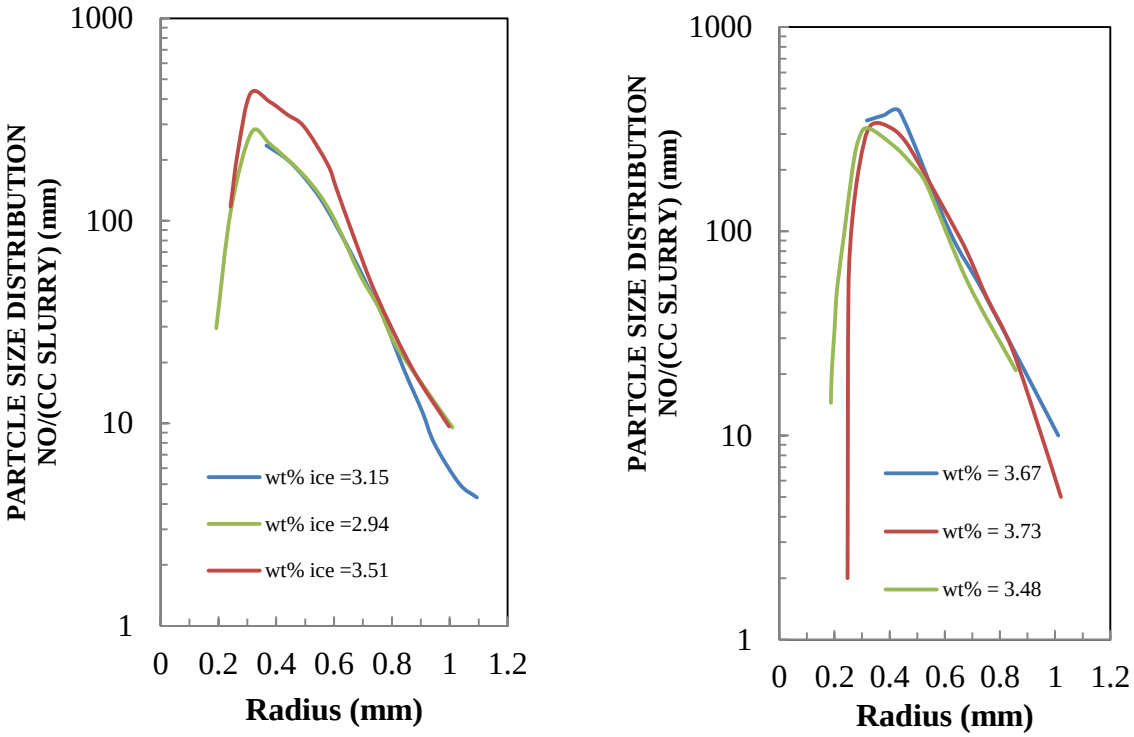

Figure 2.6 Particle size distribution:average residence time = 13 min;wt% ice≈4% =375 rpm (a) refrigeration evaporation temperature = -5.43^{O}C (b) refrigeration evaporation temperature = -4.69^{O}C [11]

Figure 2.6 shows that the minimum particle diameter and the maximum particle diameter retrieved from the experiment done at -5°C were 200 µm and 1200 µm, respectively.

2.4 Physical properties of ice

The density of ice is lower than the density of water in the liquid phase. The density of ice, ρ_I, at the temperature, T_k (in K) can be expresses as :

$$\rho_I = 917 - 0.13(T_k - 273)\ (\frac{kg}{m^3}) \quad \textbf{(2.1)}$$

The viscosity is the resistance of the body at a given moment of its deformation per unit surface of the shear layer. The ice viscosity is not a constant property but it depends on the magnitude and the duration of the stress. It is also dependent on the orientation of the crystal and temperature. Previously, the ice crystal is believed that it obeys the newton's law viscosity. Glen [12] proved that the ice crystal did not satisfy the newton's law of viscosity as shown in Figure 2.7.

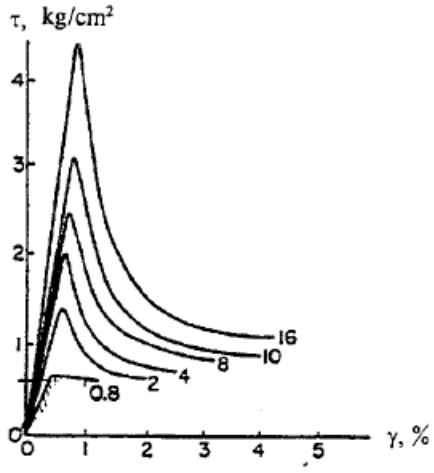

Figure 2.7 Shear-Strain diagram for ice at T_c=-15^{O}C [12]

Figure 2.7 shows that ice behaves like bingham fluid. The viscosity of ice depends on both temperature and the tangential stress according to

$$\mu_I = \frac{1 + |T_k|}{KS^{n-1}} \quad \textbf{(2.2)}$$

Where

μ_I= the viscosity of ice
S =tangential stress
K, n =empirical constant

2.5 Hydrocyclone

2.5.1 Basics principle of hydrocyclone

Hydrocyclone is the equipment which separates solid and liquid or light liquid and heavy liquid by centrifugal separation. The solid-liquid slurry is injected tangentially through the inlet opening in the upper part of the cylindrical section. As a result of the tangential entry, the fluid in hydrocyclone has the spiraling motion which generates the centrifugal force. The centrifugal force throws the high specific density material against the wall, and then they are dragged to the underflow**.** The light material which can not enter the underflow will move spiral inwards and leave via the overflow. The fluid flow pattern inside hydrocyclone is shown in Figure 2.8.

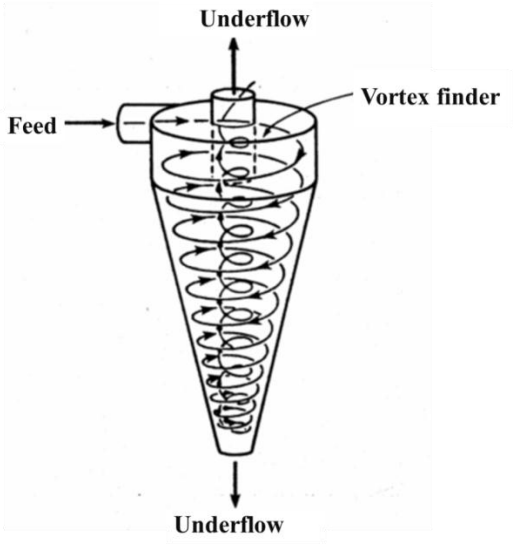

Figure 2.8 Fluid flow pattern in hydrocyclone [13]

2.5.2 Standard forces in hydrocyclone

During the separation, the particles at any point within the flow in a hydrocyclone are subjected to three forces: centrifugal force, drag force, and gravity force. The centrifugal force will throw the light density material against the wall, while the drag force is the resistance force to the particle motion.

1. **Centrifugal force**

The centrifugal force throws the large particle to the wall and removes the large particle to underflow. The centrifugal force depends on the inlet velocity. Higher velocity results in higher centrifugal force. The relationship of the velocity and the centrifugal force is shown in

$$F_C = \frac{\pi D_p^3}{6}\left(\frac{\rho_{p-}\rho_l}{r}\right) v_t^2 \quad \textbf{(2.3)}$$

Where

F_C= Centrifugal force

D_p = Diameter of particle

ρ_p= Density of particle

ρ_l= Density of liquid

2. **Drag force**

The drag force represents the resistance to flow. It depends on the size, the shape of the particle, and the density of particle. Equation (2.4) shows that the drag force for coarse particle is greater than the drag force for fine particle.

$$F_d = 3\pi D_p \mu_l v_t \quad \textbf{(2.4)}$$

Both the centrifugal force and the drag force are related to the flow pattern of fluid as following:

- If the centrifugal force exceeds the drag force, the particle moves radially outwards
- If the drag force is greater than the centrifugal force, the particle is carried inwards.

The velocity of fluid inside hydrocyclone can be resolved into three components: the vertical velocity, the radial velocity, and the tangential velocity

1. Tangential velocity

The tangential velocity is created by the tangential feed entry into hydrocyclone. The tangential velocity depends on the radius. The relation between the tangential velocity and the radius must be described into two regions: below the rim of the vortex finder and above the rim of vortex finder according to Figure 2.9. At below the rim of the vortex finder, the tangential velocity, v_t, increases considerably with decreasing radius as shown in Equation (2.5)

$$v_t r^n = constant \qquad \text{(Where } n \text{ is normally } 0.6 \leq n \leq 0.9\text{)} \qquad \textbf{(2.5)}$$

At level above the rim of the vortex finder, the tangential velocity decreases with the increase in radius. The maximum tangential velocity is near the radius of the vortex finder Tangential velocity is not dependent on the vertical position.

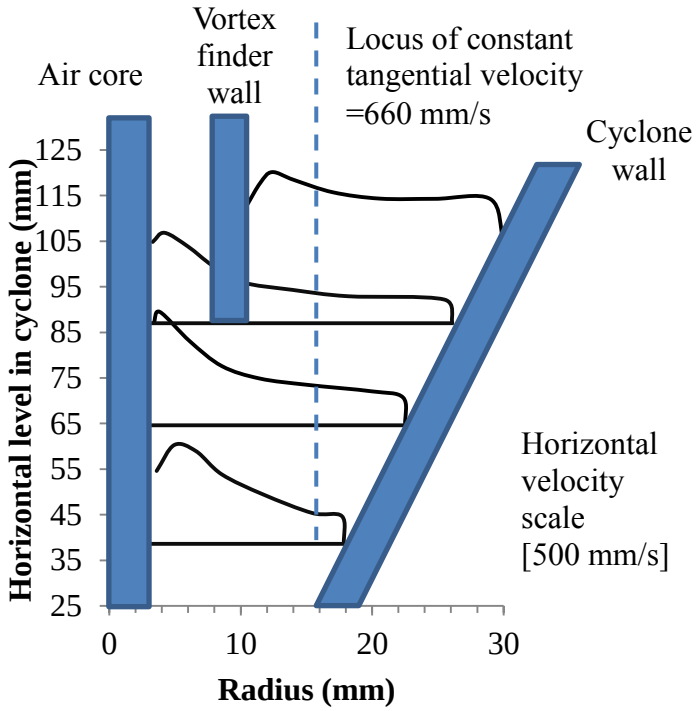

Figure 2.9 Tangential velocity profile [14]

2. Vertical velocity

There are both the upward vertical velocity at the region below the vortex finder and downward velocity at the region above the vortex finder as shown in Figure 2.10. Above the rim of vortex finder, the strong downward flow occurs when the centrifugal force is higher than the drag force. The centrifugal force will throw the particle to the wall, and then they are dragged into the underflow. Consequently, the largest downward vertical velocity occurs near the hydrocyclone wall. The downward flow is essential for

cyclone operation since it enables the particles to be separated into the underflow orifice. Sometimes, the strong downward vertical might be observed near the vortex finder.

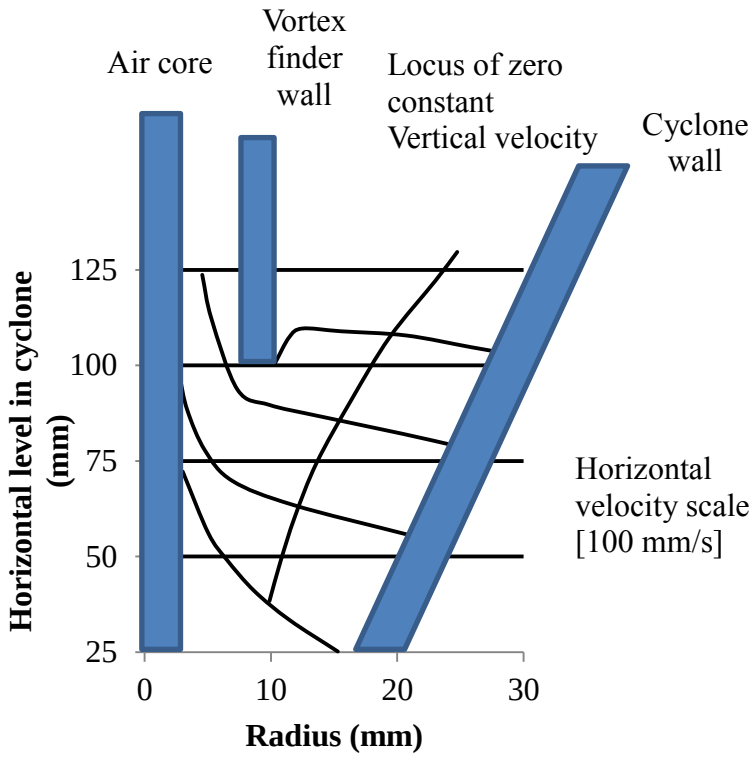

Figure 2.10 Vertical velocity profile [14]

At the region below the vortex finder, the axial velocities become upward. The region of the upward velocity and the downward velocity is separated by the locus of zero vertical velocity (LZVV). Above LZVV line, particle will move to the overflow.

3. Radial velocity

The radial velocity components are normally much smaller than the other two velocity components. The radial velocity occurs when the particle which cannot be separated into the underflow, the particle must spiral within spiral. The radial velocity increases with the increasing of the radius. Near the flat top of the cyclone, the radial velocity is inward directed to the root of the vortex finder, and this phenomenon can cause the short circuit flow.

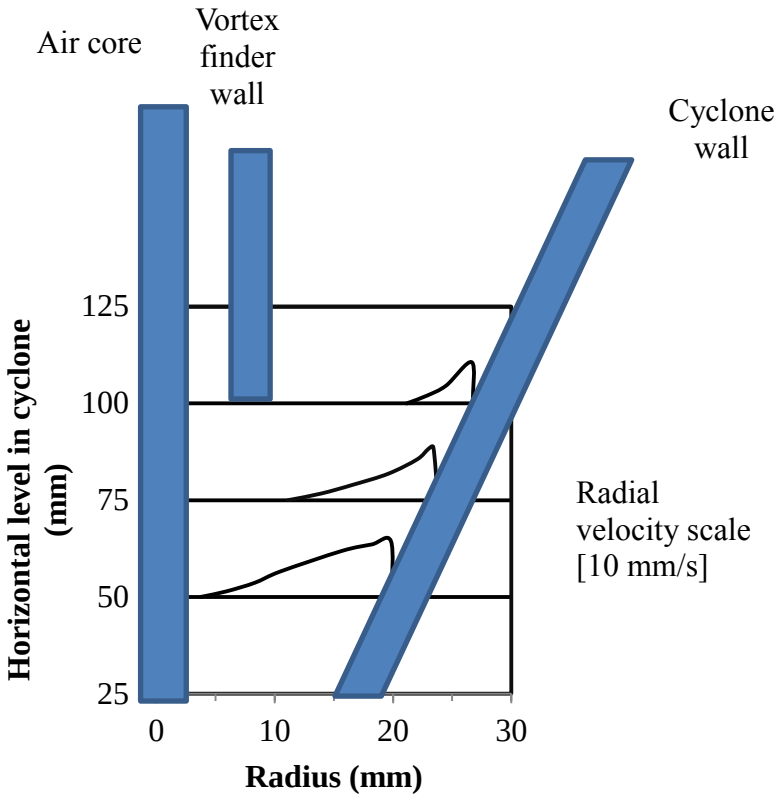

Figure 2.11 Radial velocity profile [15]

2.5.3Design factor of hydrocyclone

1. **Hydrocyclone diameter**

The diameter of the hydrocyclone is the most important variable of hydrocyclone, as it affects the cut size and capacity. Increasing hydrocyclone diameter results in decreasing the centrifugal force and poorer separation efficiency.

2. **Multicyclone arrangement**

Hydrocyclone arrangement depends on the application. Figure 2.12 shows four basic types of hydrocyclone.

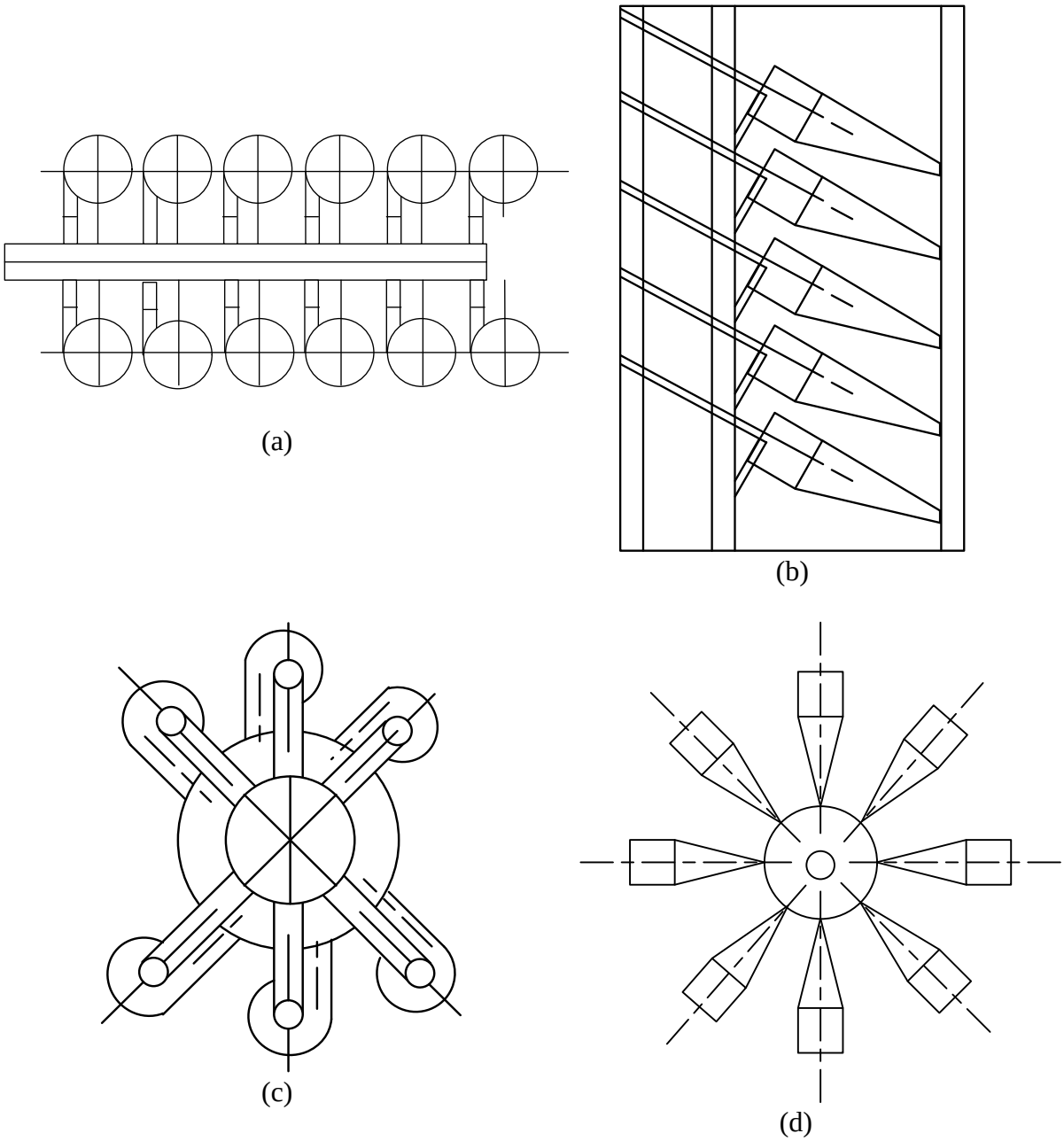

Figure 2.12 Multicyclone arrangement [14]

Figures 2.12 (a) and (b) are linear arrangement, while (c) and (d) are circular arrangement. The circular arrangement can distribute the feed better than linear arrangement, as each unit has an identical length of piping between it. The vertical-circular arrangement is highly suitable for use in the compact multiple cyclone units because it is stackable.

3. Vortex finder Diameter

The diameter of the vortex finder should be larger than the locus of maximum tangential velocity for preventing the short circuit flow, which particle leaves the hydrocyclone without separation. Additionally, the fine particles leave via the vortex finder due to the radial velocity. If the vortex finder diameter decreases, less amount of large particle is able to leave via the vortex finder. Finally, the cut size decreases. The relationship between cut size and the vortex finder diameter (D_o) is described by:

$$d_{50} \propto D_o^{1.21} \quad \textbf{(2.6)}$$

4. Feed inlet diameter

The feed inlet diameter affects the inlet velocity of the feed flow rate. Decreasing the feed inlet diameter will increase the inlet velocity, and the centrifugal force rise. Then, the separation efficiency can be improved.

5. Underflow diameter

The underflow opening of hydrocyclone must be large to discharge the coarse particles separated into the underflow. The cone angle of the overflow opening must be large enough to enable the air enter hydrocyclone. If the underflow opening is too small, the condition known as "roping the thick pulp stream of the same diameter is formed. Too large underflow opening can lead to the excessive dilute concentration of underflow outlet stream, and the unclassified particles leave through the overflow outlet.

2.5.4 Performance evaluation of hydrocyclone

1. Flow ratio (R_f)

The split ratio of the feed stream is described by

$$R_f = \frac{Volume\ flow\ rate\ at\ underflow}{Volume\ flow\ rate\ at\ inlet} \quad \textbf{(2.7)}$$

Split ratio has a significant effect on the clarification efficiency. Figure 2.13 shows the clarification efficiency increases with an increase in split ratio and reaches a maximum at a critical value of the split ratio (R_{fc}). With further increase in split ratio, the clarification efficiency will fall dramatically.

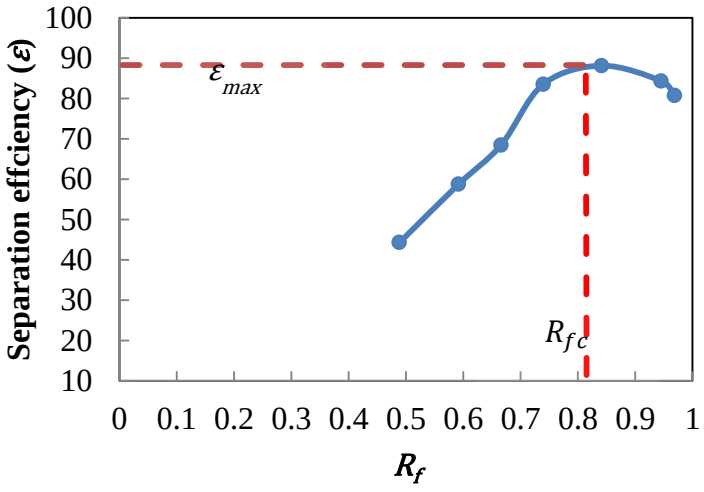

Figure 2.13 Effect of split ratio on the separation efficiency [13]

With the low split ratio, it can result in low recirculation. The low recirculation can cause the re-entrainment of settled particle near the overflow. The increase in R_f causes an increase in axial residence time and fall in tangential velocity.

2. **Efficiency** (ε)

The efficiency of hydrocyclone is defined similarly to the deoiling hydrocyclone which is shown in

$$\varepsilon = 1 - \frac{C_{light\ density,underflow}}{C_{light\ density,inlet}} \quad \textbf{(2.8)}$$

3. **Pressure drop (ΔP)**

The pressure drop is essential for the design of pumping system for a specific capacity. Overall pressure drop of hydrocyclone can be calculated as

$$\Delta P = P_{inlet} - P_{overflow} \quad \textbf{(2.9)}$$

The pressure at the overflow is set to zero, because it is assumed that the product is discharged to the atmospheric pressure. The pressure drop is equal to the inlet pressure. The increase in the pressure drop is manipulated by improving the feed flow rates. The increase in the feed flow rate improves the efficiency because the centrifugal force increases.

2.6 Basics of computational fluid dynamics

The physical aspect of any fluid flow analysis is based on three fundamental principles: (1) mass is conserved (2) F=ma (Newton's second law) (3) energy is conserved. The fundamental principle is expressed in term of the mathematical equation which is usually partial differentiation. Computational fluid dynamics is the calculation method which replaces the governing partial differential equation with the number in space and time to obtain the complete numerical description of fluid flow field. The general flow field of fluid is represented by the streamline in Figure 2.14

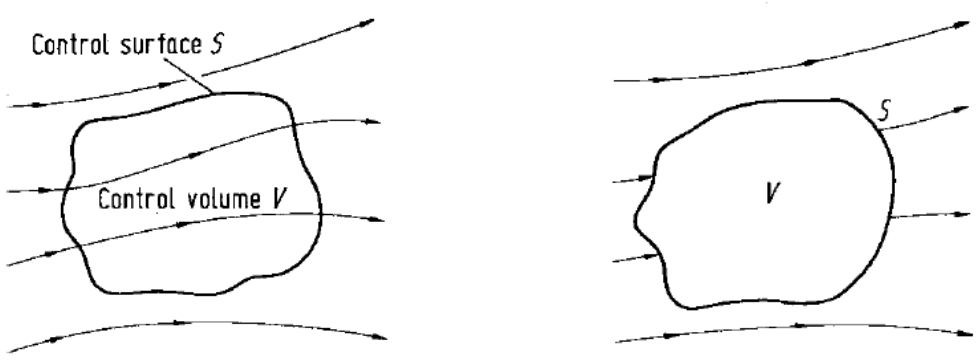

(a) (b)

Figure 2.14 Finite control volume approach [16]

The fluid flow field can be represented by the streamline. In the region which fluid flow, it can be represented as the finite control volume. The control volume may be fixed in space with the fluid is moving through it. The three fundamental principles as mentioned above are applied to calculate the fluid inside control volume. The detail of three fundamental principles is explained below:

1. **Mass conservation equation:**

$$\frac{\partial}{\partial t}(\rho) + \nabla \cdot (\rho \vec{v}) = S_m \quad \textbf{(2.10)}$$

$\frac{\partial}{\partial t}(\rho)$ represents the accumulation of mass per a control volume element. S_m is the source of mass added to the continuous phase from the dispersed second phase (e.g. due to vaporization of liquid droplets). It can be a rate of production or consumption due to chemical reactions or net exchange of species with other phases.

2. **Momentum conservation**

The momentum conservation equation is solved to give the velocity profile and the pressure profile.

$$\frac{\partial}{\partial t}(\rho \vec{v}) + \nabla \cdot (\rho \vec{v} \vec{v}) = -\nabla p + \nabla \cdot (\bar{\bar{\tau}}) + \rho \bar{g} + \vec{F} \quad \textbf{(2.11)}$$

Where p is the static pressure, $\bar{\bar{\tau}}$ is the stress tensor (described below). $\frac{\partial}{\partial t}(\rho \vec{v})$ is the rate of increase in momentum per unit volume. $\nabla \cdot (\rho \vec{v} \vec{v})$ is the change in momentum per unit volume, caused by convection. $\rho \bar{g}$ and $\vec{F}$ represent the gravitational force per unit volume and other external force (e.g., that arise from interaction with dispersed phase).

2.7 Multiphase flow modeling

There are two approaches for multiphase flow modeling: The Eulerian-Eulerian approach and Euler-Lagrangian.

1. **Euler-Lagrangian**

The fluid phase is treated as a continuum by solving the navier stokes equation, while the dispersed phase is solved by tracking a large number of particles, bubbles, or droplets. The dispersed phase can exchange momentum, mass, and energy with the fluid phase. This method is applicable when the dispersed phase occupies a low volume fraction, although the mass loading of the dispersed phase is high. This method is appropriate for the modeling of spray dryers, coal and liquid fuel combustion.

2. **Eulerian-Eulerian approach**

Two phases are treated as a continuum, as the volume of each phase can not be occupied by other phases. The volume fraction is assumed to be continuous functions of space and time. There are three different Eulerian-Eulerian multiphase models: The volume of fluid (VOF) model, the mixture, and the Eulerian model

- **2.1. Volume Of Fluid model (VOF):** designed for two or more immiscible fluids where the position of the interface between the fluids is of interest as VOF model is a surface-tracking technique. It is mostly applied for liquid–gas application e.g. the motion of the large bubble in water.
- **2.2. Mixture model:** used for multiphase flows where the phases moves at different velocities. The mixture model can model any number of secondary phases. The typical application of the mixture model is the sedimentation and cyclone separator. The mixture model is a good substitute for full Eulerian multiphase model case, as the full multiphase model might not be feasible when there is a wide distribution and the interphase drag law is unknown. The granular phase can be defined in this method, so the mixture model is applicable for the solid-liquid application
- **2.3. Full-Eulerian model:** used to model the multiphase system with any combination of liquid gases, or solids. The difference between the mixture

model and full eulerian model is that the number of secondary phases for mixture model is limited only by memory requirement.

2.8 Turbulence model classification

The navier stoke equation shown in the previous section is navier stoke equation which does not apply any additional modeling. It is suitable for solving laminar flow rather than turbulent flow. The laminar flow characteristic is that the fluid particle moves in the definite path, and no mixing between the layers. In actual, the flow is irregular, rotational, and highly disordered. The velocity components in the navier stoke equation can be decomposed into two components: time smoothed velocity ($\bar{u}_i$) and the instantaneous deviation u_i'

$$u = \bar{u}_i + u_i' \quad \textbf{(2.12)}$$

Likewise, for pressure and other scalar quantities

$$\phi = \bar{\phi} + \phi' \quad \textbf{(2.13)}$$

Where ϕ denotes a scalar such as pressure, energy, or species concentration.

Therefore, the turbulence model is applied to calculate the fluctuating velocity component. The turbulence model available in Fluent can be classified into two types:

1. **Computational fluctuated part**

The instantaneous deviation of velocity is computed. The turbulence simulation does not require any additional modeling beyond the Navier-stokes equation, for example, Direct Numerical Simulation (DNS) and Large Eddy Simulation (LES). DNS method can resolve all scales of the motion, and LES attempt to simulate the large scale motion rather than the small scale motion.

2. **Average fluctuated part**

Reynolds averaging approach does not solve all spatial; scales (time and space). The instantaneous deviation of the variable is averaged over a interval time.

$$\emptyset = \bar{\emptyset} + \emptyset' \quad \textbf{(2.14)}$$

$$\emptyset = \frac{1}{\Delta t}\int_t^{t+\Delta t} \emptyset dt \quad \textbf{(2.15)}$$

Reynolds averaging component obeys the following property:

$$\bar{\emptyset}' = 0 \quad \textbf{(2.16)}$$

Substituting expressions of this form for the flow variables into the instantaneous continuity and momentum equations and taking a time (or ensemble) average (and dropping the overbar on the mean velocity, $\bar{u}$) yield the ensemble-averaged momentum equations. They can be written in Cartesian tensor form as:

$$\frac{\partial}{\partial t}(\rho) + \nabla \cdot (\rho u_i) = 0 \quad \textbf{(2.17)}$$

$$\frac{\partial}{\partial t}(\rho u_i) + \nabla \cdot \left(\rho u_i u_j\right) = -\nabla p - \rho\overline{u_i' u_j'} + \rho g + \bar{F} \quad \textbf{(2.18)}$$

Equations (2.17) and (2.18) are called Reynolds-averaged Navier stokes (RANS) equations. They have the same general form as the instantaneous Navier-Stokes equations, with the velocities and other solution variables now representing ensemble-averaged (or time-averaged) values. This method requires less computing resource than Large Eddy simulation (LES) and Direct Numerical Simulation (DNS) approaches. The additional term for RANs is the Reynold stress $\rho\overline{u_i' u_j'}$ which must be modeled in order to close Equation (2.18)

2.9 Fluid-solid Momentum equation

Liquid-particle flows represent one class of two phase flows. When the solid particle is present in the liquid, it will affect the viscosity of liquid suspension. Below a solid concentration of about 4% by weight, most sludges exhibit a Newtonian behavior, which is a linear relationship between shear stress and shear rate where the constant of proportionality, μ_l, is the viscosity of fluid for example water. Above this concentration, most sludges behave like the bingham fluid. The curve of bingham fluid compared with the Newtonian fluid is shown in Figure 2.15.

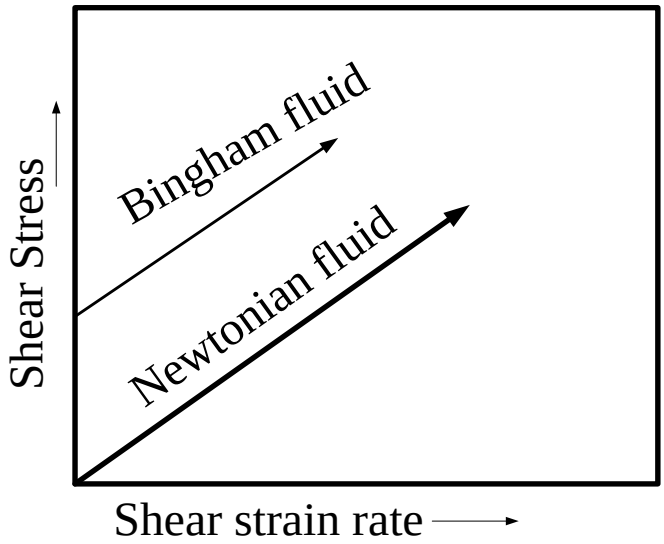

Figure 2.15 Bingham fluid [17]

Figure 2.15 shows that i) minimum shear stress is required to be exerted in order to initiate deformation of the fluid ii) The slope of curve denotes to the apparent viscosity which is not constant , but it decreases gradually with increasing shear stress. The non-constant apparent viscosity indicates the structural modification of the solid-liquid suspension when the shear stress increases. When the slope of shear stress and the shear strain or apparent viscosity is constant, it indicates that the particle aggregate breaks down. To treat this phenomenon, the Eulerian-Granular model, the extension of the Eulerian-Eulerian model, is applied to calculate the flow field of liquid-solid mixture. The main characteristic of granular flow is that the flow is not possible below a critical shear stress, and complex shear rate dependence when flowing as mentioned above.

According to Eulerian-Granular model, granular flow behaves similarly to classical the visco-plastic fluids like Bingham fluids. There are three regimes of the granular flow shown in Figure 2.16

<u>Elastic Regime</u>
- Stagnant
- Stress is strain independent
- Elasticity

<u>Plastic regime</u>
- Slow flow
- Strain rate dependent
- Soli mechanics

<u>Viscous regime</u>
- Rapid flow
- Strain rate dependent
- Kinetic theory

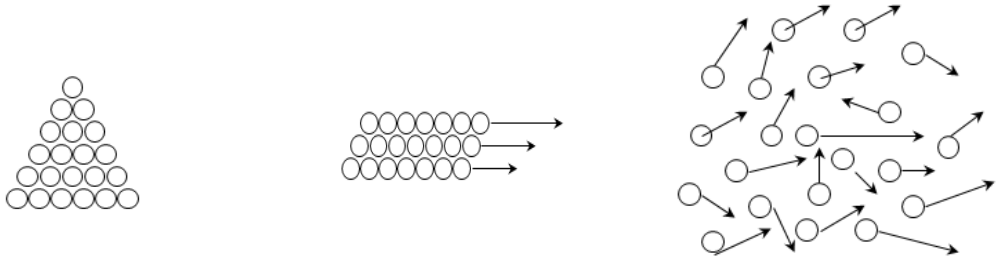

Figure 2.16 Granular flow regimes [17]

The kinetic theory of granular flow is based on similarities between the flow of a granular material, a population of particles with or without the interstitial gas. This treatment uses classical result from the kinetic theory of gas. For the granular flow, it is necessary to introduce additional term for governing equation, which considers particle-particle interaction. The analogy between the solid and the gas is that the particles are allowed to travel freely, and they are allowed to collide with neighboring particles. The kinetic theory of gases is applied to granular flow, but effect of solid phase must be considered as following:

- The number of solid particles is much less than the molecules
- The collision of gas molecule is nearly elastic. Solid particle exhibit a loss of momentum on collision where the inelasticity of the collision must be modeled through a restitution coefficient

The continuity equation for the granular phase is described by:

$$\left(\frac{\partial}{\partial t}(\alpha_s\rho_s) + \nabla\cdot(\alpha_s\rho_s\vec{v}_s)\right) = \sum_{s=1}^{n}(\dot{m}_{ls} - \dot{m}_{sl}) \qquad \textbf{(2.19)}$$

Where α_s is the solid volume fraction. Ansys Fluent uses a multi-fluid granular model to describe the flow behavior of fluid-solid mixture. The conservation of momentum for the s[th]solid phase is shown in

$$\begin{aligned}\frac{\partial}{\partial t}(\alpha_s\rho_s\vec{v}_s) + \nabla\cdot(\alpha_s\rho_s\vec{v}_s\vec{v}_s) &\\ = -\alpha_s\nabla p - \nabla P_s + \nabla\cdot\bar{\bar{\tau}}_s + \alpha_s\rho_s\vec{g} &\\ + \sum_{l=1}^{N}(K_{sl}(\overrightarrow{v_l} - \overrightarrow{v_s}) + \dot{m}_{ls}\vec{v}_{ls} - \dot{m}_{sl}\vec{v}_{sl}) &\\ + \left(\overrightarrow{F_s} + \vec{F}_{lift,s} + \vec{F}_{vm,s}\right)\end{aligned} \qquad \textbf{(2.20)}$$

Where P_s is the s[th]solid pressure, K_{sl}= K_{ls} is the momentum exchange coefficient between fluid and solid phase *l* and solid phase s, N is the total number of phases.

1. **Fluid solid interphase exchange coefficient**

The fluid-solid exchange coefficient K_{sl} can be written in the general form:

$$K_{sl} = \frac{\alpha_s \rho_s f}{\tau_s} \tag{2.21}$$

Where drag function (f) is defined differently for the different exchange-coefficient models, and τ_s, the particulate relaxation time, is defined as

$$\tau_s = \frac{\rho_s d_s^2}{18\mu_l} \tag{2.22}$$

2. **Solid-solid exchange coefficient**

$$K_{ls} = \frac{3(1 + e_{ls})\left(\frac{\pi}{2} + C_{fr,ls}\frac{\pi^2}{8}\right)\alpha_s \rho_s \alpha_l \rho_l (d_l + d_s)^2 g_{0,ls}}{2\pi(\rho_l d_l^3 + \rho_s d_s^3)} |\vec{v}_l - \vec{v}_s| \tag{2.23}$$

Where

e_{ls} = The coefficient of restitution

$C_{fr,ls}$ = The coefficient of friction between the l^{th} and s^{th} solid –phase particles $(C_{fr,ls} = 0)$

d_l = The diameter of the particles of solid *l*

$g_{0,ls}$ = The radial distribution coefficient

3. **Solid stress tensor $(\nabla \cdot \bar{\bar{\tau}}_s)$**

Solid stress occurs due to inter-particle collisions. It can be modeled using a collisional solids stress tensor in the solid phase momentum equation only. The solid stress tensor accounts for the interaction within solid phase

$$\left(\nabla \cdot \bar{\bar{\tau}}_s\right) = -P_s \bar{I} + 2\,\alpha_s \mu_s \bar{S} + \alpha_s \left(\lambda_s - \frac{2}{3}\mu_s\right)\nabla \cdot \vec{u}_s\, \bar{I} \tag{2.24}$$

$$\bar{S} = \frac{1}{2}(\nabla \vec{u}_s + (\nabla \vec{u}_s)^T) \tag{2.25}$$

Where

P_s= solids pressure

λ_s= solid bulk viscosity

μ_s= Solid shear viscosity

4. **Solid pressure (P_s)**

Solid pressure is the pressure exerted on the containing wall due to the presence on the particle. The solid pressure is composed of a kinetic term and the second term due to particle collisions

$$P_s = \alpha_s \rho_s \theta_s + 2\rho_s(1 + e_{ss})\alpha_s^2 g_{0,ss}\theta_s \tag{2.26}$$

Where

e_{ss} = the coefficient of restitution for particle collision

$g_{0,ss}$= the radial distribution function
θ_s = the granular temperature

5. Radial distribution function $(g_{0,ss})$

The radial distribution, $g_{0,ss}$, is a correction factor that modifies the probability of collision between grains when the solid granular phase becomes dense.

$$g_{0,ss} = \frac{S + d_p}{S} \tag{2.27}$$

Where S is the distance between grains

6. Granular temperature (θ_s)

The granular temperature for the s[th] solid phases is proportional to the kinetic energy of the random motion of the particles. The transport equation derived from kinetic theory takes the form

$$\frac{3}{2}\left[\frac{\partial}{\partial t}(\rho_s \alpha_s \theta_s) + \nabla \cdot (\rho_s \alpha_s \vec{v}_s \theta_s)\right] = (-P_s \bar{I} + \bar{\tau}_s) : \nabla \vec{v}_s + \nabla \cdot \left(k_{\theta_s} \nabla \theta_s\right) - \gamma_{\theta_s} + \emptyset_{ls} \tag{2.28}$$

Where

$(-P_s \bar{I} + \bar{\tau}_s) : \nabla \vec{v}_s$ = The generation of energy by the solid stress tensor
$k_{\theta_s} \nabla \theta_s$ = The diffusive flux of granular energy
k_{θ_s} =The diffusion coefficient

7. Solid Shear Stress (μ_s)

The solid stress tensor contains shear and bulk viscosities arising from particle momentum exchange due to translation and collision. A frictional component of viscosity can also be included to account for the viscous plastic transition that occurs when particles of a solid phase reaches the maximum solid volume fraction

$$\mu_s = \mu_{s,col} + \mu_{s,kin} + \mu_{s,fr} \tag{2.29}$$

Each component of solid shear stress is calculated as following:

Collisional viscosity $(\mu_{s,col})$

$$= \frac{4}{5}\alpha_s \rho_s d_s g_{0,ss}(1 + e_{ss})\left(\frac{\theta_s}{\pi}\right)^{1/2} \alpha_s \tag{2.30}$$

Kinetic viscosity $(\mu_{s,kin})$

$$= \frac{\alpha_s d_s \rho_s \sqrt{\theta_s \pi}}{6(3 - e_{ss})}\left[1 + \frac{2}{5}(1 + e_{ss})(3e_{ss} - 1)\alpha_s g_{0,ss}\right] \tag{2.31}$$

Frictional viscosity $(\mu_{s,fr})$

$$= \frac{P_s \sin \emptyset}{2\sqrt{I_{2D}}} \tag{2.32}$$

Where P_s is the solids pressure, $\emptyset$ is the angle of internal friction, and $I_{2D}$is the second invariant of the viatoric stress tensor.
The frictional viscosity accounts for the friction between particles. The frictional stress is significant when the solids volume fraction exceeds a critical value of 0.5.

8. Bulk viscosity (λ_s)

The solid bulk viscosity accounts for the resistance of the granular particles to compression and expansion. It has the following of Lunet.al:

$$\lambda_s = \frac{4}{3}\alpha_s \rho_s d_s g_{0,ss}(1 + e_{ss})\left(\frac{\theta_s}{\pi}\right)^{1/2} \quad \textbf{(2.33)}$$

2.10 CFD review of hydrocyclone

Narasimh [18] studied the effect of spigot diameter and inlet water velocities on the water split and particle classification in the hydrocyclone with CFD simulation in order to predict the cut size. The discrete phase modeling was applied to model the solid movement to track the particle trajectory. CFD simulation was validated by comparing with the experimental results. This study revealed that the increase in feed flow rate and decrease in spigot diameter improved the separation sharpness of hydrocyclone.

Medronho [19] studied the separation of microorganism and mammalian cells using computational fluid dynamics. They aimed at understanding the complex flow inside hydrocyclone apparatus. Turbulence model used in this research is Reynold Stress Model (RSM) due to high swirl effect which occurs in hydrocyclone includes anisotropic turbulence. The Volume Of Fluid model (VOF) was used to account for the gas/liquid interface of air core. Discrete phase modeling or Euler-Larangian is chosen to calculate the dispersed phase. The results show that the air core naturally appeared as a result of the low pressure region along the central axis.

Ukkaracheneeyakorn [20] studied the hydrocyclone as a classifier. The effect of design and the operating parameter: overflow diameter, vortex finder diameter, and the length of hydrocyclone and pressure drop were investigated. The results showed that increasing the pressure drop and the overflow diameter, whereas reducing the vortex finder diameter causes the decreasing of the cut size diameter (d_{50}). Reducing the overflow diameter and increasing the vortex finder could increase the sharpness index.

Delgadillo [21] studied the effect of three turbulence model: the renormalization group k-ε model, the Reynold stress model, and the large eddy simulation on the accuracy of hydrocyclone simulation. The results showed that the large-eddy simulation produces some detailed feature turbulence, and the results were closer to the experimental data than other two turbulence models.

2.11 Reynold Stress Model

Reynold Stress Model (RSM) is the most complex type of RANs turbulence model that Ansys Fluent can provides. RSM abandons the isotropic eddy-viscosity hypothesis. RSM also solves transport equations for the Reynold stress with the equation for dissipation rate. RSM equation accounts for the effects of streamline curvature, swirl, rotation, and rapid changes in strain rate. It can predict complex flow. The example application of RSM is cyclone flows, highly swirling in combustor, rotating flow passage, and the stress-induced secondary flow in ducts. The exact transport equation for the transport of the Reynolds stress($\rho\,\overline{u_i' u_j'}$) may be written as follows:

$$\frac{\partial}{\partial t}\left(\rho\,\overline{u_i' u_j'}\right) + C_{ij} = D_{T,ij} + D_{L,ij} + P_{ij} + G_{ij} + \emptyset_{ij} + \varepsilon_{ij} \quad \textbf{(2.34)}$$

Where

Convection term

$$C_{ij} = \frac{\partial}{\partial x_k}\left(\rho u_k \overline{u_i' u_j'}\right) \quad \textbf{(2.35)}$$

Turbulent diffusion

$$D_{T,ij} = -\frac{\partial}{\partial x_k}\left[\rho\overline{u_i' u_j' u_k'} + \overline{p\left(\delta_{kJ} u_i' + \delta_{\iota k} u_j'\right)}\right] \quad \textbf{(2.36)}$$

Molecular diffusion

$$D_{L,ij} = \frac{\partial}{\partial x_k}\left[\mu \frac{\partial}{\partial x_k}\left(\overline{u_i' u_j'}\right)\right] \quad \textbf{(2.37)}$$

Stress production

$$P_{ij} = -\rho\left(\overline{u_i' u_j'}\frac{\partial u_j}{\partial x_k} + \overline{u_j' u_k'}\frac{\partial u_i}{\partial x_k}\right) \quad \textbf{(2.38)}$$

Buoyancy production

$$G_{ij} = -\rho\beta\left(g_i\overline{u_j'\theta} + g_j\overline{u_\iota'\theta}\right) \quad \textbf{(2.39)}$$

Pressure strain

$$\emptyset_{ij} = \overline{p\left(\frac{\partial u_\iota'}{\partial x_J} + \frac{\partial u_J'}{\partial x_\iota}\right)} \quad \textbf{(2.40)}$$

Dissipation

$$\varepsilon_{ij} = -2\mu\overline{\frac{\partial u_\iota'}{\partial x_k}\frac{\partial u_J'}{\partial x_k}} \quad \textbf{(2.41)}$$

CHAPTER 3 METHODOLOGY

The purpose of this research is to design a hydrocyclone for desalination process with computational fluid dynamics. The research methodology can be described step by step as Figure 3.1

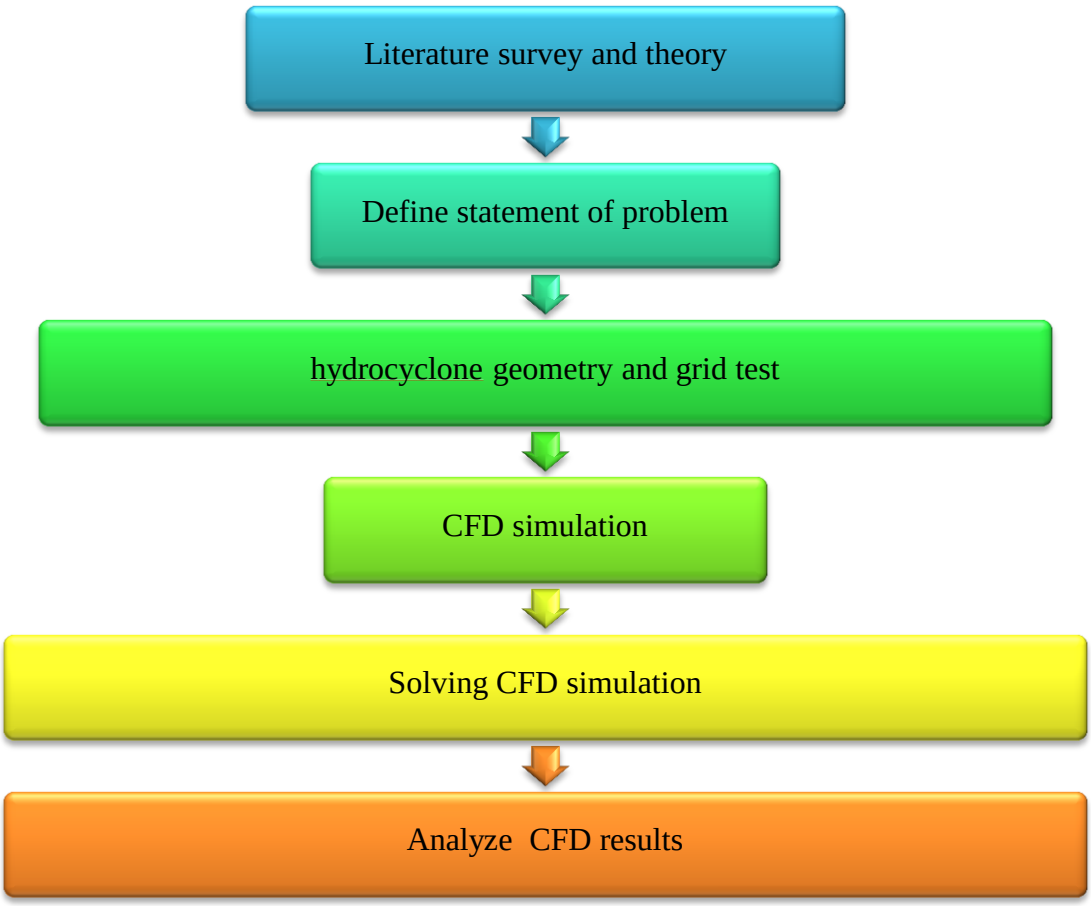

Figure 3.1 Methodology scheme

Before performing CFD simulation, the basic principle of freezing desalination process must be studied in order to determine the sufficient parameters for inputting into CFD simulation. Literatures review of CFD modeling for hydrocyclone must be reviewed to find the suitable approach for multiphase modeling. Finally, the hydrocyclone geometry and its operating condition of hydrocyclone for concentrating ice slurry from the brine slurry will be proposed.

3.1 Studying freezing desalination process

The freezing desalination is based on the principle that ice crystal can form at low temperature without impurity. When the temperature of salt solution is lowered than the freezing curve of salt solution but still stays above the solubility line, the ice crystal will be formed exclude the impurity. Figure 2.4 shows the eutectic phase diagram for NaCl solution. The natural sea water exists in the region A. If the temperature is reduced to below the eutectic line or exists in region D, salt and ice will become crystal. The solid-liquid separation requires that the salt solution must be in region C.

The natural sea water composed of many inorganic salts and organic salt e.g. $CaCO_3$, $MgCO_3$, and $MgSO_4$. The sea water must enter the crystallizer process. The overall crystallization process designed is shown in Figure 3.2

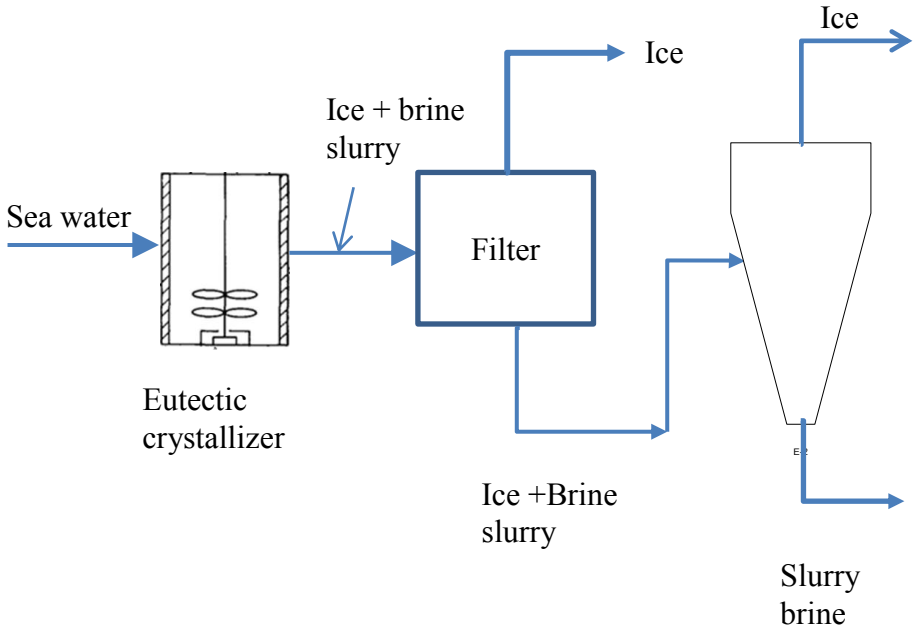

Figure 3.2 Overall crystallization process

The sea water is cooled by the free Liquid Natural Gas (LNG) in the crystallizer. Then the ice will be removed by the solid-liquid separator. The remaining ice will be recovered with hydrocyclone. The operating conditions of the eutectic crystallizer and the ice filter have been performed with Aspen Plus simulation. Hydrocyclone is used to separate the ice and brine by difference density. All of aspen simulation results are shown in Table A.1. The selected condition of the sea water exiting the eutectic crystallizer is -35°C and 5 bar, and then sent to filtration equipment to remove some of ice before feeding to hydrocyclone. The density of sea water and ice are 1222 and 917 kg/m^3, respectively. During the separation with ice filter and hydrocyclone, it is assumed that all system is adiabatic. Therefore, the density of sea water and ice entering hydrocyclone are equal to that of exiting the eutectic crystallizer. Table 3.1 shows the parameters for fluid dynamics calculation

Table 3.1 Parameters for CFD Simulation

Material	**Density (kg/m^3)**	**Viscosity (kg/ms)**
Sea water	1221	0.0039
Ice	917	-

The solid fraction of ice depends on the performance of the ice-filter or the filtration fraction. The relation between the filtration fraction of the ice filter and the solid feed fraction in hydrocyclone is shown in Appendix A. In order to determine the optimum operating condition of hydrocyclone, the solid fraction should be considered.

3.2 Creating geometry by ICEM CFD

The important task for success in separating ice slurry from the brine slurry is to select the geometry of hydrocyclone which can separate small density materials. Rietema design geometry is used to separate the solid from the liquid. Ruiyun's work reveals that Rietema hydrocyclone was not applicable for concentrating ice slurry [22]. The geometry of hydrocyclone in this research is retrieved from the deoiling hydrocyclone of HY1 [23], because the deoiling hydrocyclone can separate the oil and water which have small density difference, similarly to ice and sea water. Figure 3.3 shows the geometry of hydrocyclone and their notations, their proportions are shown in Table 3.2. Hydrocyclone is aligned in the horizontal direction.

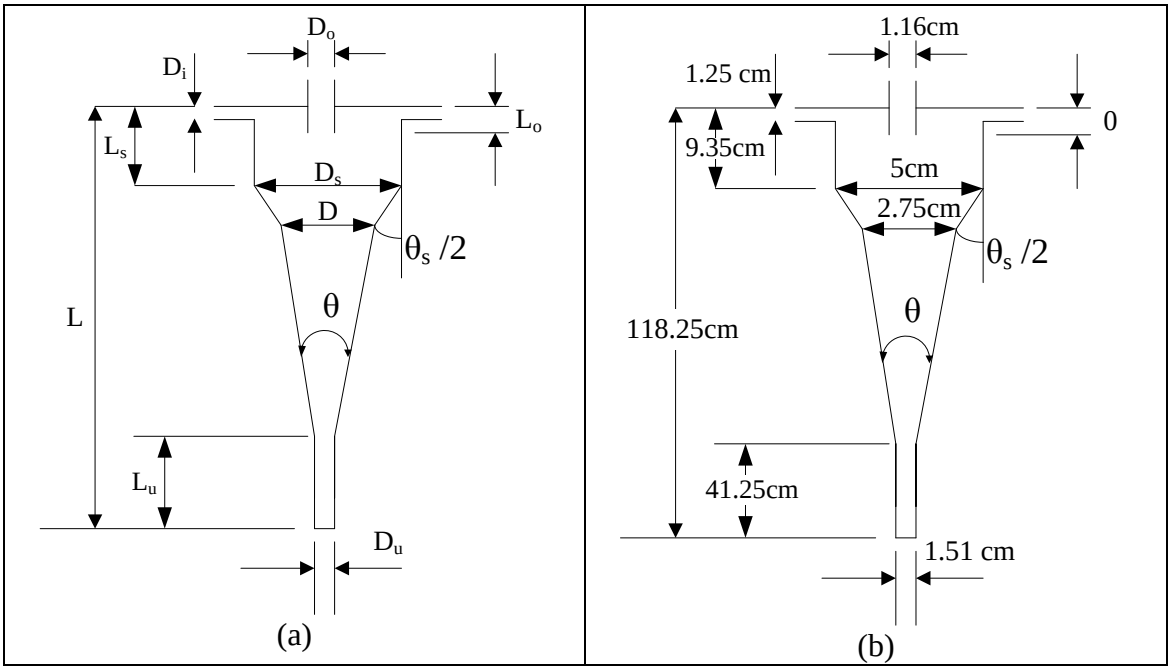

Figure 3.3 Hydrocyclone geometry (a) HY1 design proportion (b) 5 cm diameter of HY1 geometry

Table 3.2 Hydrocyclone geometry proportions [23]

Ratio	L/D	θ(°)	D_s/D	L_s/D	θ_s(°)	A_i/A	L_o/D	D_u/D	L_u/D
Value	43	1.2	1.82	3.4	1.25	0.21	1.51	0.55	15

Tetra mesh is used to create the geometry of hydrocyclone, as tetrahedral mesh support the complex geometry. The mesh proposed can be diagnosed and then fixed for example checking hole, gap and bad quality element. The finer element can be created by adjusting the scale factor and max element size. The mesh quality must be higher than 0.2.

After studying the ice-sea water with the standard geometry of HY1, the overflow and the underflow diameter are adjusted to study their influences on the flow pattern, split ratio, and the purity of ice. The variations of overflow area and underflow diameter are represented as the ratio of overflow diameter to underflow diameter.

$$\frac{D_o}{D_u} = \frac{Overflow\ diameter\ of\ hydrocyclone}{Underflow\ diameter\ hydrocyclone} \quad \textbf{(3.1)}$$

The ratio of the overflow diameter to underflow diameter is varied from 0.47 to 1.16. The ratio D_o/D_u of the standard geometry present in Figure 3.3 is 0.77. Table 3.3 and Table 3.4 show the underflow diameter, overflow diameter and ratio of D_o/D_u . All geometries in Table 3.3 and Table 3.4 are shown in Figure 3.5 and Figure 3.6.

Table 3.3 Variation of overflow diameter ($\boldsymbol{D_u}$ = 1.51 cm)

Case	$\boldsymbol{D_o}$ (cm)	$\boldsymbol{D_o/D_u}$
a	0.82	0.55
b	0.94	0.66
c	1.296	0.86
d	1.4152	0.94

Table 3.4 Variation of underflow diameter ($\boldsymbol{D_u}$= 1.16 cm)

Case	$\boldsymbol{D_u}$ (cm)	$\boldsymbol{D_o/D_u}$
a	1	1.16
b	1.3	0.89
c	1.68	0.69
d	1.83	0.63

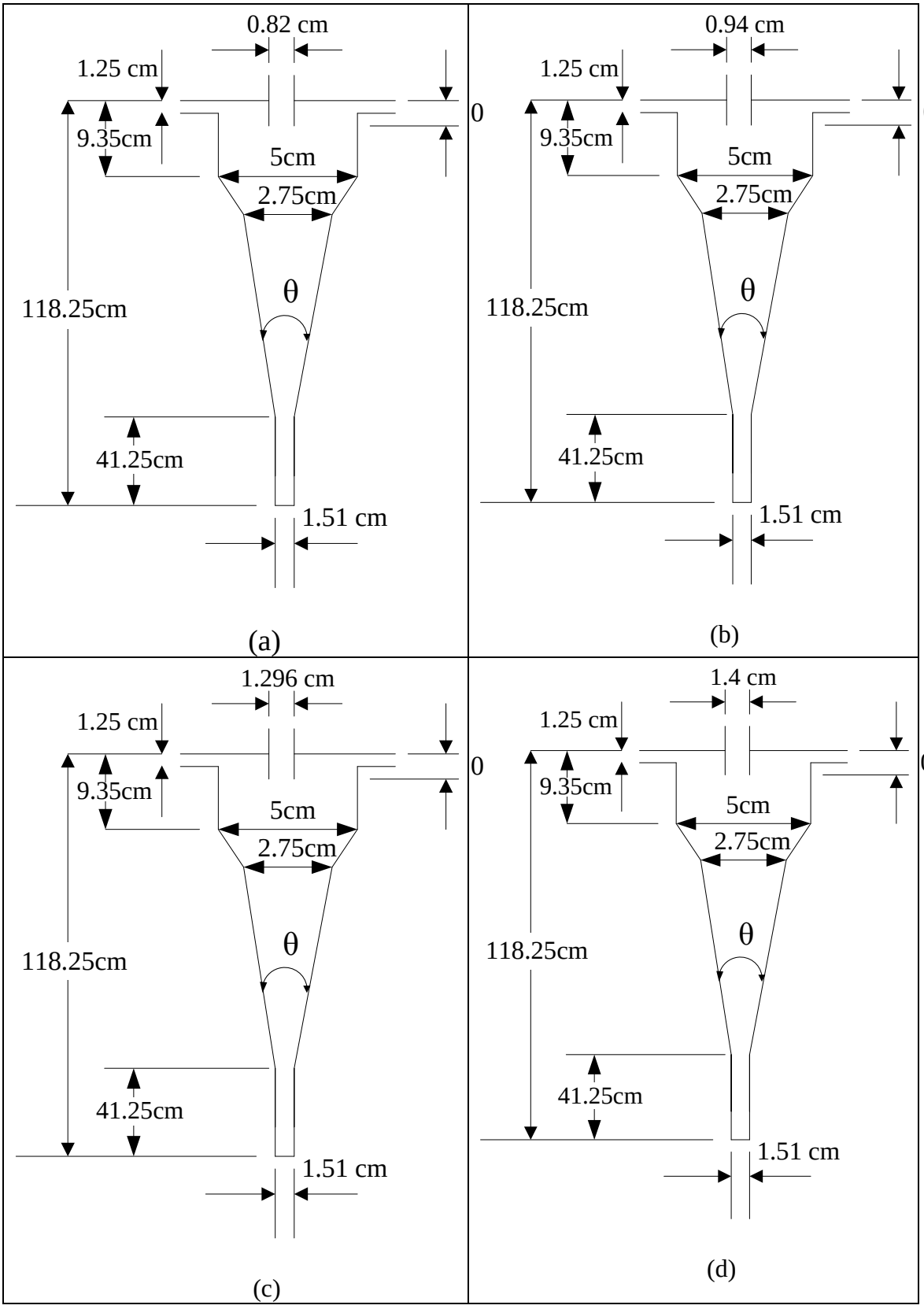

Figure 3.4 Hydrocyclone geometry of overflow diameter variation (a) $\boldsymbol{D_o/D_u}$= 0.55 (b) $\boldsymbol{D_o/D_u}$= 0.66 (c) $\boldsymbol{D_o/D_u}$= 0.86 (d) $\boldsymbol{D_o/D_u}$ = 0.94

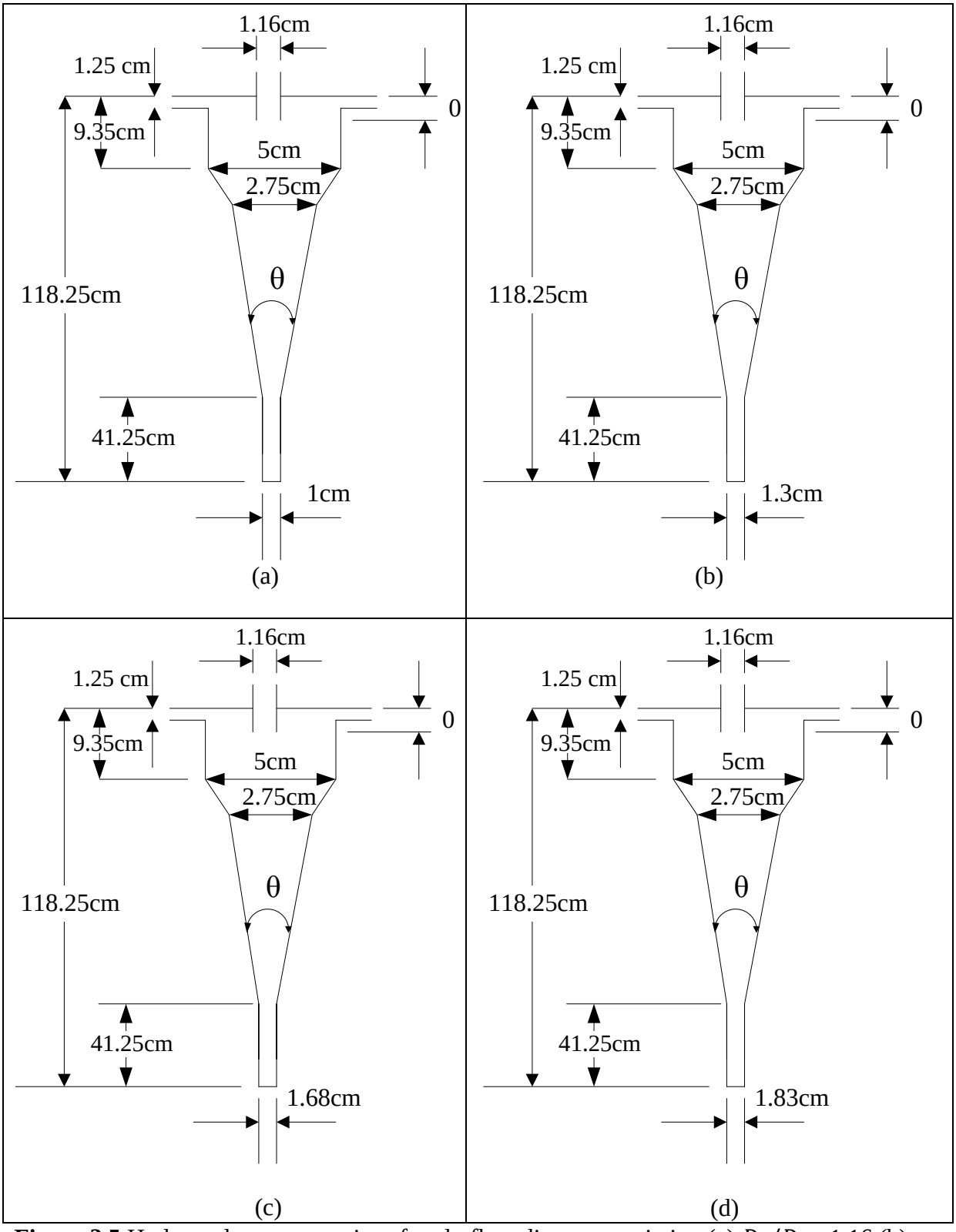

Figure 3.5 Hydrocyclone geometries of underflow diameter variation (a) D_o/D_u= 1.16 (b) D_o/D_u= 0.89 (c) D_o/D_u= 0.69 (d) D_o/D_u= 0.63

3.3 Mesh Independence test

Finer element of hydrocyclone provides the better result of CFD simulation, but it also takes longer computational time. The mesh independence test is carried out to find the optimum node number. The mesh independence test is tested with the single phase water feed flow rate of 5 m/s. Five different mesh sizes between 120,000-400,000 nodes were examined to find the optimum node number.

Table 3.5 Node number for mesh independence test

Case	Node number	Element number
1	120,620	699,421
2	163,336	950,304
3	230,127	1,343,336
4	338,594	1,983,402
5	403,496	2,366,670

The outlet boundary is set as the pressure-outlet condition. To select the number of node, the relative difference of mass flow rate per number of nodes is required to indicate the optimum number of node. The relative difference of overflow (Δ_o) and underflow (Δ_u) are defined by

$$\Delta_o = \frac{|m_{O,x} - m_{O,y}|}{x - y} \quad \textbf{(3.2)}$$

$$\Delta_u = \frac{|m_{U,x} - m_{U,y}|}{x - y} \quad \textbf{(3.3)}$$

Where, x and y are the number of nodes. The optimum number of nodes is selected by the criterion that the relative difference of the mass flow rate at overflow and underflow between nodes must be less than 5×10^{-8}

3.4 Problem formulation

3.4.1 Governing equation

The key to successfully modeling the high swirling flow inside hydrocyclone is a selection of turbulence model. Turbulence models have been categorized into two categories: Direct Numerical Simulation (DNS), Large Eddy Simulation (LES), and Reynold Averaging component (RANs). Direct numerical simulation requires no additional modeling, but it is impractical due to highly computationally expensive. The flow inside hydrocyclone is anisotropic turbulence and has rapid strain change. LES falls between DNS and RANs. LES requires transient simulation modeling; consequently, LES takes longer computational time to obtain the stable flow. Therefore, Reynold Averaging component (RANs) equations must be considered. Bhaskar [24] carried out the study of difference turbulence model such as standard k-ε, RNG k-ε, and RSM by comparing the simulation results and the experimental results of the water exiting the spigot opening. The results indicate that RSM model better agree with the experimental results than other type of RANs model, because it provides the marginal error of 4-8%. RSM model is the most suitable turbulence modeling approach, because it accounts for the effect of streamline curvature, swirl, rotation, and rapid changes in strain rate.

$$\frac{\partial}{\partial t}(\rho u_i) + \nabla \cdot (\rho u_i u_j) = -\nabla p - \rho \overline{u_i' u_j'} + \rho g + \bar{F} \quad \textbf{(3.4)}$$

RSM abandons the assumption of isotropic turbulence; thus it requires additional modeling of Reynold stress terms term. Equations of RSM model are shown in section 2.11

3.4.2 Multiphase model set up

There are two approaches for multiphase flow modeling: Eulerian-Eulerian approach and Euler-Lagrangian approach. The difference between Eulerian-Eulerian approach and Euler-Lagrangian is that the dispersed phase in the Eulerian-Larangian is not treated as continuum, and the control volume of dispersed phase moves with the fluid. Eulerian-Lagrangian approach is suitable for the solid volume fraction mixture below 10%. Above 10% of ice fraction, Eulerian-Eulerian approach must be applied.
The Eulerian-Granular model is the extension of Eulerian-Eulerian approach applied to calculate the fluid-solid flow behavior for the separation of ice and sea water. The momentum equation of fluid-solid is shown in

$$\begin{aligned}\frac{\partial}{\partial t}(\alpha_s\rho_s\vec{v}_s) + \nabla\cdot(\alpha_s\rho_s\vec{v}_s\vec{v}_s) \\ = -\alpha_s\nabla p - \nabla p_s + \nabla\cdot\overline{\overline{\tau_s}} + \alpha_s\rho_s\vec{g} \\ + \sum_{l=1}^{N}(K_{ls}(\overrightarrow{v_l} - \overrightarrow{v_s}) + \dot{m}_{ls}\vec{v}_{ls} - \dot{m}_{sl}\vec{v}_{sl}) \\ + (\overrightarrow{F_s} + \vec{F}_{lift,s} + \vec{F}_{vm,s})\end{aligned} \tag{3.5}$$

Where $\sum_{l=1}^{N}(K_{ls}(\overrightarrow{v_l} - \overrightarrow{v_s}) + \dot{m}_{ls}\vec{v}_{ls} - \dot{m}_{sl}\vec{v}_{sl})$ is the interaction term between fluid-solid phases. The fluid-solid interphase exchange coefficient models available in Fluent 14 are Wen-Yu, Gidaspow, and Symlal-Orbien. Wen-Yu model is appropriate for dilute phase calculation, and Gidaspow is mostly applied to calculate the dense fluidized bed model. Symlal-Orbien predicts the accurate results when compared with other drag models. The range of ice solid fraction in hydrocyclone feed is 0.1-0.4, Symlal-Orbien and Gidaspow must be considered. The validating results for drag force coefficient. can be obtained from the CFD modeing of Fluidized bed reactor. Almuttahar [25] studied the CFD modeling of air and fluid catalytic cracking (FCC) particles in the riser of high density, and the effect of drag models on the simulation results are investigated by comparing the simulated profiles of fluid and solid velocity with the experimental data. Symlal-Orbien provides the better agreement results with the experimental data. Consequently, the drag model, Symlal-Orbien, is chosen to calculate the solid phase.

The Symlal-Orbien fluid-solid momentum exchange coefficient is described by

$$K_{sl} = \frac{3}{4}\frac{\alpha_s\alpha_l\rho_g}{v_{r,s}^2 d_s}\cdot C_D\cdot\left(\frac{Re_s}{v_{r,s}}\right)\cdot|\vec{v}_s - \vec{v}_l| \tag{3.6}$$

$$C_D = \left(0.63 + \frac{4.8}{\sqrt{Re_s/v_{r,s}}}\right)^2 \tag{3.7}$$

$$Re_s = \frac{\rho_l\, d_s}{\mu_l} \tag{3.8}$$

$$v_{r,s} = 0.5\left(A - 0.06Re_s + \sqrt{(0.06\cdot Re_s)^2 + 0.012Re_s(2B - A) + A^2}\right) \tag{3.9}$$

With

$$A = \alpha_l^{4.14} \quad \textbf{(3.10)}$$

$$B = 0.8 \times \alpha_l^{1.28} \text{ for } \alpha_l \leq 0.85 \quad \textbf{(3.11)}$$

$$B = \alpha_g^{2.65} \text{ for } \alpha_g > 0.85 \quad \textbf{(3.12)}$$

The granular phase parameter is calculated as following:

Solid pressure (P_s)
$$P_s = 2\rho_s (1 + e_{ss})\alpha_s^2 g_{0,ss}\theta_s \quad \textbf{(3.13)}$$

Radial distribution ($g_{0,ss}$)
$$g_{0,ss} = \left[1 - \left(\frac{\alpha_s}{\alpha_{s,max}}\right)^{\frac{1}{3}}\right]^{-1} \quad \textbf{(3.14)}$$

Collisional viscosity ($\mu_{s,col}$)
$$\mu_{s,col} = \frac{4}{5}\alpha_s\rho_s d_s g_{0,ss}(1 + e_{ss})\left(\frac{\theta_s}{\pi}\right)^{1/2}\alpha_s \quad \textbf{(3.15)}$$

Kinetic viscosity $(\mu_{s,kin})$
$$\mu_{s,kin} = \frac{\alpha_s d_s \rho_s \sqrt{\theta_s \pi}}{6(3 - e_{ss})}\left[1 + \frac{2}{5}(1 + e_{ss})(3e_{ss} - 1)\alpha_s g_{0,ss}\right] \quad \textbf{(3.16)}$$

Granular bulk viscosity (λ_s)
$$\lambda_s = \frac{4}{3}\alpha_s\rho_s d_s g_{0,ss}(1 + e_{ss})\left(\frac{\theta_s}{\pi}\right)^{1/2} \quad \textbf{(3.17)}$$

3.4.3 Boundary and the numerical scheme

The volume of feed inlet can be specified by both the magnitude velocity and the pressure inlet. In this research, the inlet velocity magnitude of 11-25 m/s is defined. The overflow and the underflow were assigned as the pressure outlet set to zero. The outflow boundary can not be applied to the overflow and the underflow, because Fluent assumes that the split fraction is equal in both overflow and underflow. The assumption for modeling ice-sea water mixture is as following:

- The system is adiabatic
- The hydrocyclone wall effect is negligible.
- The ice distribution in ice-brine slurry is equal across the feed inlet
- The overflow and underflow boundary is opened to the air

The hydrocyclone is adiabatic or insulated in order to control the operating temperature inside hydrocyclone and maintain the physical properties of ice and sea water: e.g. density and the viscosity. To verify this assumption, the CFD simulation including energy equation has been runned. It shows that the operating temperature can be controlled with the insulator. The results and setting boundary of energy case are shown in Figure C.17 and Figure C.20, respectively. The Fluent solver is 3-D double precision solver, Phase-Simple Coupled (PC-SIMPLE), and all quantities are discretized with the first order upwind scheme. PC-SIMPLE is the extension of the SIMPLE algorithm to the multiphase flow. Fluent 14 allows you to choose the discretization scheme from several upwind scheme, first-order upwind scheme, and the QUICK scheme. The assumption of the first order upwind scheme is that the scalar value stored at the cell centers equal to the face center. Higher order upwind scheme means the scalar value at face is discretized from the cell value, so the second order upwind scheme provides the

more accurate results than the first order upwind scheme, but take more computational time. In this work, Eulerian-Granular model coupled with Reynold Stress Model (RSM) is highly computational expensiv; consequently, the first order upwind scheme is applied instead of. The convergence criteria should fall below 10^{-5}, hence the convergence is assigned as 10^{-6}.

3.5 Analyzing the result

Hydrocyclone is applied to separate the ice, light density material, from the brine, heavy density material. Three key parameters for hydrocyclone design are separation efficiency (ε), and the split fraction (R_f). In the first, the inlet velocity of hydrocyclone and solid volume fraction is adjusted to provide the better separation efficiency. The velocity profile and the pressure profile are plotted over the radial position to obtain the flow characteristics. Then the diameter of underflow and underflow are adjusted to observe the effect of flow split ratio and the purity of ice in the overflow stream ($X_{v,ice}$).

$$\varepsilon = 1 - \frac{C_{ice,underflow}}{C_{ice,inlet}} \tag{3.18}$$

$$X_{v,ice} = \frac{Volume\ flow\ rate\ of\ ice\ at\ the\ overflow\ (\frac{m^3}{s})}{Volume\ flow\ rate\ of mixture\ \ at\ the\ overflow\ (\frac{m^3}{s})} \tag{3.19}$$

$$R_f = \frac{Volume\ flow\ rate\ at\ underflow}{Volume\ flow\ rate\ at\ inlet} \tag{3.20}$$

CHAPTER 4 RESULT AND DISCUSSION

CFD simulation is used to simulate hydrocyclone for concentrating ice slurry from brine. Firstly, the flow pattern of fluid inside will be studied. Then the operating condition: inlet velocity and the solid ice fraction are adjusted to find the condition which gives the separation efficiency exceeds 80%. Then, the configurations are adjusted to study the effects on the separation behavior.

4.1 Mesh Independence test

Before carrying the CFD simulation of ice-sea water mixture, the grid Independence test is performed to find the appropriate number of nodes for hydrocyclone simulation. Finer mesh provides higher accuracy of CFD simulation, but it also takes more computational time. Therefore, the optimum number of node must be determined. Larger size of equipment requires higher number of node. In this research, 5-cm diameter of hydrocyclone according to HY1 design proportion is selected. The node number of hydrocyclone is varied from 120,620-403,496. The mass flow rates of overflow and underflow are used to validate the node number because mass flow rates are used for the separation efficiency calculation. The operating condition for mesh independence test is water-single phase flowing into hydrocyclone with the inlet velocity of 5 m/s. The mesh independence results are shown Figure 4.1.

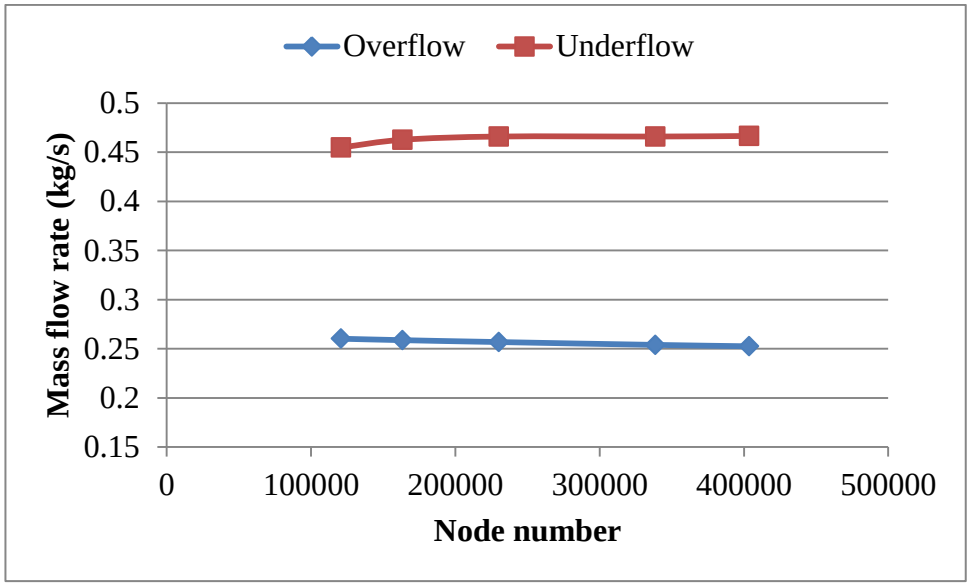

Figure 4.1 Mass flow rate at overflow and underflow (kg/s)

The mass flow rates of overflow and underflow are calculated in term of relative difference per node of overflow (Δ_o) and underflow (Δ_u).

Table 4.1 Relative difference per node

Node	Δ_o	Δ_u
120,620→163,336	3.90×10^{-8}	1.84×10^{-7}
163,336→230,127	2.88×10^{-8}	4.98×10^{-8}
230,127→338,594	2.65×10^{-8}.	2.77×10^{-8}
338,594→403,496	2.14×10^{-8}.	2.45×10^{-8}

The relative difference of mass flow rate at overflow and mass at between nodes must be less than 5×10^{-8}. 338,594 nodes are required for 5 cm diameter of hydrocyclone

4.2 Effect of inlet velocity

Theoretically, higher velocity increases the centrifugal force, so the increase of inlet velocity increases the separation efficiency. The inlet velocity is varied from 11 m/s to 25 m/s to determine the optimum velocity which provides the best separation efficiency. All simulations are performed at the solid ice fraction of 0.2.

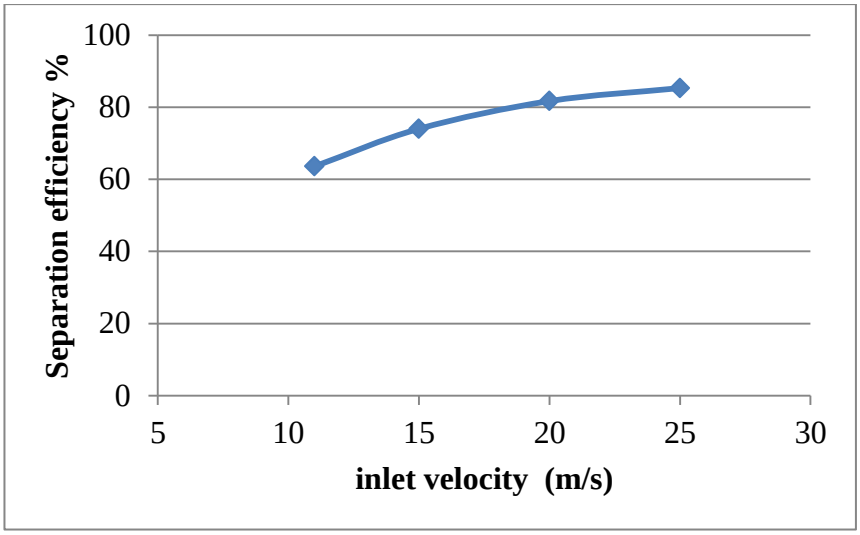

Figure 4.2 Effect of inlet velocities on the separation efficiency , operating condition: ice fraction = 0.2 Temperature = -30°C, pressure = 5 bar

Figure 4.2 shows that higher inlet velocities provide higher separation efficiency. The results of inlet velocity and separation efficiency were in agreement with the experiment investigated by Yuan [13]. The certain level of pressure drop or feed flow rate is needed to generate enough centrifugal force for separation. With further increase in velocity above 20 m/s, the efficiency increased slowly. The overall pressure profile and volume fraction are illustrated to investigate the effect of inlet velocities. Figure 4.3 shows total pressure distribution along the radius distance 4.5 cm below of vortex finder. The total pressure gradually decreases when the radius decreases inwards to the center of hydrocyclone. The maximum pressure occurs near hydrocyclone wall due to tangential entry of hydrocyclone feed. The low pressure region occurs at the center of hydrocyclone. Below the atmospheric pressure, it is assumed that the air can enter into hydrocyclone. This indicates that the air core can forms in only case of inlet velocity = 11 m/s. The overall pressure profile in hydrocyclone is illustrated in Figure 4.3. The negative pressure occurs at the vortex finder and the cylindrical extrude length of underflow.

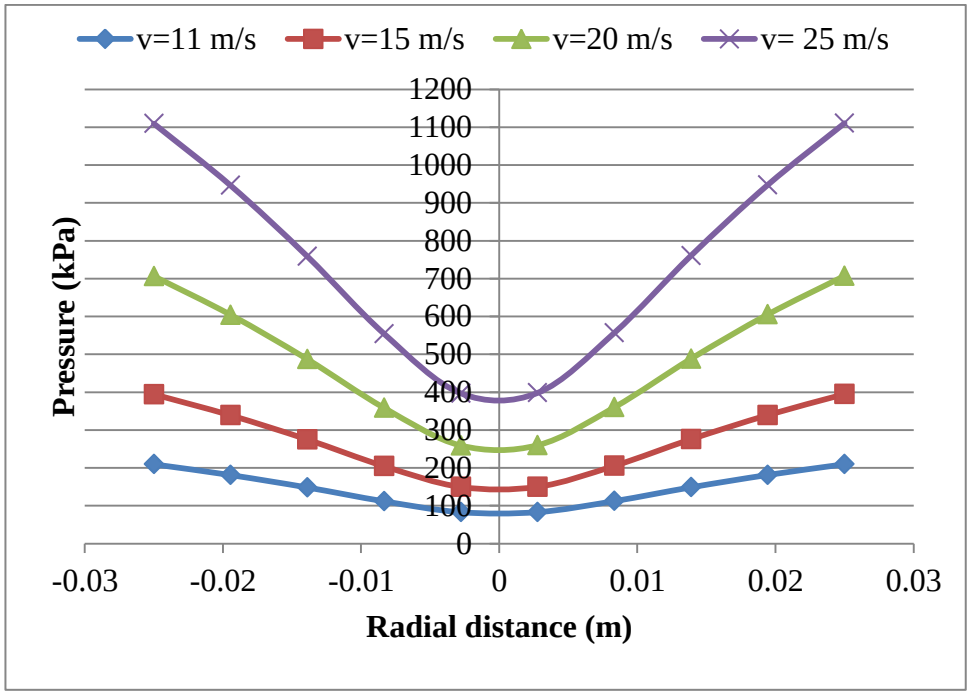

Figure 4.3 Effect of inlet velocity on pressure profile below 4.5 cm of vortex finder

The flow characteristics of ice-sea water are represented by the radial velocity, axial velocity, and the tangential velocity profile at level of 4.5 cm below the vortex finder.

Figure 4.4 (a) shows both positive axial velocity and the negative axial velocity. The positive axial velocity means the material goes to the overflow and the negative value means the material goes to the underflow side. The positive axial velocity is concentrated at the center of hydrocyclone. Near the hydrocyclone wall, the axial velocity is downward. This flow removes the particle to the underflow.

Figure 4.4 (b) shows the tangential velocities as function of radial distance. The tangential velocity magnitude increases with the increasing radius. The tangential velocity near the hydrocyclone wall is close to the inlet velocity of hydrocyclone. The higher tangential velocity represents higher centrifugal force. The relation between the centrifugal force and the tangential velocity is described by:

$$F_c \; \alpha \; v_t^2 \qquad \textbf{(4.1)}$$

Figure 4.4 (c) shows the radial velocity profile which are similar to the tangential velocity profile. The radial velocity is always inward, and the magnitude of radial velocity is highest near hydrocyclone wall. The effects of radial velocity is negligible, as the magnitudes of radial velocity profile are much smaller than the axial velocity and the tangential velocity

When the effect of radial velocity can be negligible, only gravity force and centrifugal force mainly affects the particle motion. In this study, the gravity force also enhances the centrifugal force due to the alignment of hydrocyclone. Due to higher centrifugal force, ice tends to move spiral inwards and move via the overflow, the ice is concentrated at the center of hydrocyclone axis. The ice distribution is illustrated in Figure 4.6

Figure 4.6 shows the maximum ice volume fraction located at hydrocyclone axis is 0.5 because the inlet velocity above 20 m/s provides higher centrifugal force. The ice distribution is low near hydrocyclone wall.

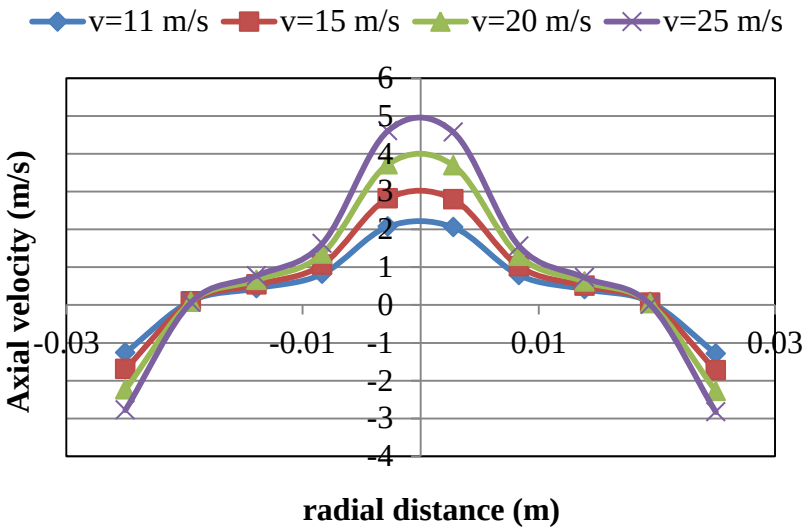

(a)

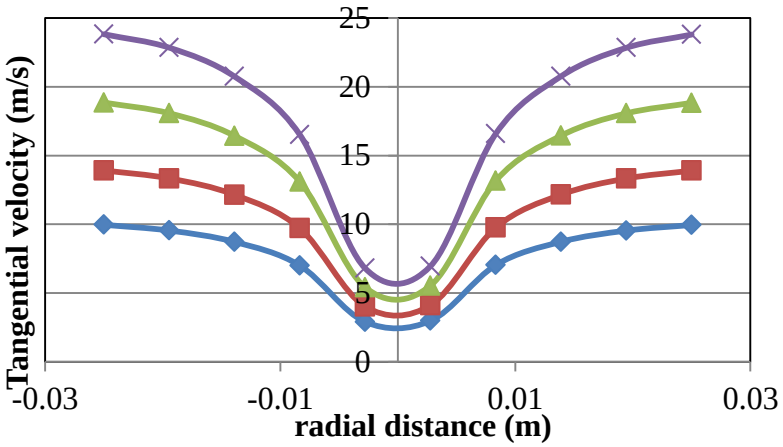

(b)

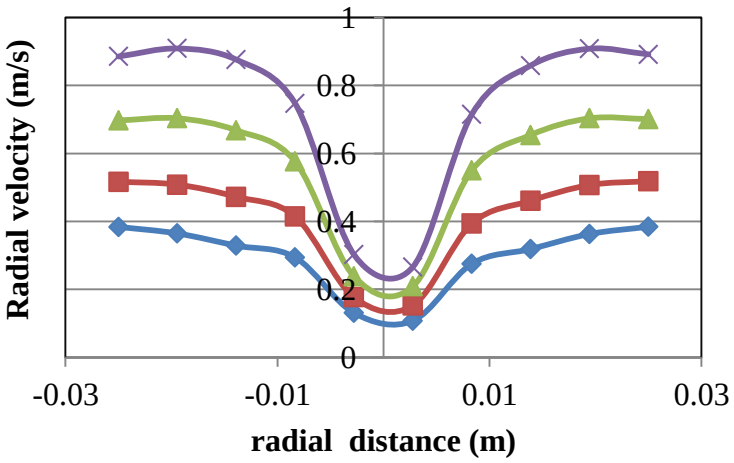

(c)

Figure 4.4 Effect of inlet velocity profile of ice (a) axial velocity (b) tangential velocity (c) radial velocity

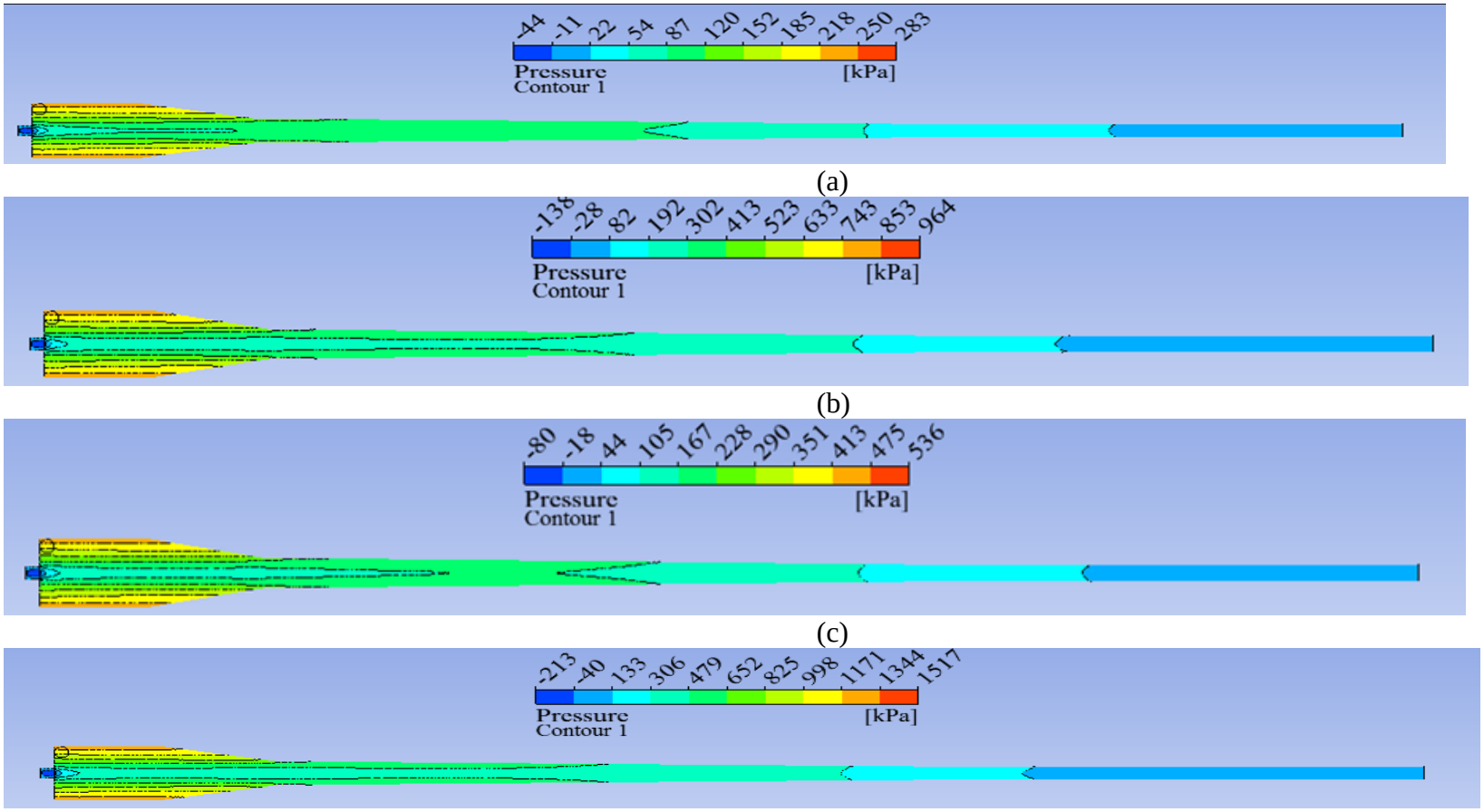

Figure 4.5 Pressure profile at the middle plane (a) Inlet velocity =11 m/s (b) Inlet velocity = 15 m/s (c) Inlet velocity = 20 m/s (d) Inlet velocity = 25 m/s

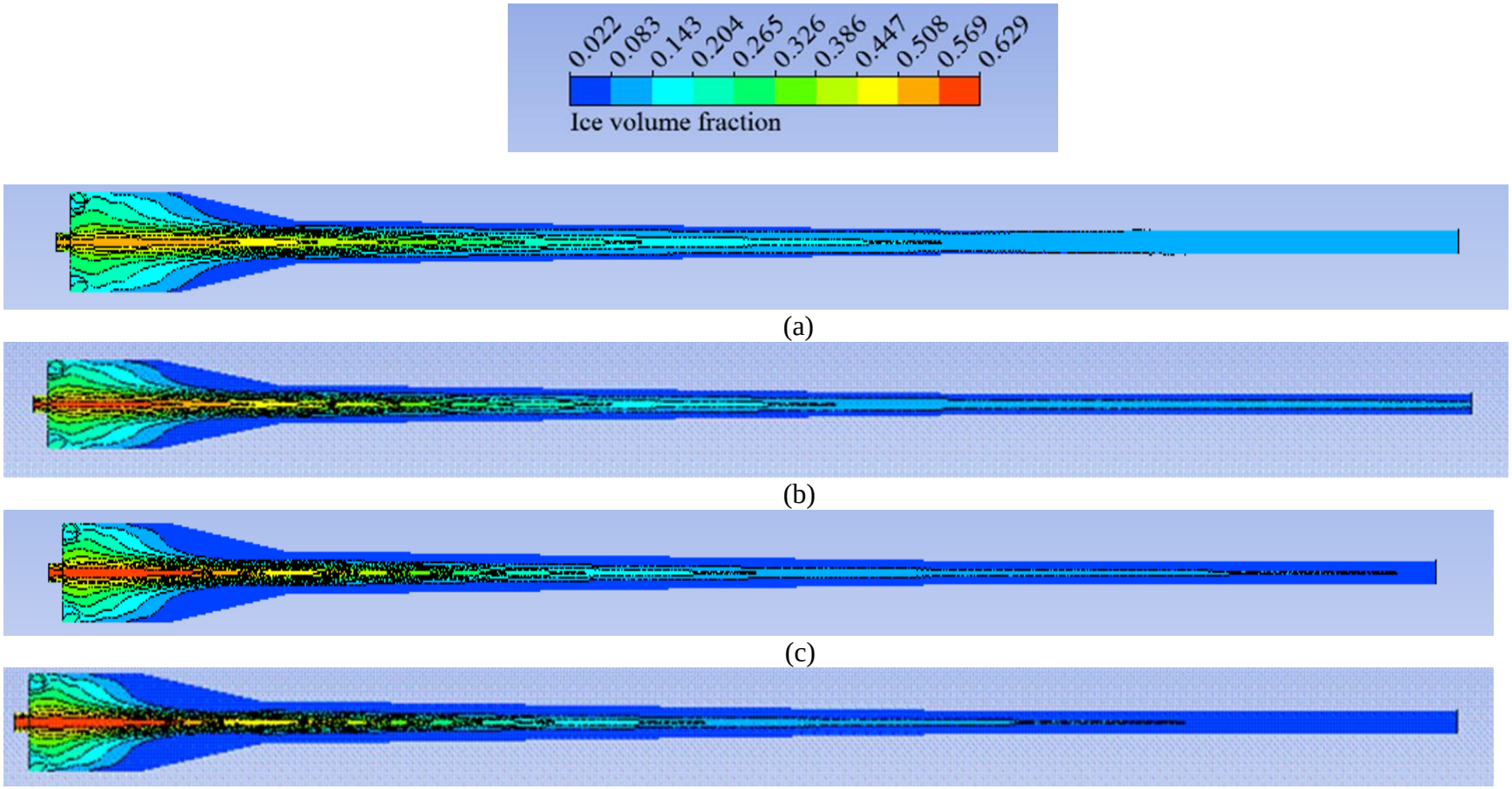

Figure 4.6 Contour of ice volume fraction at the symmetry plane (a) Inlet velocity =11 m/s (b) Inlet velocity = 15 m/s (c) Inlet velocity =20 m/s (d) Inlet velocity =25 m/s

4.3 Effect of solid concentration

Hydrocyclone is suitable for low solid concentration feed. Higher solid concentration results in poorer separation, because increasing solid volume fraction increase the resistance to flow. The solid fraction in this case is varied from 0.1 to 0.4 while the inlet velocity is kept at 20 m/s. Figure 4.7 shows the relationship between the separation efficiency and the inlet ice fraction. The separation efficiency reaches 80%, when the solid fraction is less than 0.2. The parameter which indicates the resistance to flow is the granular viscosity represented by Figure 4.8. The bulk granular viscosity of ice is calculated by

$$\lambda_s = \frac{4}{3}\alpha_s \rho_s d_s g_{0,ss}(1+e_{ss})\left(\frac{\theta_s}{\pi}\right)^{1/2} \quad \textbf{(3.14)}$$

The bulk viscosity of ice is a function of the solid fraction(α_s), the density, and the radial distribution ($g_{0,ss}$). The radial distribution is the probability of particle collision described by:

$$g_{0,ss} = \left[1 - \left(\frac{\alpha_s}{\alpha_{s,max}}\right)^{\frac{1}{3}}\right]^{-1} \quad \textbf{(3.17)}$$

Equation (3.17) indicates that higher solid fraction results in higher probability of collision. According to Equations (3.14) and (3.17), the increase in solid fraction raises the bulk viscosity value. The drag resistance to the particle motion also rises because of the increase in the ice viscosity. The increase in slurry viscosity in Figure 4.8 agrees with the feed concentration effect investigated by Yuan [13]. The increase in feed concentration raises the possibility of hindered settling. Then the separation efficiency decreases.

Figure 4.9 shows the ice distribution inside hydrocyclone. In case of solid volume fraction of ice =0.1, ice is concentrated near only the center of hydrocyclone. For the case which inlet ice volume fraction is high at 0.4, the ice distributes throughout hydrocyclone due to higher greater resistance to flow. When the ice solid fraction of 0.1 enters into hydrocyclone, the ice volume fraction in the overflow stream is 0.29. While inlet ice fraction is 0.4, the outlet fraction of ice in the overflow stream is 0.63. Low inlet ice fraction gives three times concentrated ice slurry, while the ice is one and half times concentrated ice slurry. With lower ice fraction, ice tends to move to the overflow rather than that of high solid fraction. The velocity vector of ice is illustrated in Error! Reference source not found.. It can be seen that with lower ice fraction, the ice tend to move to the overflow side rather than the high solid fraction case due to the drag force effect.

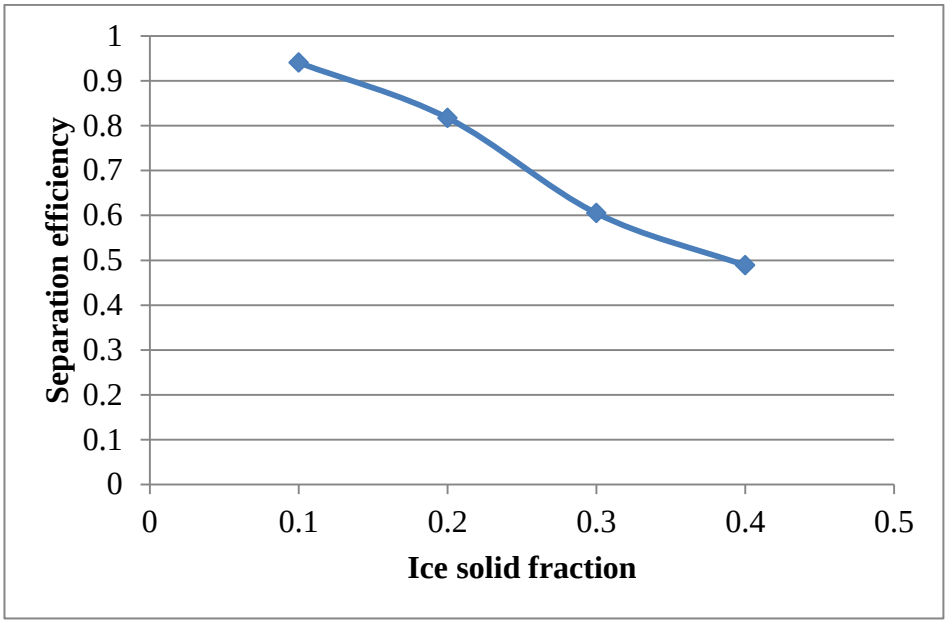

Figure 4.7 Effect of ice solid fraction on the separation efficiency

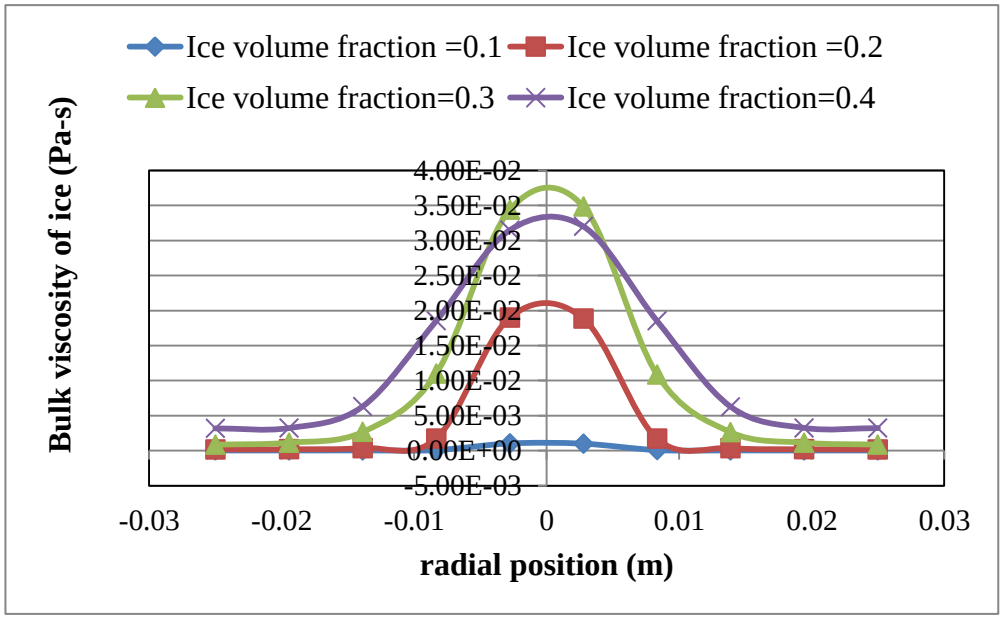

Figure 4.8 Bulk viscosity of ice calculated by Symlal-Orbien

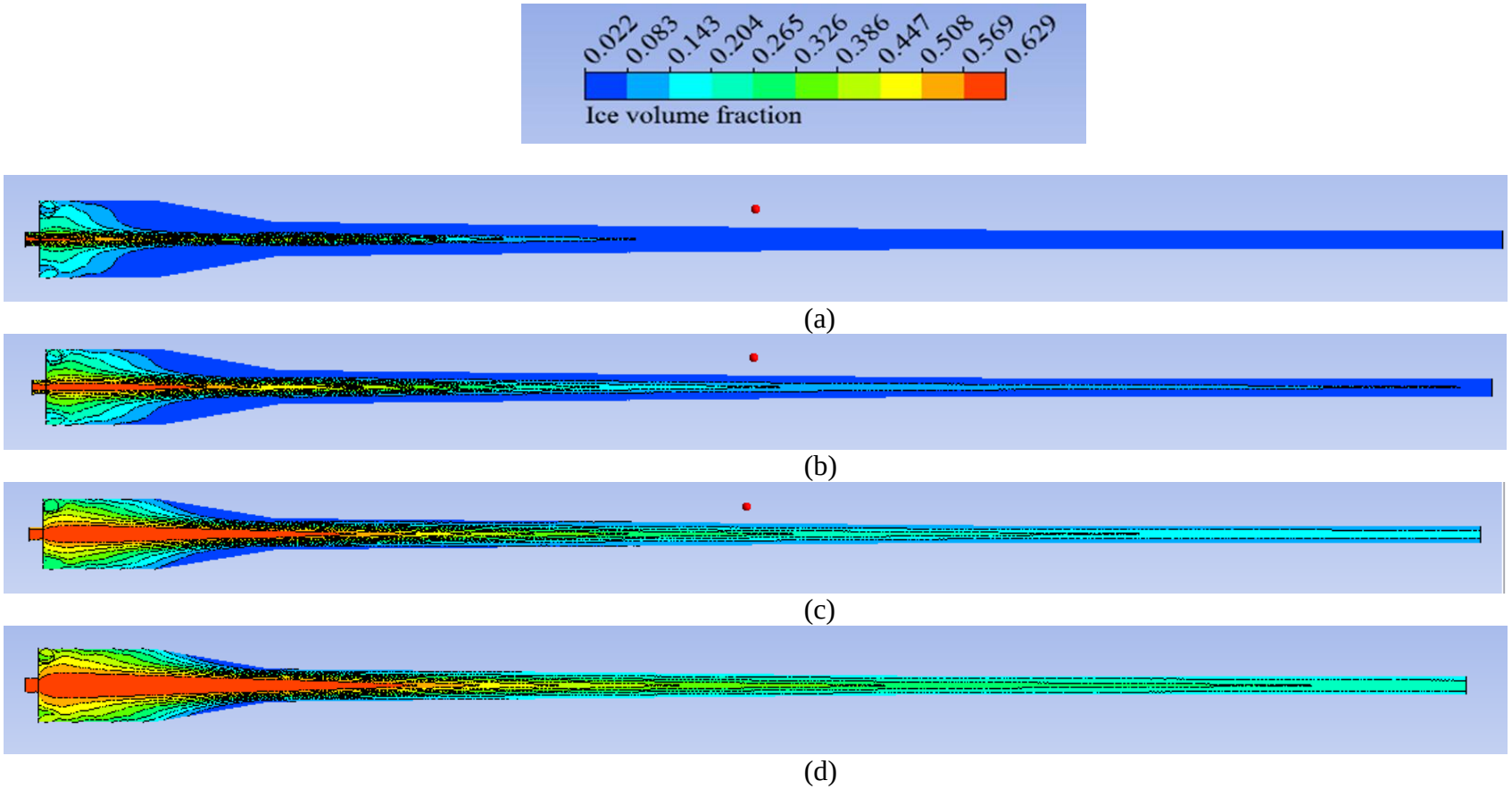

Figure 4.9 Ice volume fraction at the middle plane of hydrocyclone (a) Inlet ice volume fraction =0.1 (b) Inlet ice volume fraction =0.2 (c) Inlet ice volume fraction =0.3 (d) Inlet ice volume fraction = 0.4

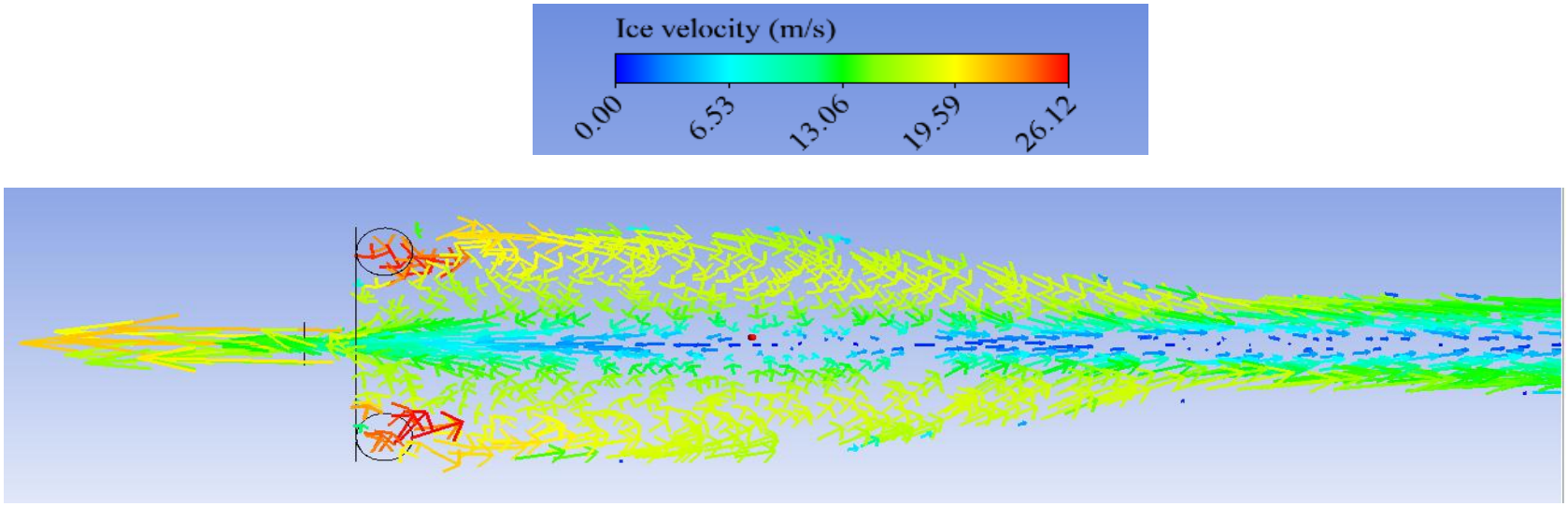

(a)

(b)

Figure 4.10 Velocity vector plot of slurry at the middle plane of hydrocyclone (a) Ice inlet fraction = 0.1 (b) Ice inlet fraction = 0.4

4.4 Effect of overflow diameter and underflow diameter

This part focuses on the geometry adjustments of the existing hydrocyclone. The overflow diameter and the underflow diameter are varied to determine their effects on the flow pattern of ice, the split ratio, and purity of ice. All simulations were performed at under the constant 20 % v/v ice solid concentration operating at inlet velocity of 20 m/s. Firstly, the overflow diameter is varied from 0.82 to 1.4 cm while another dimensions e.g. hydrocyclone length and the cone angle are same as the standard hydrocyclone. Secondly, the underflow diameter is varied from 1 to 1.83 cm while another dimensions e.g. total length of hydrocyclone and diameter of reducing section are kept constant. All geometries are thoroughly presented in Figures 3.5 and 3.6

The decrease of the underflow diameter results in the reduction of cone angle. After performing the simulation of underflow diameter variation and the overflow diameter variation, it was found that influence of overflow diameter increase on the separation is similar to that of underflow diameter reduction. To represent all of results concisely, the split fraction, purity of ice, and the phase recovery will be plotted over the ratio of overflow to underflow diameter (D_o/D_u) based on the overflow diameter variation and underflow diameter variation. Figure 4.12 to Figure 4.14 show that underflow diameter adjustment develops the higher gradient of split fraction, phase recovery, and the purity over the ratio (D_o/D_u) of than that of overflow diameter adjustment, because reducing the underflow diameter also affects the cone angle. At lower cone angle, ice tends to move the overflow.

Figure 4.11 shows that increasing D_o/D_u results in higher split fraction of slurry to overflow side, but the lower ice purity in the overflow stream. The variation of D_o/D_u on the overflow diameter adjustment from 0.82 to 1.4 cm increases percent split fraction of overflow stream from 20 to 60%, but reduces the ice purity from 57 to 37 % v/v. The main reason why the product purity is lowered at higher split fraction is shown in Figure 4.13 and Figure 4.14. Sea water recovery in the overflow stream continuously rises at higher value of D_o/D_u, while the ice recovery gradually increases. Figure 4.15 shows that the increase of D_o/D_u ratio increases the separation efficiency of hydrocyclone. The curves in Figure 4.11, Figure 4.12, and Figure 4.15 are similar to the previous study performed by Yu [26]. He performed the experiment of underflow diameter effect on hydrocyclone separation efficiency. His study revealed that decreasing the underflow diameter or increasing the D_o/D_u ratio would increase the separation efficiency because of the flow rotation inside the hydrocyclone unit due to the detention of more slurry. Therefore, more heavy material would be separated to the underflow.

To select the optimum ratio D_o/D_u of hydrocyclone, the purity of ice, split fraction, and ice recovery must be considered. The results of the adjustment in underflow diameter and underflow diameter are analyzed together. The D_o/D_u ratio of the standard hydrocyclone is 0.76. At low range of D_o/D_u (0.54-0.68), the purity of ice is higher than 50 % v/v, but percent recovery of is only 50 to 70%. At high range of D_o/D_u (0.86-1.08), the purity of ice reduces from approximately 47 to 36 % v/v, but split fraction of the overflow stream percent Ice also increases. Ice recovery for higher range of D_o/D_u reaches approximately 99%. To select the optimum value of D_o/D_u ratio, the separation efficiency and the purity of ice should be considered. The D_o/D_u ratio of the standard hydrocyclone or 0.66 is considered as the optimum value, because it provides the separation efficiency 80% and the purity is higher than 50% v/v of ice.

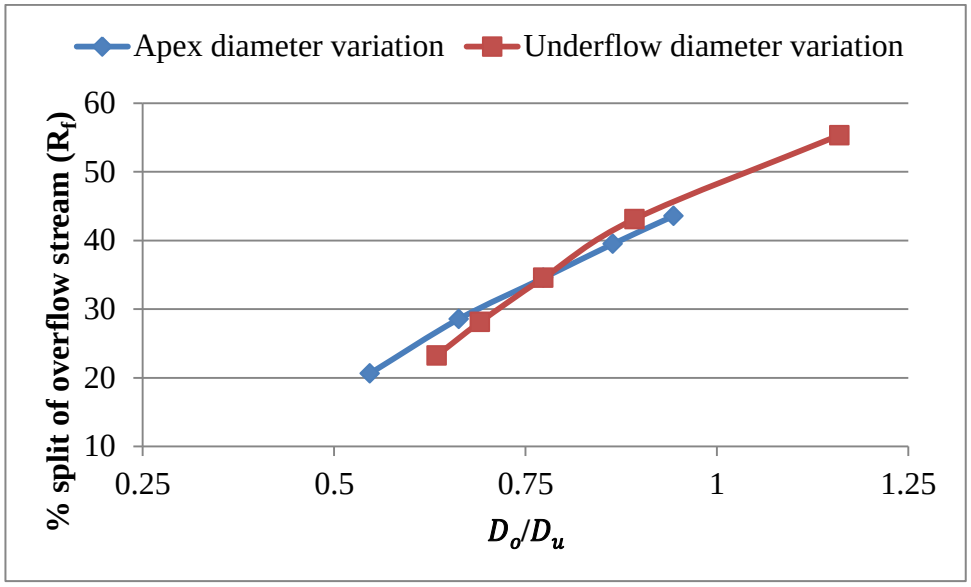

Figure 4.11 percent split fraction of the overflow stream operating at the inlet velocity of 20 m/s and ice concentration of 20 % v/v

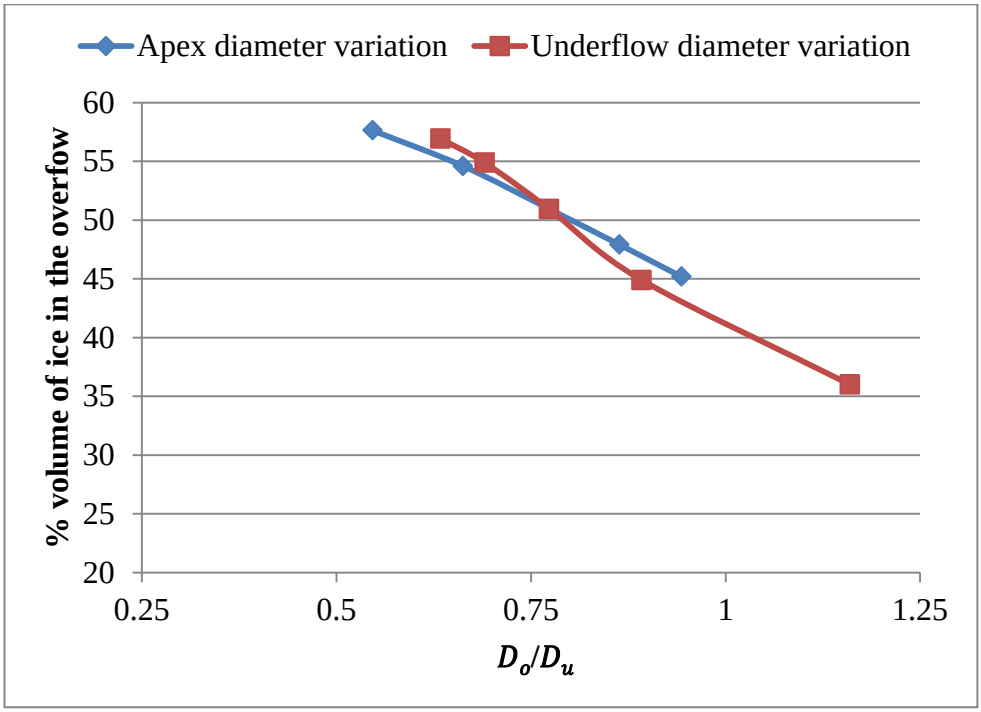

Figure 4.12 Purity of ice at the overflow opening operating at the inlet velocity of 20 m/s and ice concentration of 20 % v/v

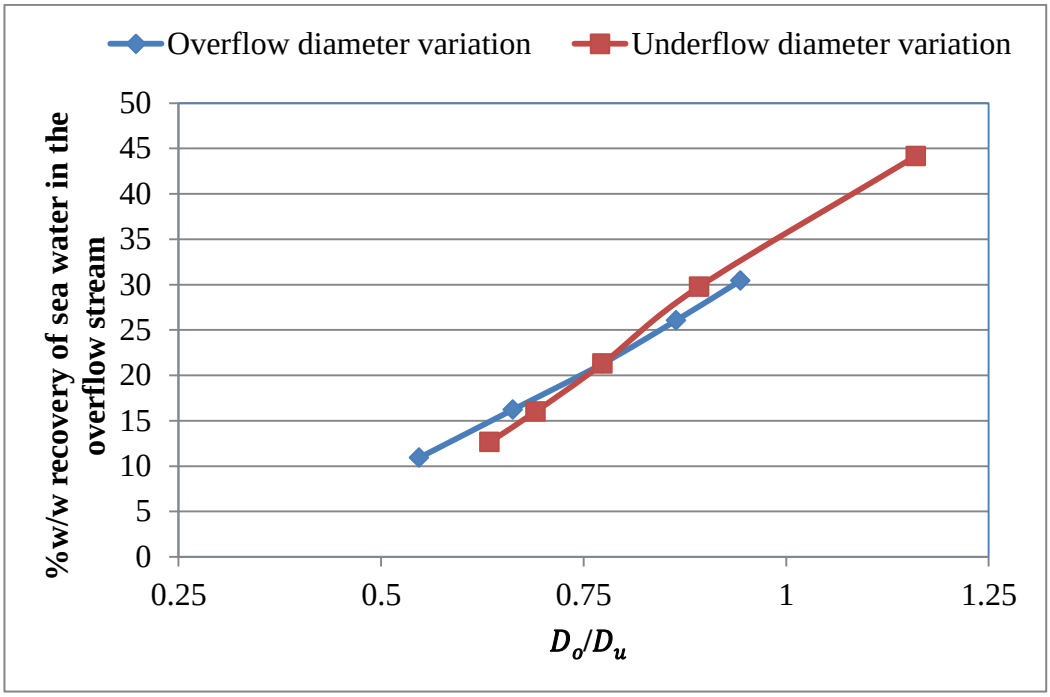

Figure 4.13 Sea water recovery in the overflow stream at the overflow opening operating at the inlet velocity of 20 m/s and ice concentration of 20 % v/v

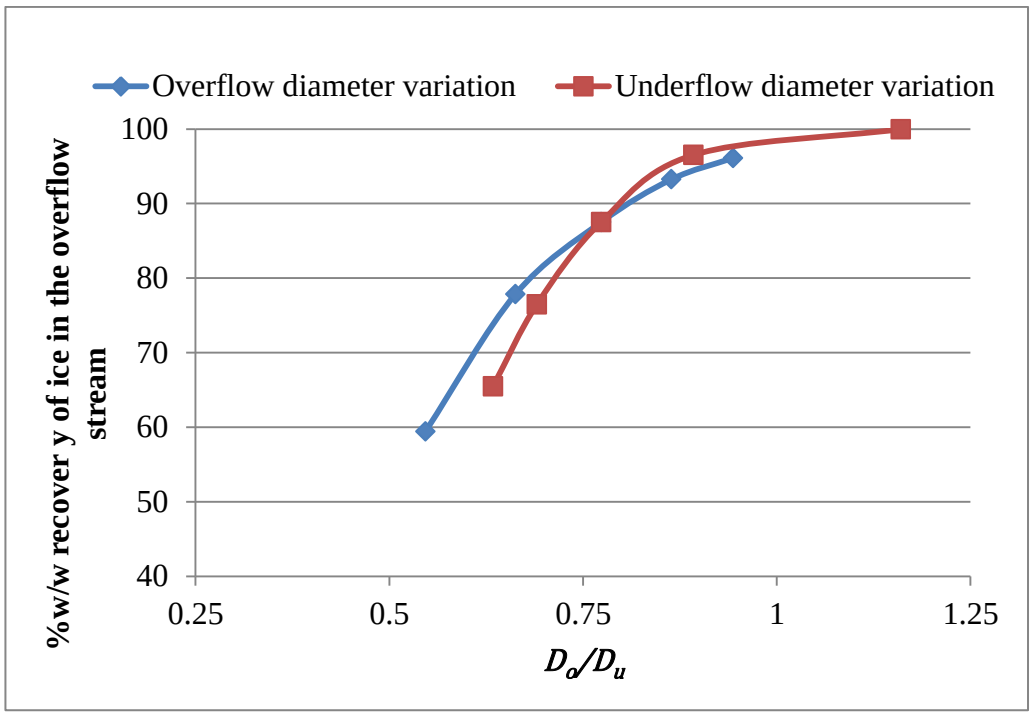

Figure 4.14 Ice recovery in the overflow stream at the overflow opening operating at the inlet velocity of 20 m/s and ice concentration of 20 % v/v

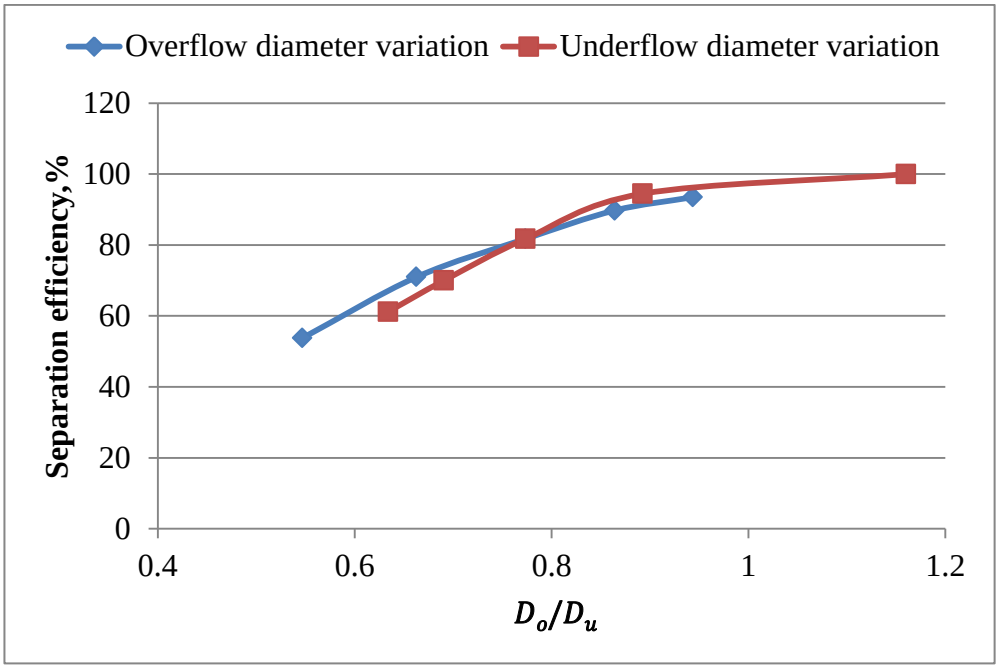

Figure 4.15 Effect of ratio D_o/D_u on the separation efficiency

CHAPTER 5 CONCLUSION AND RECOMMENDATION

5.1 Conclusion

In this work, CFD model of ice-sea water slurry for desalination process is investigated. The obstacle for concentrating ice slurry from brine with the wash column encourages this simulation. The selected configuration of a hydrocyclone is HY1 geometry, because it successfully separates the oil and the water which have closet density together. The overall configuration is 5 cm diameter and 116 cm height. The mesh independence test done with the single phase water at 5 m/s of inlet velocity shows that 330,000 node required for CFD calculation. Reynold Stress Model (RSM) and Eulerian-Granular model is applied to calculate the turbulent characteristics of ice-sea water slurry mixture inside hydrocyclone. The results of the CFD simulation is divided into two parts: effect of the operating conditions and the geometry on the separation efficiency of hydrocyclone.

The first part studies the effects of the operating conditions: the inlet velocity and the solid fraction of feed to hydrocyclone. The increasing inlet velocity generates higher centrifugal force. The operating condition which the separation efficiency of hydrocyclone exceeds 80 % based on the concentration of 20 % v/v is the inlet velocity at least 20 m/s. Above 20 m/s of inlet velocity, the separation efficiency gradually increases. However, higher inlet velocity also causes higher pressure drop which means higher operating cost. The increment of solid concentration from 0.1 to 0.4 results in the decrease of separation efficiency from 90 to 48%. Therefore, the lower ice concentration provides the better separation of hydrocyclone.

The second part focused on the study of overflow opening and underflow opening on the separation behavior of hydrocyclone. Both overflow diameter and underflow diameter are varied to study their effects on the split fraction, ice purity, and phase recovery in the similar trend. Therefore, the ratio of overflow diameter and underflow diameter will be used to analyze the separation performance of hydrocyclone. Adjusting the overflow diameter and underflow diameter does not enhance the higher separation efficiency in practice, because low range of overflow to underflow diameter provides lower capacity but higher purity of ice. The medium value of overflow diameter to underflow diameter (0.76) is considered as the optimum value.

In conclusion, the CFD model based on Eulerian-Granular model was used to investigate the separation behavior of ice-sea water slurry for the desalination process. The simulation provides the valuable information of operating condition for hydrocyclone such as, the inlet velocity, solid concentration, overflow diameter and the underflow diameter. The separation efficiency can be improved by increasing inlet velocity and lowering solid concentration.

5.2 Recommendation

The following recommendations for further study of this research are as following:

1. In this work, the Eulerian-Granular model is applied to calculate the fluid-solid behavior of ice and sea water mixture. The bulk viscosity of ice is calculated by Symlal-Orbien law. To develop the better model, the ice viscosity is proposed by Glen should be inputted instead of Symlal-Orbien
2. The size distribution of ice for this work is inputted as the constant size, but the ice can break and agglomerate. Smaller ice particles reduce the separation efficiency. To include the effect of agglomeration and breakage, the population balance equation should be added into the existing model for accounting the ice crystal fracture

REFERENCE

1. Nareerat_Wiriyapong, **Water Shortage for Thailand by 2015?**, [online], Available: http://www.readbangkokpost.com/easybusinessnews/agriculture/water_shortage_for_thailand_by.php [15/04/2554].

2. Lattemann, S. and Höpner, T., 2003, **Seawater Desalination : Impacts of Brine and Chemical Discharge on the Marine Environment**, Balaban Desalination Publications, L'Aquila, pp. 20-23.

3. Nelson, K.H., Thompson, T.G., and University of Washington. Dept. of, O., 1954, **Deposition of Salts from Sea Water by Frigid Concentration**, University of Washington, Dept. of Oceanography, Seattle, Wash., pp.135-148.

4. Stepakoff, G.L., Siegelman, D., Johnson, R., and Gibson, W., 1974, "Development of a Eutectic Freezing Process for Brine Disposal", **Desalination**, Vol. 15, No. 1, pp. 25-38.

5. Barduhn, A.J. and Manudhane, A., 1979, "Temperatures Required for Eutectic Freezing of Natural Waters", **Desalination**, Vol. 28, No. 3, pp. 233-241.

6. resource, C.e.-l., **Solutions and Solubility**, [online], Available: http://eleceng.dit.ie/gavin/id_crystal/main.php?page=solu_01 [3/05/2554].

7. Chemguide, **Solid-Liquid Phase Diagrams: Salt Solution**, [online], Available: http://www.chemguide.co.uk/physical/phaseeqia/saltsoln.html [15/04/2554].

8. Howe, E.D., 1974, **Fundamentals of Water Desalination**, M. Dekker, New York, pp.314-332

9. Franceschini, O., **Dewatering of Sludge by Freezing**, [online], Available: epubl.ltu.se/1402-1617/2010/024/LTU-EX-10024-SE.pdf [15/04/2554].

10. Evans, W.K., Suksangpanomrung, A., and Nowakowski, A.F., 2008, "The Simulation of the Flow within a Hydrocyclone Operating with an Air Core and with an Inserted Metal Rod", **Chemical Engineering Journal**, Vol. 143, No. 1–3, pp. 51-61.

11. Margolis, G., Sherwood, T.K., Brian, P.L.T., and Sarofim, A.F., 1971, "The Performance of a Continuous Well Stirred Ice Crystallizer", **Ind. Eng. Chem.**

Fund. Industrial & Engineering Chemistry Fundamentals, Vol. 10, No. 3, pp. 439-452.

12. Voitkovskii, K.F., 1962, **The Mechanical Properties of Ice**, Air Force Cambridge Research Laboratories, Geophysics Research Directorate; [available from the Office of Technical Services, U.S. Dept. of Commerce, Washington, Bedford, Mass., pp.217-230

13. Claxton, D., Svarovsky, L., and Thew, M.T.,"**Hydrocyclones** '96", 1996, London, pp., 135-149.

14. Svarovsky, L., 1977, **Solid-Liquid Separation**, Butterworths, London; Boston, pp.170-180

15. Anon., 2003, "**Solid Liquid Separation**", Kidlington, Oxford, UK.

16. Wendt, J.F., Anderson, J.D., and Von Karman Institute for Fluid, D., 1992, **Computational Fluid Dynamics : An Introduction**, Springer-Verlag, Berlin; New York, pp.250-272

17. Gidaspow, D., 1994, **Multiphase Flow and Fluidization : Continuum and Kinetic Theory Descriptions**, Academic Press, Boston, pp.78-100

18. Narasimha, M., Sripriya, R., and Banerjee, P.K., 2005, "CFD Modelling of Hydrocyclone--Prediction of Cut Size", **International Journal of Mineral Processing**, Vol. 75, No. 1-2, pp. 53-68.

19. Medronho, R.A., Schuetze, J., and Deckwer, W.D., 2005, "Numerical Simulation of Hydrocyclones for Cell Separation", **Latin American applied research = Pesquisa aplicada latino americana = Investigación aplicada latinoamericana.**, Vol. 35, No. 1, p. 1.

20. Ukkaracheneeyakorn, N., 1998, **Hydrocyclone as a Classifier** = ไฮโดรไซโคลนกับงานคัดแยกขนาด.

21. Delgadillo, J.A. and Rajamani, R.K., 2005, "A Comparative Study of Three Turbulence-Closure Models for the Hydrocyclone Problem", **International Journal of Mineral Processing**, Vol. 77, No. 4, pp. 217-230.

22. Ruiyun, Z., Wenji, S., Kaijun, D., and Ziping, F.,2011. "Cfd Simulation on Ice Slurry Concentrating Hydrocyclone". **Mechanic Automation and Control**

Engineering (MACE), 2011 Second International Conference on, 15-17 July 2011, pp., 5642-5644.

23. Elsayed Ahmed, E.A., 2005, **Application of Hydrocyclone for Cell Separation in Mammalian Cell Perfusion Cultures**, Braunschweig, Techn. University, pp.120-140

24. Bhaskar, K.U., Murthy, Y.R., Raju, M.R., Tiwari, S., Srivastava, J.K., and Ramakrishnan, N., 2007, "CFD Simulation and Experimental Validation Studies on Hydrocyclone", **Minerals engineering.**, Vol. 20, No. 1, pp. 60-71.

25. Almuttahar, A. and Taghipour, F., 2008, "Computational Fluid Dynamics of High Density Circulating Fluidized Bed Riser: Study of Modeling Parameters", **Powder Technology Powder Technology**, Vol. 185, No. 1, pp. 11-23.

26. Yu Jianghua, Y.Q., and Youngchul Kim, Performance Analysis of a Hydrodynamic Separator for Treating Particulate Pollutants in Highway Rainfall Runoff. **Environmetal Engineering Research**

APPENDIX A

ASPEN PLUS SIMULATION DATA

A.1. Eutectic crystallization loop

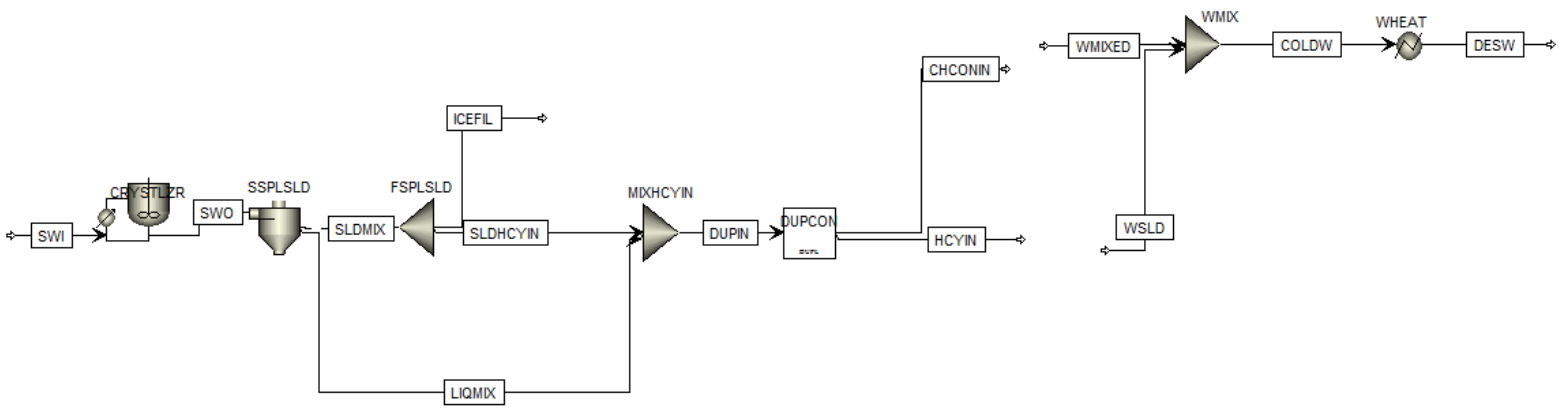

Figure A.1 Aspen Plus Simulation Process

Table A.1 Aspen Plus simulation data

Parameter& Description	Feed pressure@selected operating temperature = 35°C							
	1 barg		3 barg		5 barg		7 barg	
From	SWI	SWO	SWI	SWO	SWI	SWO	SWI	SWO
To		CRYSTZR		CRYSTZR		CRYSTZR		CRYSTZR
Substream: MIXED	CRYSTZR		CRYSTZR		CRYSTZR		CRYSTZR	
Phase:								
Component Mole Flow	Liquid	All	Liquid	All	Liquid	All	Liquid	All
Mass Flow (kg/hr)	5.467269	5.467272	5.467269	5.467272	5.467269	5.467272	5.467269	5.467272

Parameter& Description	Feed pressure@selected operating temperature = 35°C							
	1 barg		3 barg		5 barg		7 barg	
Volume Flow (m^3/hr)	100	100	100	100	100	100	100	100
Temperature (°C)	35	-30	35	-30	35	-30	35	-30
Pressure (bar)	2.01325	2.01325	4.01325	4.01325	6.01325	6.01325	8.01325	8.01325
Vapor Fraction	0	0	0	0	0	0	0	0
Liquid Fraction	1	0.118407	1	0.118407	1	0.118407	1	0.118407
Solid Fraction	0	0.881593	0	0.881593	0	0.881593	0	0.881593
Molar Enthalpy (kcal/mol)	-67.8928	-70.0531	-67.892	-70.0531	-67.8913	-70.0531	-67.8905	-70.0531
Mass Enthalpy (kcal/kg)	-3711.88	-3829.99	-3711.84	-3829.99	-3711.8	-3829.99	-3711.76	-3829.99
Enthalpy Flow	-0.37119	-0.383	-0.37118	-0.383	-0.37118	-0.383	-0.37118	-0.383
Molar Entropy (cal/mol-K)	-37.7115	-45.7829	-37.7121	-45.9169	-37.7126	-45.9954	-37.713	-46.0512
Mass Entropy (cal/cm-K)	-2.06179	-2.50308	-2.06182	-2.5104	-2.06185	-2.5147	-2.06187	-2.51775
Molar Density (kmol/cm^3)	55.82281	51.82784	55.82772	51.82779	55.83262	51.82774	55.83752	51.82769
Mass Density (kg/m^3)	1021.037	947.9653	1021.126	947.9644	1021.216	947.9635	1021.306	947.9626
Average Molecular Weight	18.29067	18.29066	18.29067	18.29066	18.29067	18.29066	18.29067	18.29066
Phase: Liquid								
Density (kg/m^3)	1021.037	1221.76	1021.126	1221.749	1021.216	1221.737	1021.306	1221.726
Viscosity (cp)	0.694998	3.907823	0.695002	3.907807	0.695006	3.907789	0.69501	3.907771
surface tension (dyne/cm)	71.7078	90.41374	71.70786	90.41369	71.70792	90.41362	71.70798	90.41356

A.2. Filtration fraction

The solid fraction of feed to hydrocyclone depends on the filtration fraction of ice filter.

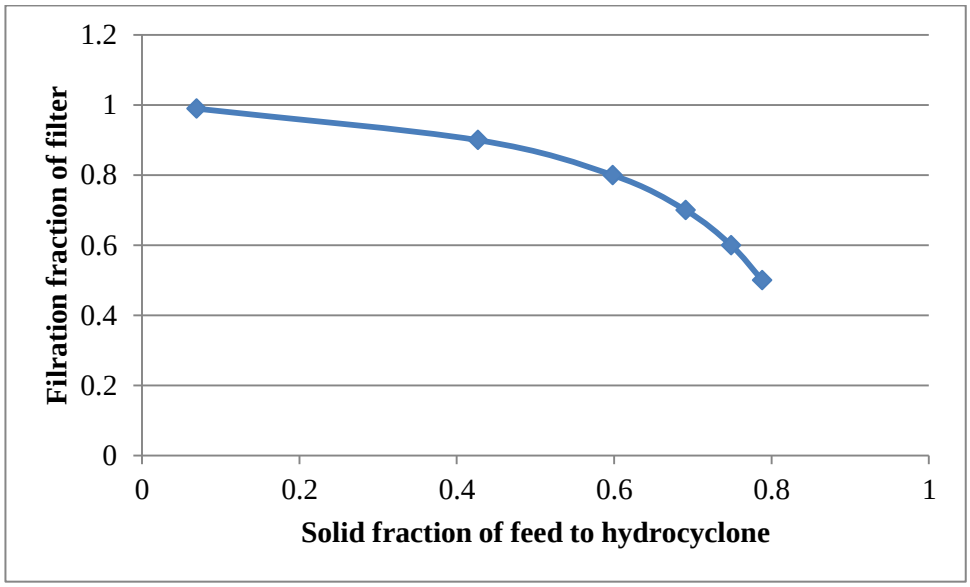

Figure A.2 Filtration fraction

APPENDIX B

EXPERIMENTAL RESULTS

B.1. Effect of inlet velocity and solid concentration [13]

Yuan [13] studies the separation of yeast with hydrocyclone. They used the liquid-liquid type hydrocyclone for use with light dispersion, which was originally developed for the separation of dispersed oil in water. His study investigated the effect on the separation performance of operating conditions including split ratio and feed flow rate or feed pressure, shear effect on yeast cells, and feed concentration of hydrocyclone.

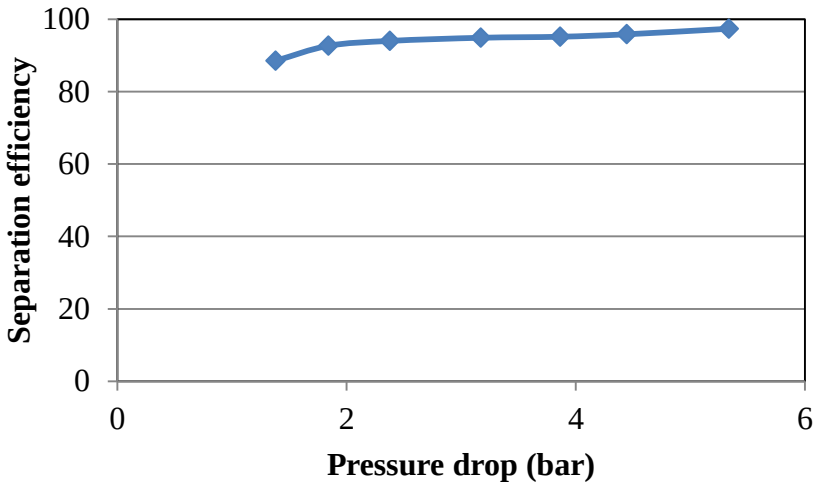

Figure B.1 Effect of pressure drop on the separation efficiency: HY1 nylon powder in water C_i = 0.50 % v/v ,T = 17°C [13]

The efficiency increased with increase in pressure drop or feed flow rate. The certain level of pressure drop or feed flowrate is needed to generate enough centrifugal force for particles to settle. With further increase in feed flow rate after around 2 bar, however, the efficiency increased slowly.

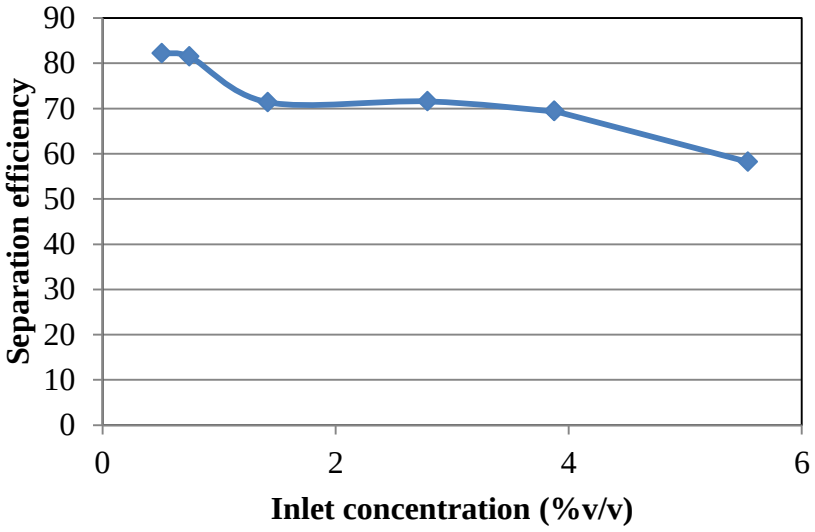

Figure B.2 Feed Concentration Effect on the clarification efficiency: Geometry hydrocyclone HY2 brewing yeast in sucrose water 2.3 % (w/w),operating conditions: ΔP = 4.8 bar [13]

The separation efficiency of hydrocyclone has been believed to decrease with increase in feed concentration because the level of effective viscosity hindered settling and

hindered discharge increase with increase in feed concentration. Within the range of feed concentration from 0.35 to 0.80%, the efficiency fell slightly since neither significant feed concentration reached to above 0.8%, the hindered settling become severe.

B.2 Effect of D_o/D_u

The effect of the underflow diameter was previously investigated by Yu [26]. He examined the separation characteristics of particles in the rainfall runoff from paved roads using ϕ 7.5cm hydrocyclone of Rietema design. Figure shows the geometry of hydrocyclone

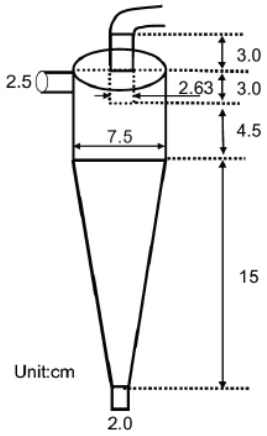

Figure B.3 Rietema design of hydrocyclone [26]

The underflow diameter was adjusted from 0.5 to 2 cm. Then the results were analyzed in term of ratio of D_o/D_u. Figure B.4 shows the relationship between the split fraction and the ratio of D_o/D_u

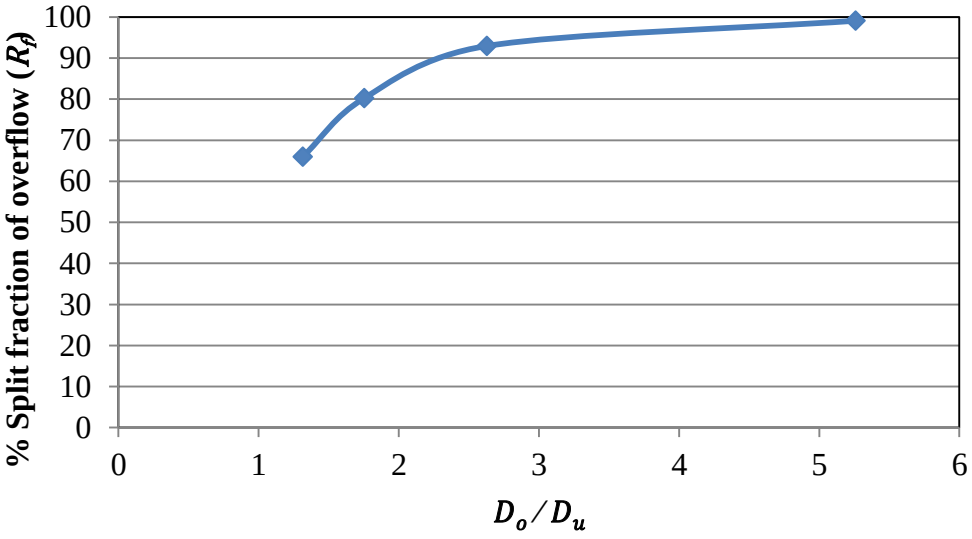

Figure B.4 Effect of ratio on the split fraction of overflow stream

The geometry of the hydrocyclone and the relative size of the outlet, allow the greatest part of the water and part of the water and part of the finest particles to exit as overflow, while most particles with less water exit as underflow. The behavior of hydrocyclone separation is regulated by adjusting the underflow diameter. The results are analyzed in term of D_o/D_u. The percentage of the overflow volume increases with increasing D_o/D_u ratio, while the percentage of the underflow volume increases. The separation efficiency of the hydrocyclone was evaluated by means of the following indicator

$$\varepsilon = \frac{Mass\ flow\ rate\ in\ the\ underflow}{Mass\ flow\ rate\ in\ the\ inlet} \quad \textbf{(B.1)}$$

Figure B.5 shows the variation in the removal efficiency with respect to the outlet size. The removal efficiency decreased with decreasing outlet size (D_u), or the removal efficiency increase with the increasing of D_o/D_u. When the underflow outlet is reduced, the flow rotation inside the unit will be enhanced due to the detention of much more slurry; consequently, more particles are separated to the underflow. However, if the underflow outlet is too little, it may clog with coarse particles during practical application. The effect of the D_o/D_u showed a weak increasing trend for the removal efficiency.

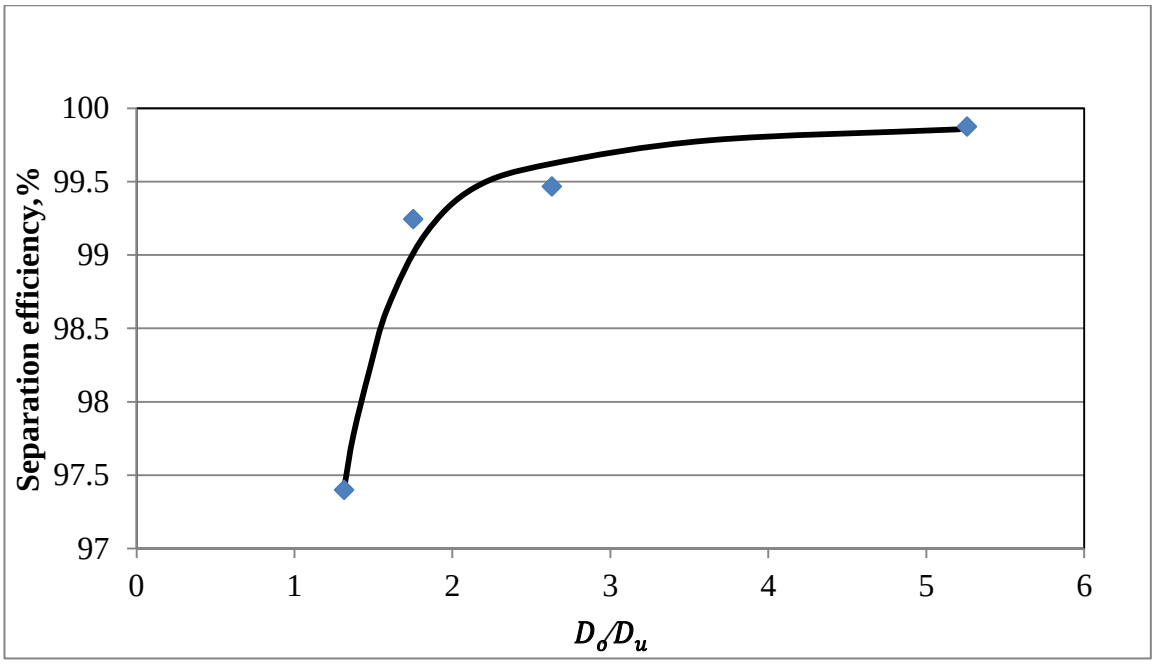

Figure B.5 Effect of D_o/D_u ratio on the separation efficiency of hydrocyclone

APPENDIX C

FLUENT SETTING

C.1. Problem specification

The ice-slurry enters hydrocyclone with the inlet velocity of 20 m/s, and hydrocyclone is applied to concentrate ice slurry from the brine slurry . The operating condition of hydrocyclone is specified as shown in

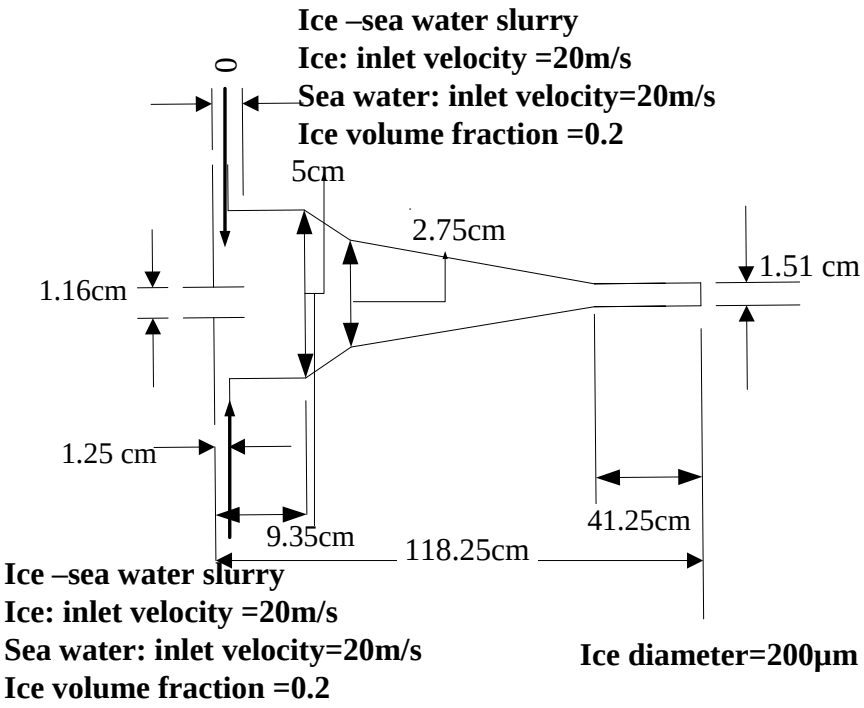

Figure C.1 Thesis Problem Statement

C.2. Setting Fluent

1. Preparation

1.1. Draw geometry of hydrocyclone with solidwork and compute mesh file with ICEM CFD

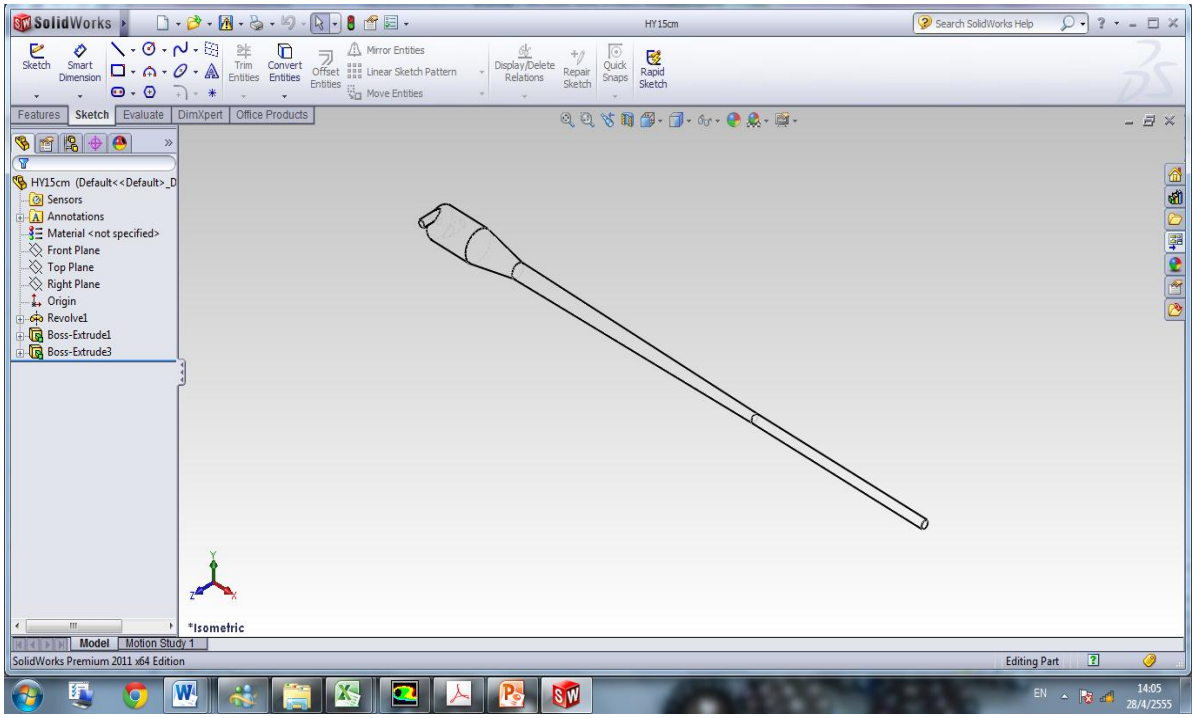

Figure C.2 Solidwork of hydrocyclone

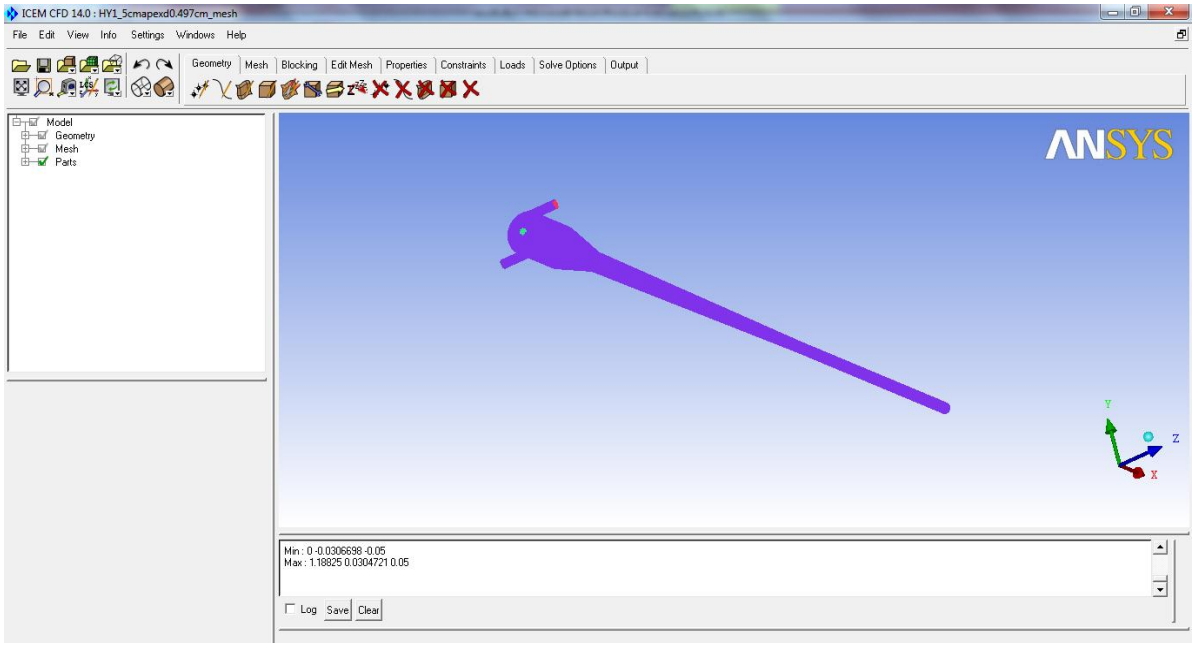

Figure C.3 ICEM CFD of Hydrocyclone

1.2. Load file mesh of hydrocyclone into Fluent: Read→Mesh

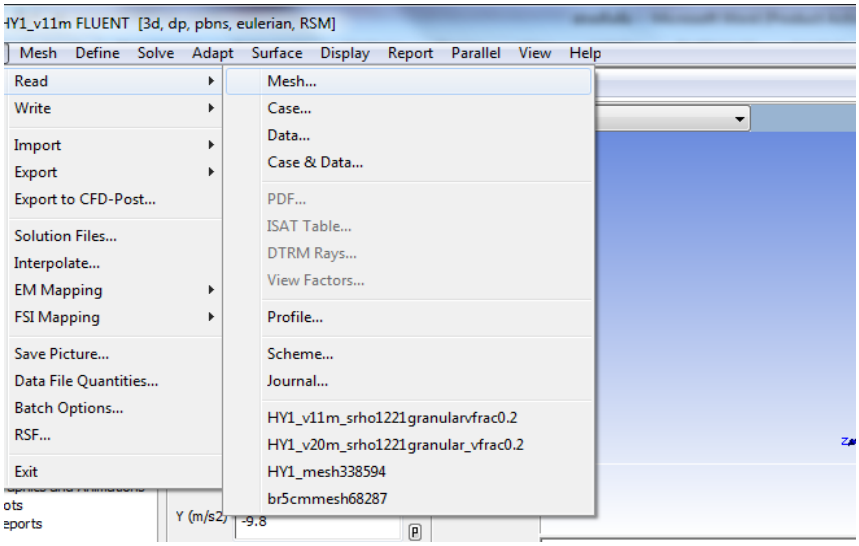

Figure C.4 Reading mesh

2. Set solver type

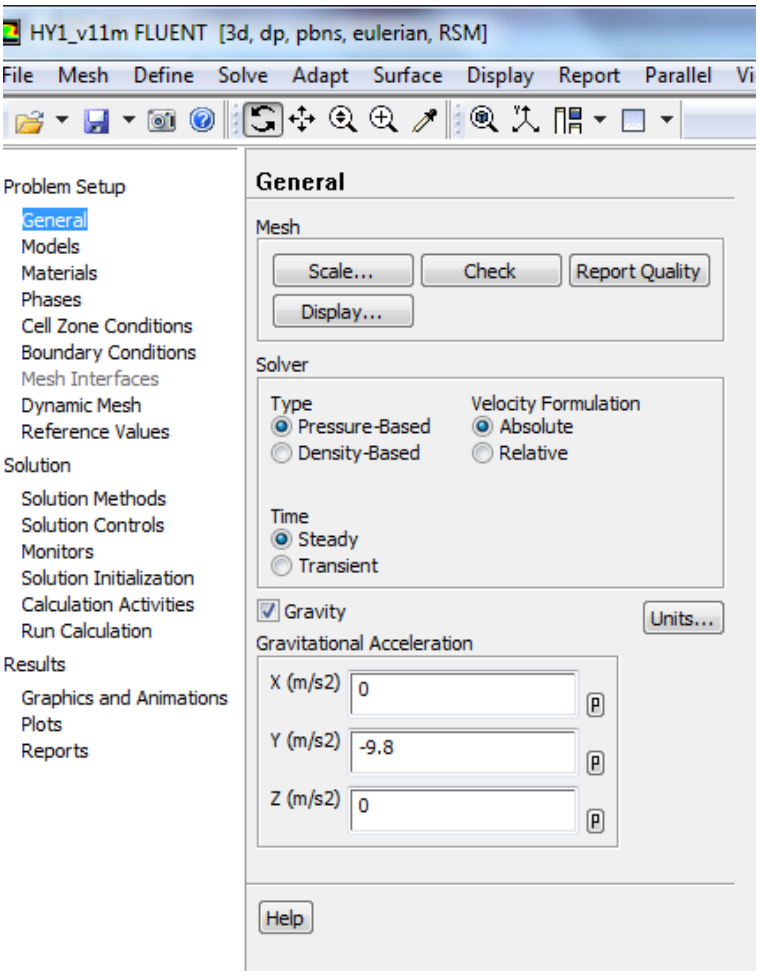

Figure C.5 Solver type setting

3. Turbulence model

Model→Viscous model→Reynold stress model

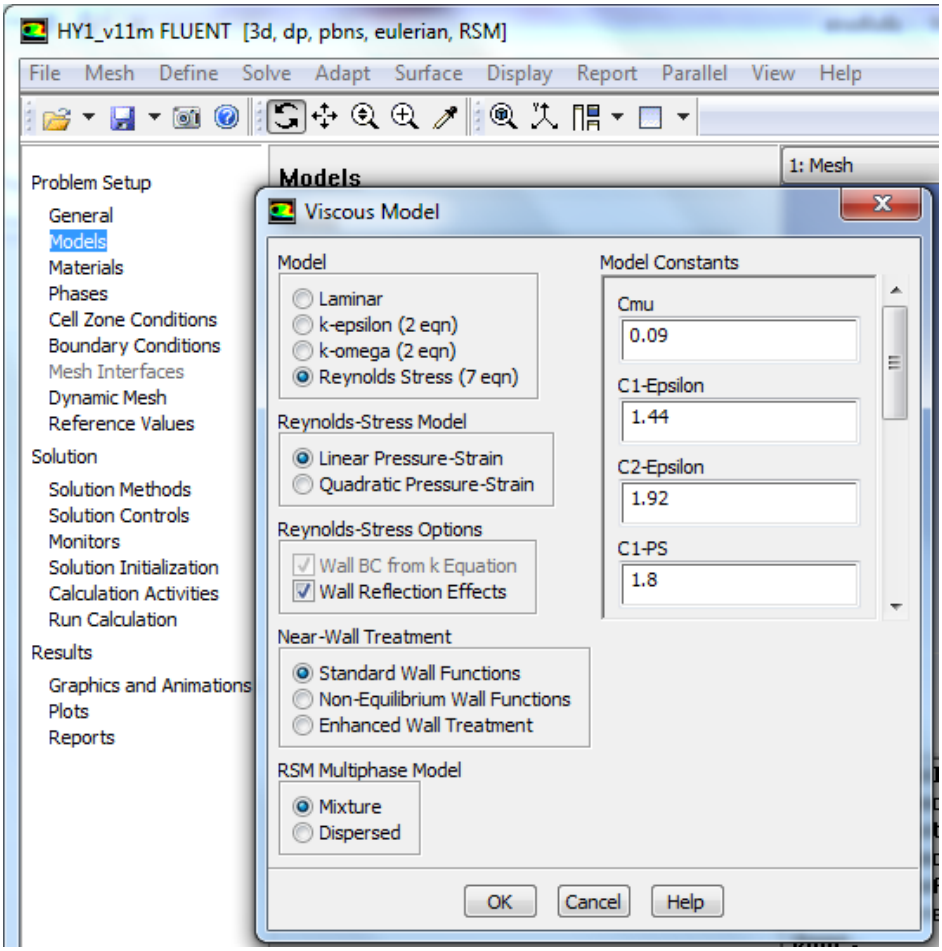

Figure C.6 Turbulence model set up

4. Multiphase model

Models→Multiphase→Eulerian

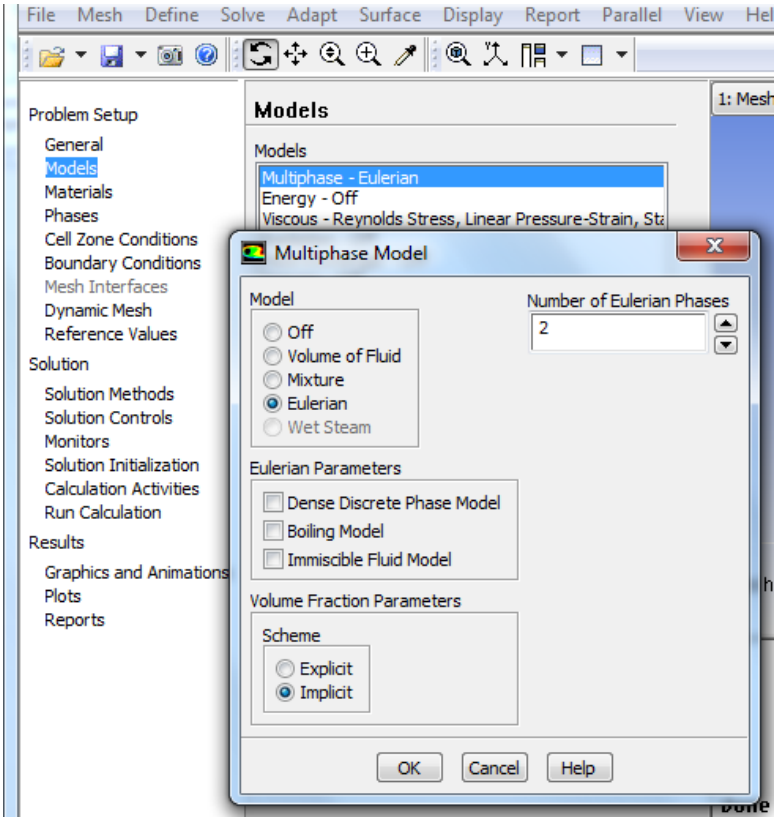

Figure C.7 Multiphase model set up

5. Creating material: Material→Create

5.1. Enter the physical properties of sea water: density = 917 kg/m^3 and viscosity =0.0039 kg/m-s and then click create

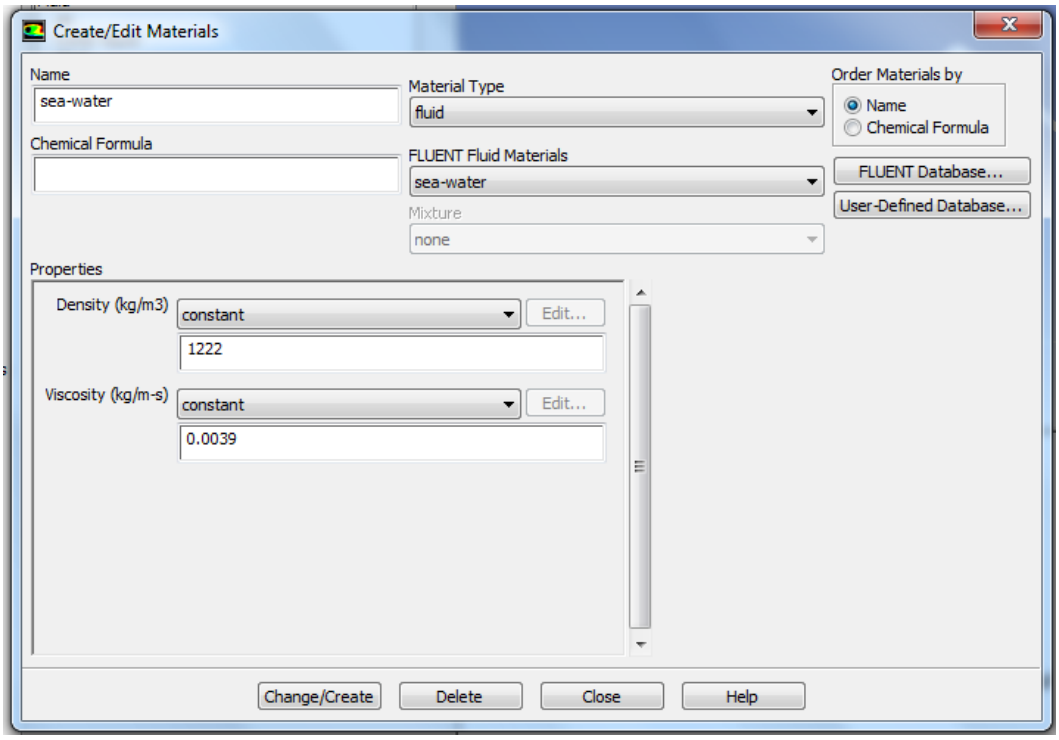

Figure C.8 Creating material of sea water

5.2. To create the ice material, choose the fluent database and then copy and type the name of material: ice

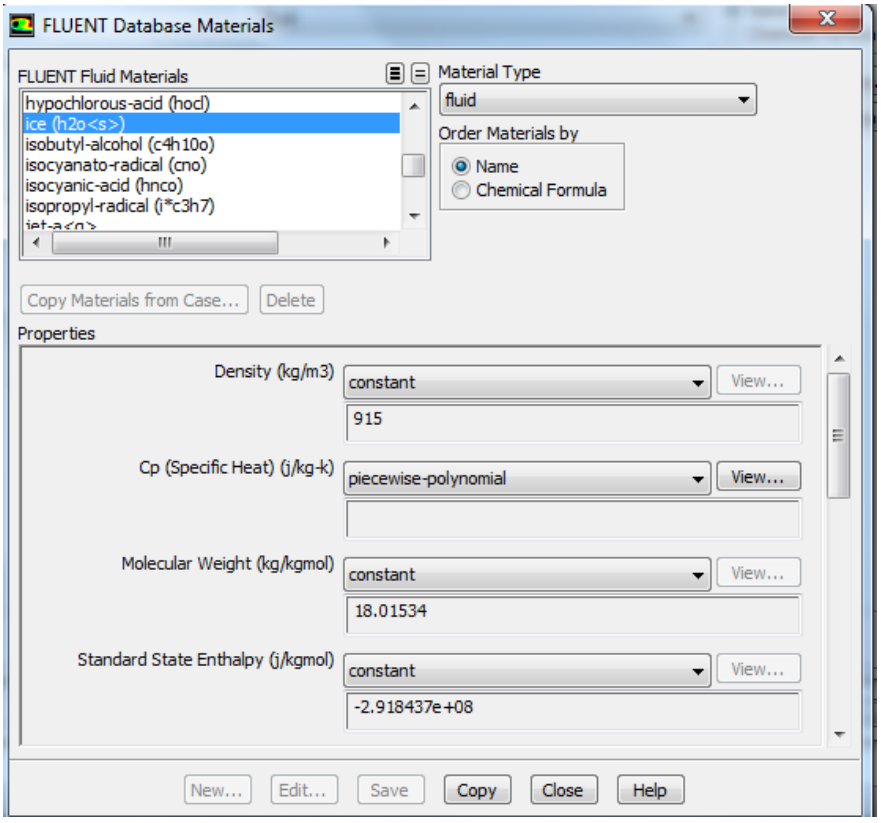

Figure C.9 Using Fluent Database

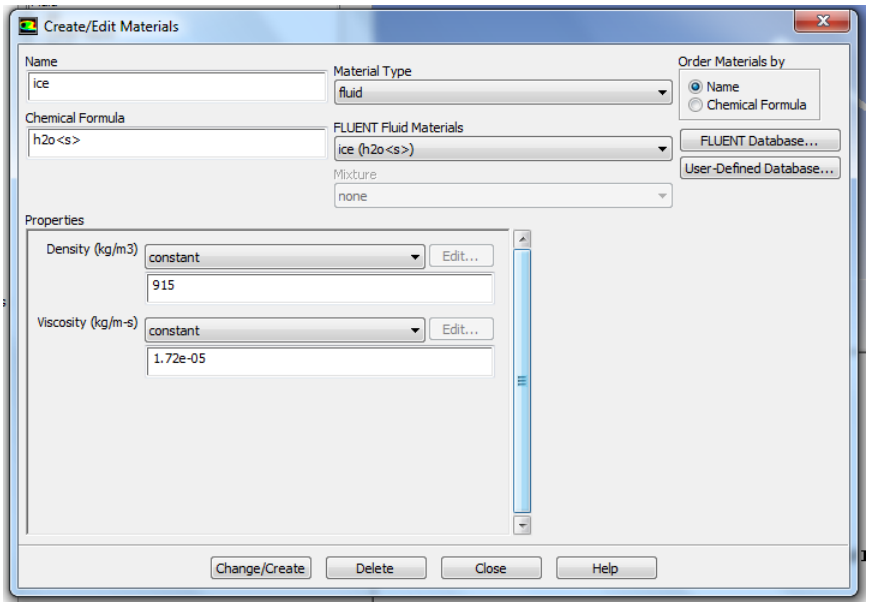

Figure C.10 Creating ice material

6. Phases

6.1. Define primary phase: Phase→Phase 1-primary phase →sea water

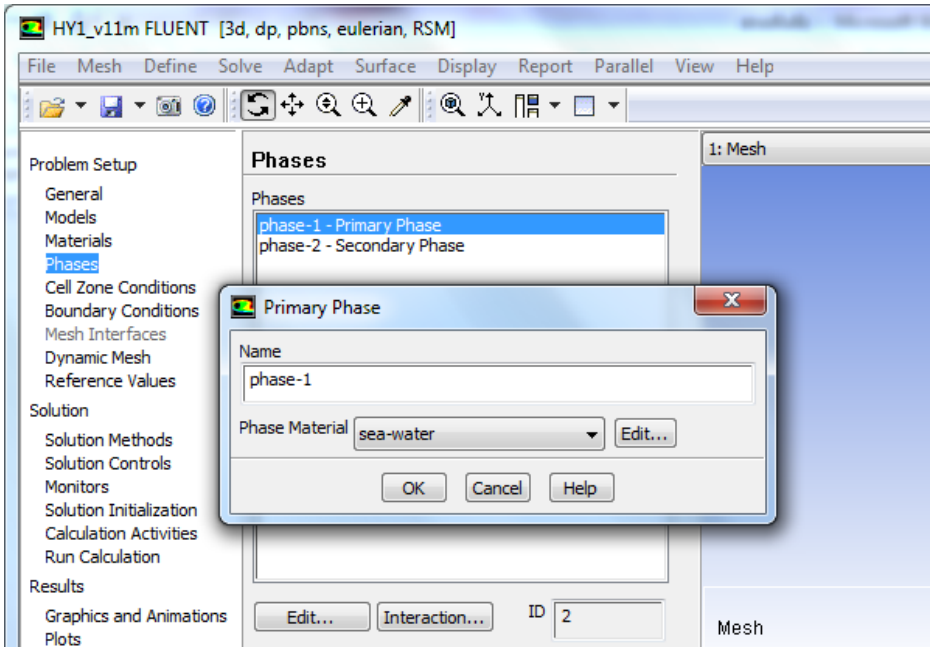

Figure C.11 Defining primary phase

6.2. Define secondary phase: Phase→Phase 2-secondary phase→Ice

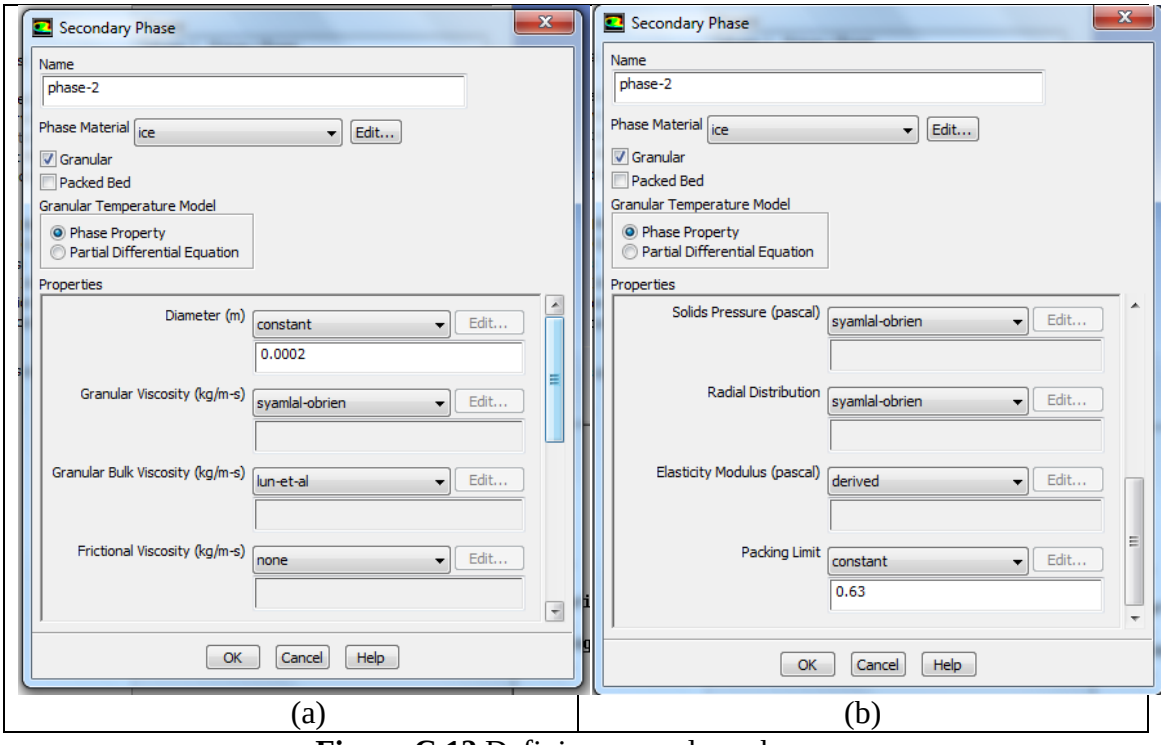

(a) (b)

Figure C.12 Defining secondary phase

7. Setting boundary conditions

7.1. Set the boundary conditions as following:

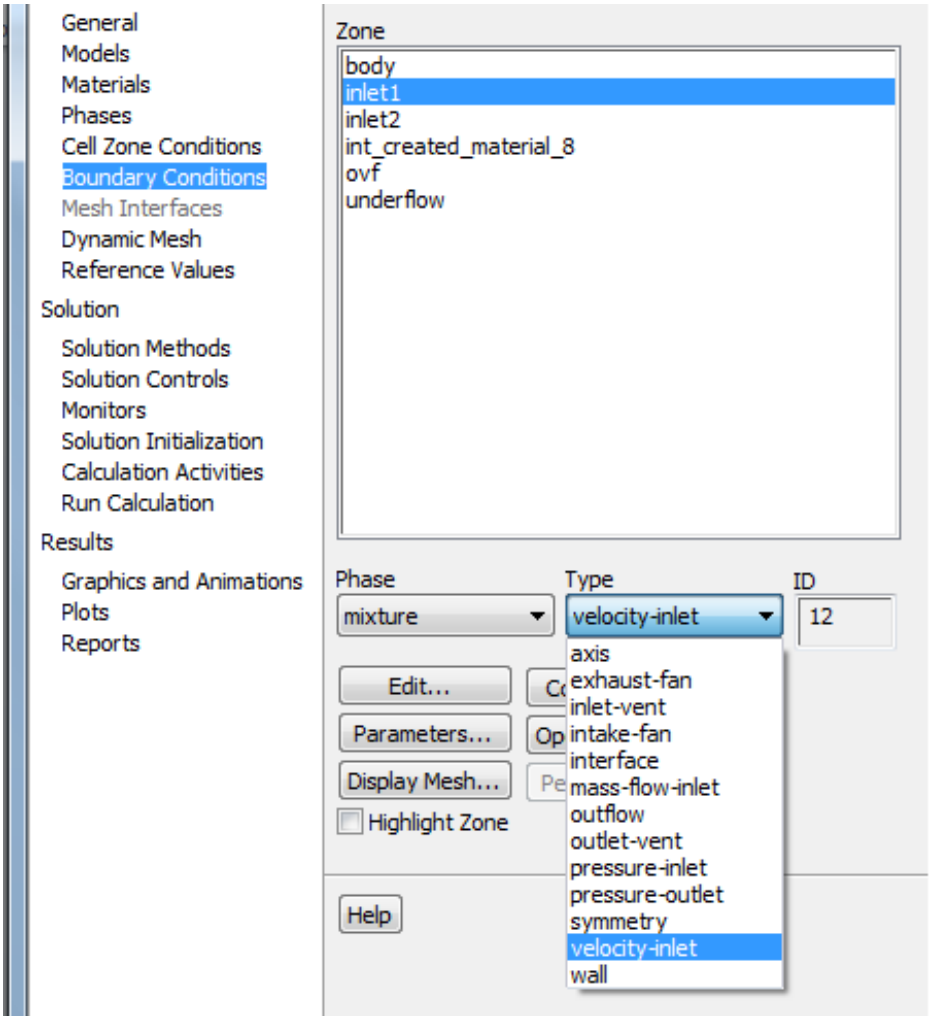

Figure C.13 Defining boundary conditions

- Boundary→inlet 1→velocity inlet
- Boundary→inlet 2→velocity inlet
- Boundary→ovf→pressure-outlet
- Boundary→underflow→pressure-outlet

7.2.Specify the inlet velocity magnitude as following:

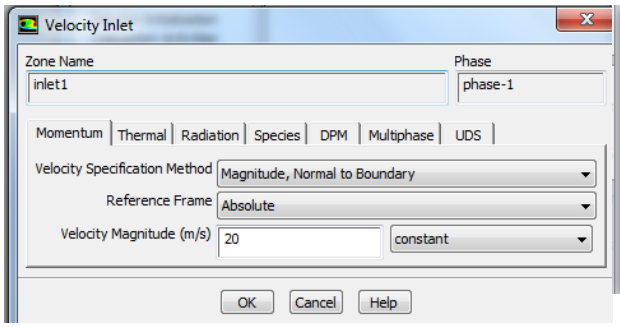

(a)

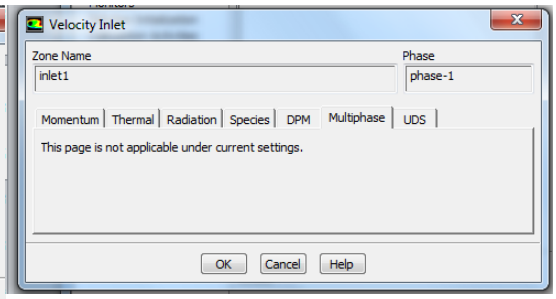

(b)

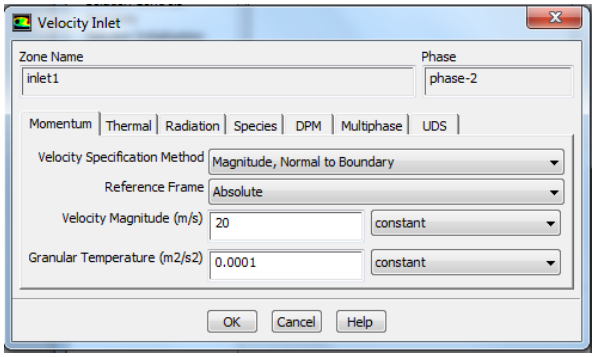

(c)

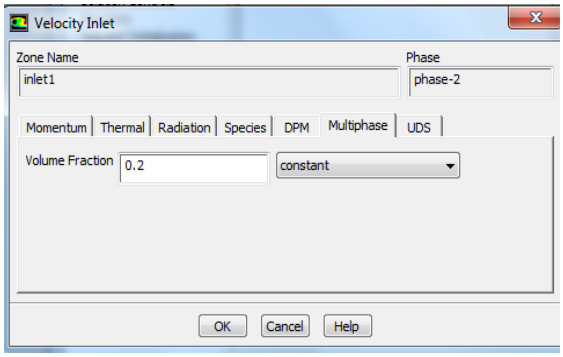

(d)

Figure C.14 Defining inlet velocity

7.3.Specify the outlet pressure of overflow (ovf) and underflow to zero

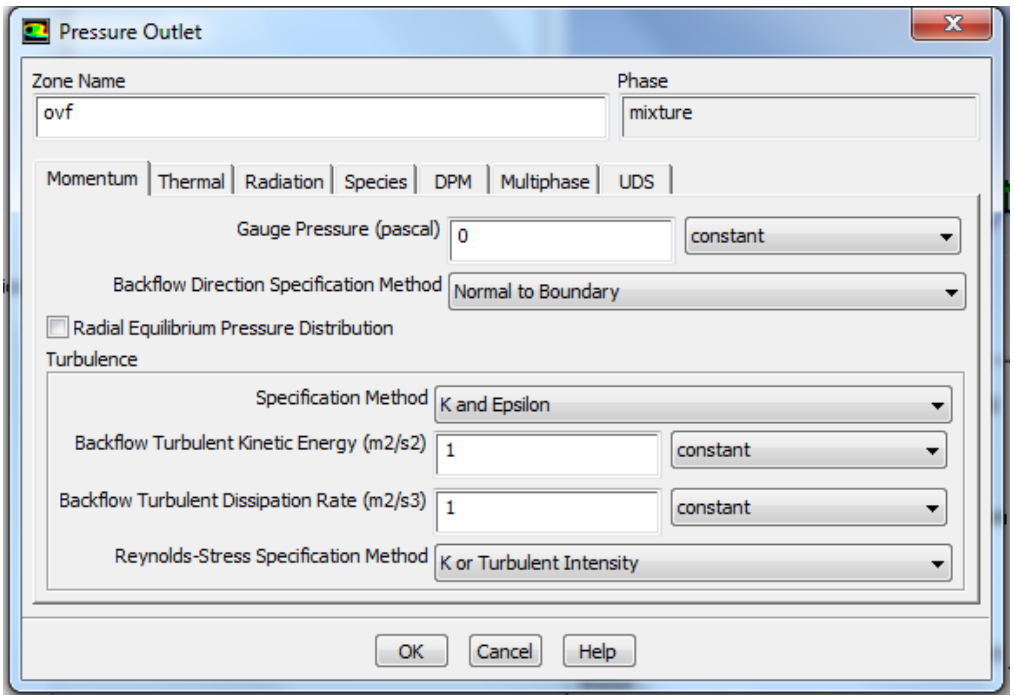

Figure C.15 Pressure outlet condition

8. Check the solution method

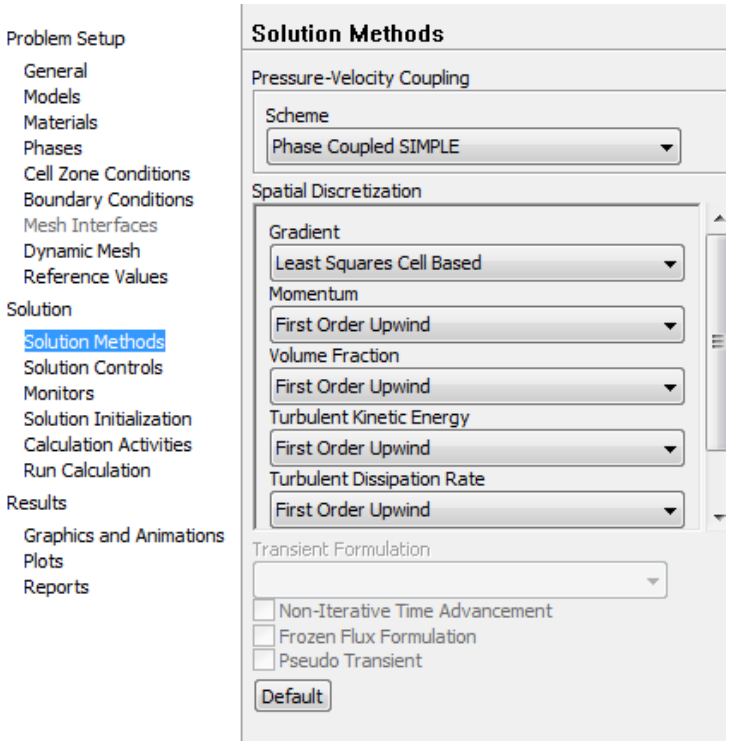

Figure C.16 Solution method of CFD

9. Click solution initialization and then start runing

C.3 Fluent setting for energy case

1. Click Model→Energy

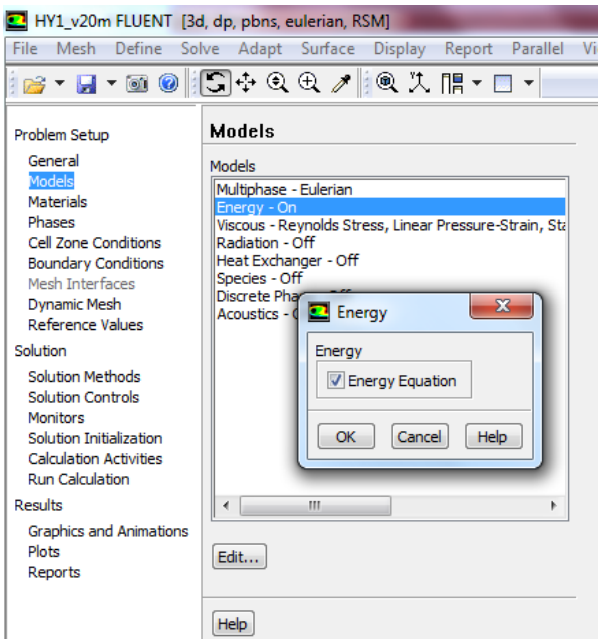

Figure C.17 Energy case

2. Setting Adiabatic case

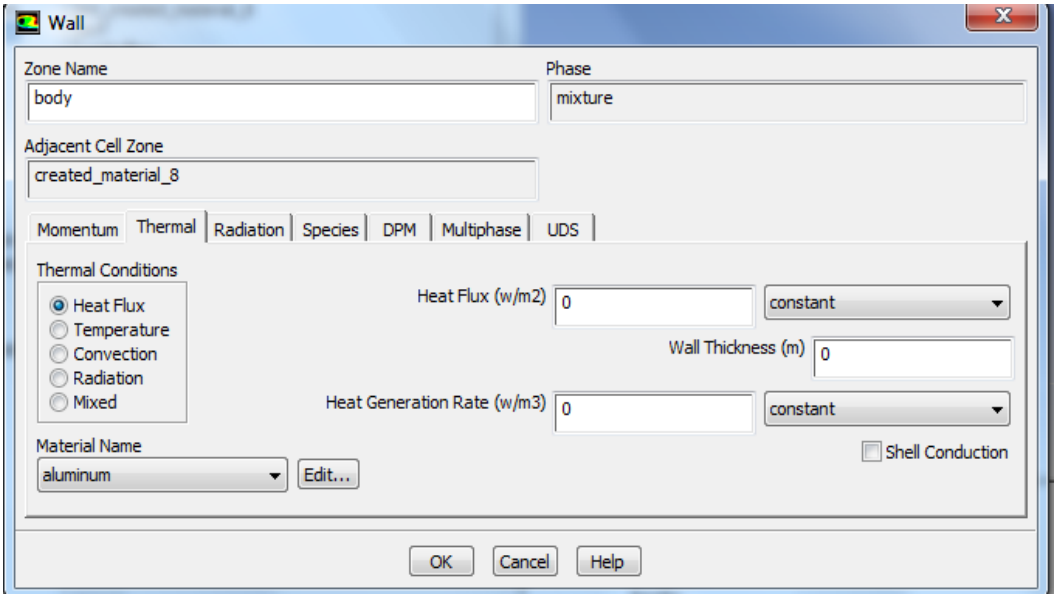

Figure C.18 Setting adiabatic case

3. Setting heat transfer coefficient

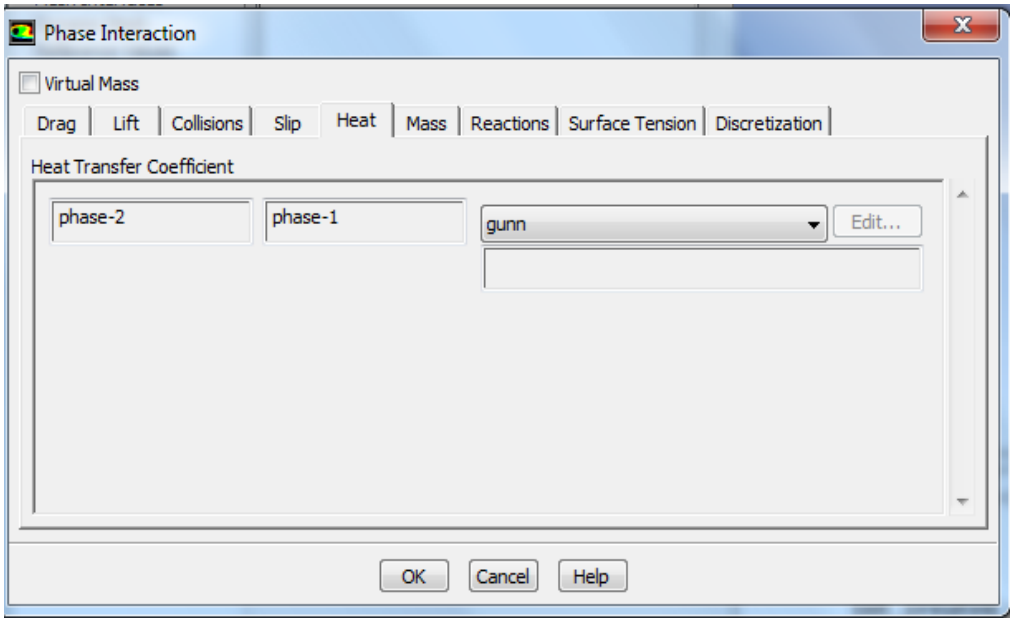

Figure C.19 Setting heat transfer coefficient

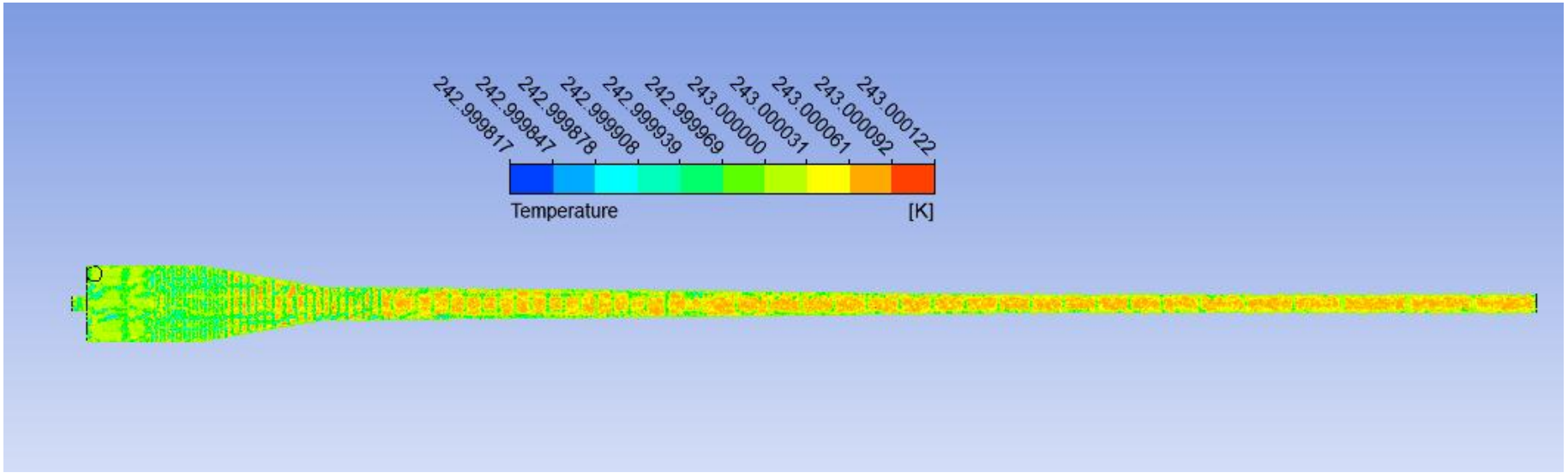

Figure C.20 Temperature contour at the middle plane of hydrocyclone

CURRICULUM VITAE

NAME	Ms. Jitsopin Srudhiprom
DATE OF BIRTH	1 April 1988
EDUCATIONAL BACKGROUND	
HIGH SCHOOL	The Demonstration School of Ramkhamhaeng University, 2005
BACHELOR'S DEGREE	Bachelor of Engineering (Chemical Engineering), with the First Class Honors Sirindhorn International Institute of Technology, Thammasat University, 2009
MASTER'S DEGREE	Master of Engineering (Chemical Engineering) King Mongkut's University of Technology Thonburi, 2011